DURBAN UNIVERSITY OF TECHNOLOGY

OPTIMIUM CONDITIONS FOR THE PRODUCTION OF SUB-MICRON COBALT POWDER

Andricia Hareepersad

2014

OPTIMIUM CONDITIONS FOR THE PRODUCTION OF SUB-MICRON COBALT POWDER

SUBMITTED IN FULFILLMENT OF THE REQUIREMENTS FOR THE DEGREE OF

MASTER OF TECHNOLOGY: CHEMICAL ENGINEERING IN THE FACULTY OF ENGINEERING, SCIENCE, AND BUILT ENVIRONMENT AT THE DURBAN UNIVERSITY OF TECHNOLOGY

ANDRICIA HAREEPERSAD

SUPERVISORS:

P. Musonge

F. M. Swalaha

V. L. Pillay

JUNE 2014

DECLARATION

I, the undersigned, solemnly declare that the project has been completed entirely by me and this project work has not been submitted in whole or in part for a degree at another University.

A Hareepersad	Place	Date
---	---	---

Approval by Supervisor

NAME: **Prof Paul Musonge**

SIGNATURE: _____

CONTACT: **(031)-373 2415**

QUALIFICATION: **PhD (Chemical Engineering) , University of London**

DATE: _____

ABSTRACT

Cobalt powder is a grey metallic powder that is produced by the thermal decomposition and reduction of a cobalt compound. The challenge faced by Shu Powders Africa was that sub-micron cobalt powder had never been produced in a two-step furnace by any manufacturer in the cobalt powder industry. Hence there was no prior information to guide this type of processing. Therefore this research set out to investigate the production of sub-micron cobalt powder through a two-step furnace to determine the optimum parameters for this process.

For the company to remain competitive, it was imperative to begin producing sub-micron cobalt powder. Sub-micron cobalt powder is much more valuable and profitable to produce. The second production line would be operational due to the production of sub-micron cobalt powder hence creating job opportunities for the local community.

Sub-micron cobalt powder shares the same chemical composition and physical characteristics as cobalt powder. The only differences are particle size (0.60 - 0.90 µm), oxygen content (0.30 - 0.80%) and the microscopic structure which is the particle size distribution d_{90} (7 - 10 µm). The approach taken was to understand the variables that had a large effect on the powder. The effects needed to be established by determining how it impacted on the quality of the powder which is pertinent to making sub-micron cobalt powder. Due to the experience in producing cobalt powder, variables that had a large effect on normal cobalt powder production were assumed to be the same variables that would impact the production of sub-micron cobalt powder. Some of these effects were also confirmed by literature.

A strategy of statistical design of experiments was used to evaluate the conditions for sub-micron cobalt powder production. Design of experiments assisted in planning the experimental design matrices for both experiments. For the furnace experimentation a 2^4 factor design was selected. For the jet mill experimentation a 2^3 factor design was selected. Response surface methodology was used to determine optimum ranges of the variables at various process conditions. The central composite rotatable design laid out the design in which the variables interacted with one another at different process conditions. Evaluation of results was based on the generated model. Models such as the 3D surface model, cubic model and the contour model were generated to graphically illustrate the effects that the variables have on the response.

Analysis of furnace data indicated that the optimal response was achieved at a temperature range (445 - 460)°C, hydrogen gas range (225 - 250) Nm^3/h, belt speed (80 - 90) mm/min, and carbon dioxide gas range (80 - 90) Nm^3/h. Analysis of the jet mill experimental data indicated that the optimal response particle size distribution, was achieved at a classifier speed range of (5500 - 6000) rpm, AFG grinding bin range (30 - 35) kgs and grinding gas pressure of (4.0 - 4.5) bar.

The study confirms the efficiency of a two-step furnace to produce sub-micron cobalt powder at high volumes. The advantage of the two-step furnace was the increased throughput of 2.3-2.7 tons/day whilst in industry furnace throughputs are 1.3-1.6 tons/day. This represented a 60% increase in productivity over conventional furnaces. The response surface methodology also proved to be a suitable technique for process optimization.

ACKNOWLEDGEMENTS

I am indebted to all those who offered expert advice and critical comment. I would like to express my gratitude to the following:

1. My supervisors Prof Paul Musonge, Dr Feroz Mahomed Swalaha and Prof V.L. Pillay.
2. My mother Renuka Hareepersad for her support and encouragement and my late father Mr. M. S. Hareepersad for his spiritual guidance.
3. In particular special thanks are due to the Shareholder of Shu Powders Africa Pty (Ltd), Robert. T. Martin.
4. My colleagues at Shu Powders Africa for their continuous support and hard work.
5. The company Foxmet and Mr. Cedric Sheridan for the diamond tool tests.
6. The company Sandvik and Mr. Pete Fuller for providing data on the performance of submicron carbide applications.

TABLE OF CONTENTS

CONTENT			PAGE NO.
DECLARATION			i
APPROVAL BY SUPERVISOR			ii
ABSTRACT			iii
ACKNOWLEGDEMENTS			v
LIST OF FIGURES			xii
LIST OF TABLES			xvii
LIST OF EQUATIONS			xxii
LIST OF ABBREVIATIONS			xxiii
CHAPTER 1: INTRODUCTION			**1**
1.1	Background		1
1.2	Scope		3
1.3	Sub-micron cobalt production – Furnace		4
1.4	Sub-micron cobalt production – Jet mill		6
1.5	Thesis Outline		7
CHAPTER 2: LITERATURE REVIEW			**8**
2.1	History of Cobalt		8
	2.1.1	Refined cobalt	9
	2.1.2	Cobalt matte, alloys and chemicals	9
	2.1.3	Super alloys	9
	2.1.4	Magnetic alloys	10
	2.1.5	Other cobalt based alloys	10

2.2 Cobalt Properties 13

2.2.1 Physical properties 13

2.2.2 Mechanical properties 14

2.2.3 Chemical properties 14

2.3 Cobalt Production Processes 15

2.3.1 Production of cobalt powder from cobalt oxalate 16

2.3.2 Production of cobalt powder from cobalt hydroxide 19

2.3.3 Production of cobalt powder from cobalt carbonate 20

2.3.4 Other processes 24

2.3.5 Uses of sub-micron cobalt powder 25

2.4 Milling Processes for Cobalt Powder 28

2.4.1 Air classifier mills 28

2.4.2 Hammer mills 29

2.4.3 Pin mills 29

2.4.4 Spiral jet mills 30

2.4.5 Fluidized bed jet mills 31

2.5 Design of Experiments 33

2.5.1 Pre-experimental planning 33

2.5.2 Type of experimental design 34

2.5.3 Conducting the experiment 35

2.5.4 Performing the statistical analysis on the data 35

2.5.5 Conclusion and recommendation 35

2.6 Full Factorial Experiment 36

2.7 Response Surface Methodology 39

2.7.1 Central composite design 41

2.7.2 The three types of response surface methodology 43

CHAPTER 3: FURNACE AND JET MILL TECHNOLOGY 46

3.1 The Furnace Process 46

3.2 The Jet mill Process 52

3.2.1 Jet mill description 52

3.2.2 Important variables - jet mill process 54

CHAPTER 4: EXPERIMENTAL METHODS 56

4.1 Approach for Experimentation 56

4.1.1 Process 56

4.1.2 Cobalt powder and cobalt carbonate 56

4.1.3 Standard operating procedures 57

4.1.4 Design of experiments and response surface methodology 57

4.1.5 Furnace and Jet mill 57

4.1.6 Particle size, oxygen content and particle size distribution 57

4.2 The Furnace Process 58

4.3 The Jet mill Process 59

4.4 Particle Size 61

4.4.1 The fsss sub-sieve sizer machine process 62

4.5 Oxygen Content 64

4.6 Particle Size Distribution 65

4.7 Design of Experiments 67

4.7.1 Furnace experimentation 67

4.7.2 Jet mill experimentation 69

4.8 Design Expert Software 71

CHAPTER 5: RESULTS AND DISCUSSION 72

5.1 Design of Experiments for Furnace Experiment 1 72

5.1.1 Response variable fsss 72

5.1.2 Response variable oxygen 79

5.1.3 Trends observed for furnace experimentation 1 85

5.2 Response Surface Methodology for Furnace experimentation 4 87

5.2.1 Response variable fsss 90

5.2.2 Response variable oxygen 93

5.2.3 Trend observed for furnace experimentation 4 97

5.3 Jet mill Experimentation 99

5.4 Response Surface Methodology for Jet mill Experimentation 1 99

5.4.1 Response variable particle size distribution 102

5.4.2 Response variable milling time 105

5.4.3 Trends observed for jet mill experimentation 1 109

5.5 Response Surface Methodology for Jet mill Experimentation 3 109

5.5.1 Response variable particle size distribution 113

5.5.2 Response variable milling time 116

5.5.3 Trends observed for jet mill experimentation 3 120

5.6 Discussion of Furnace and Jet mill Experimentation 121

CHAPTER 6: CONCLUSIONS AND RECOMMENDATION S 124

6.1 Conclusion 124

6.2 Recommendation 124

CHAPTER 7: REFERENCES 125

CHAPTER 8: APPENDIX 128

8.1 Furnace Experimentation 2 128

8.1.1 Design of experiments 2 - Furnace 128

8.1.2 Response variable fsss 130

8.1.3 Response variable oxygen 134

8.1.4 Trends observed for furnace experimentation 2 138

8.2 Furnace Experimentation 3 140

8.2.1 Response surface methodology for furnace experimentation 3 140

8.2.2 Response variable fsss 144

8.2.3 Response variable oxygen 148

8.2.4 Trends observed for furnace experimentation 3 153

8.3 Jet mill Experimentation 2 154

8.3.1 Response surface methodology for jet mill experimentation 2 154

8.3.2 Response variable particle size distribution 157

8.3.3 Response variable milling time 160

8.3.4 Trends observed for jet mill experimentation 2 164

8.4 Design Expert Software 165

8.5 Understanding the Terms and Options in Design Expert 170

CHAPTER 9: APPENDIX B **173**

9.1 Sequence Furnace Start-up 173

9.2 Sequence Jet mill Start-up 174

9.3 The Fsss Analysis Procedure 175

9.4 The Particle Size Distribution analysis procedure 177

LIST OF FIGURES

Figure 1.1:	Block diagram of the two-step furnace process for the production of sub-micron cobalt powder	1
Figure 2.1:	The global end use of cobalt powder	10
Figure 2.2:	A cobalt-nickel arsenide	11
Figure 2.3:	Uses of cobalt powder	11
Figure 2.4:	The location of the main deposits of the central African copper belt	12
Figure 2.5:	World production of primary cobalt	12
Figure 2.6:	Overview of different cobalt ore and salt production Processes	15
Figure 2.7:	Scanning electron micrograph of cobalt oxalate	17
Figure 2.8:	Scanning electron micrograph of cobalt carbonate	20
Figure 2.9:	An example of a hydrometallurgical process	24
Figure 2.10:	Diamonds in a cobalt metal for a diamond saw	27
Figure 2.11:	Air classifier mill	28
Figure 2.12:	Hammer mill operation	29
Figure 2.13:	Pin mill configuration	30
Figure 2.14:	Spiral jet mill	31
Figure 2.15:	Fluidized bed jet mill	32
Figure 2.16:	Fishbone diagram for brainstorm of factors	34
Figure 2.17:	Examples of factorial, fractional factorial and composite design	36
Figure 2.18:	Two-level factorial vs. one factor at a time	38
Figure 2.19:	The sequential nature of response surface methodology	39

Figure 2.20: Central composite design example 40

Figure 2.21: Strategy of experimentation 43

Figure 2.22: Response surface and contour plot illustrating a surface with a maximum 44

Figure 2.23: Response surface and contour plot illustrating a surface with a minimum 44

Figure 2.24: Response surface and contour plot illustrating a saddle point (mini-max) 45

Figure 3.1: Process flow diagram of the furnace 49

Figure 3.2: Schematic diagram of the AFG unit 52

Figure 3.3: Process flow diagram of the jet mill 53

Figure 4.1: Experimental brainstorming for the research 56

Figure 4.2: Schematic diagram for the jet mill process 60

Figure 4.3: Fisher sub-sieve sizer WLP-208 61

Figure 4.4: Fisher sub-sieve sizer principle 61

Figure 4.5: Fundamentals of the technology 65

Figure 4.6: Demonstration of 3 axis values 66

Figure 5.1: Half-normal probability for experimentation 1 for fsss (µm) un-selected effects 74

Figure 5.2: Half-normal probability for experimentation 1 for fsss (µm) selected effects 75

Figure 5.3: Pareto chart for experimentation 1 for fsss (µm) un-selected effects 75

Figure 5.4: Pareto chart for experimentation 1 for fsss (µm) selected effects 76

Figure 5.5: Model graph for the effects of temperature (°C) on fsss (µm) 78

Figure 5.6: Model graph for the effects of hydrogen gas flow rate (Nm^3/h) on fsss (μm) 78

Figure 5.7: Model graph for the effects of belt speed (mm/min) on fsss (μm) 79

Figure 5.8: Half-normal probability for experimentation 1 for oxygen (%) un-selected effects 80

Figure 5.9: Half-normal probability for experimentation 1 for oxygen (%) selected effects 80

Figure 5.10: Pareto chart for experimentation 1 for oxygen (%) un-selected effects 81

Figure 5.11: Pareto chart for experimentation 1 for oxygen (%) selected effects 81

Figure 5.12: Model graph for the effects of temperature (°C) on oxygen (%) 83

Figure 5.13: Model graph for the effects of hydrogen gas flow rate (Nm^3/h) on oxygen (%) 84

Figure 5.14: Model graph for the effects of belt speed (mm/min) on oxygen (%) 84

Figure 5.15: The design trend between fsss and oxygen for experimentation 4 89

Figure 5.16: Normal Plot vs. Residual for fsss 92

Figure 5.17: Normal Plot vs. Residual for oxygen 95

Figure 5.18: 3D surface Model for particle size vs. temperature and belt speed interaction 96

Figure 5.19: 3D surface Model for oxygen size vs. temperature and belt speed interaction 96

Figure 5.20: Overlay plot highlighted in white indicating the area of the optimum results 97

Figure 5.21: The design trend between psd and milling time for experimentation 1 101

Figure 5.22: Normal Plot vs. Residual for psd 104

Figure 5.23: Normal Plot vs. Residual for milling time 107

Figure 5.24: 3D surface Model for particle size distribution vs. AFG weight and classifier speed interaction 107

Figure 5.25: 3D surface Model for milling time vs. classifier speed and grinding gas pressure interaction 108

Figure 5.26: The design trend between psd and milling time for experimentation 3 112

Figure 5.27: Normal Plot vs. Residual for psd 115

Figure 5.28: Normal Plot vs. Residual for milling time 118

Figure 5.29: 3D surface Model for particle size distribution vs. grinding gas pressure and classifier speed interaction 119

Figure 5.30: 3D surface Model for milling time vs. grinding gas pressure and classifier speed interaction 119

Figure 5.31: Overlay plot highlighted in white indicating the area of the optimum results 120

Figure 5.32: SEM of the sub-micron cobalt powder produced from the furnace 121

Figure 5.33: Particle size distribution from the jet mill experimentation 122

Figure 5.34: Compacity of this sub-micron cobalt powder in comparison to conventional powders 122

Figure 5.35: Hardness of this sub-micron cobalt powder in comparison to conventional powders 123

Figure 5.36: Microstructure achieved with this sub-micron cobalt powder 123

Figure 8.1: Half-normal probability for experimentation 2 for fsss (µm) selected effects 130

Figure 8.2: Pareto chart for experimentation 2 for fsss (µm) selected effects 131

Figure 8.3: Model graph for the effects of temperature (°C) and fsss (µm) 132

Figure 8.4: Model graph for the effects of belt speed (mm/min) and fsss (µm) 133

Figure 8.5: Model graph for the effects of temperature (°C) and belt speed (mm/min) on fsss (µm) 133

Figure 8.6: Half-normal probability for experimentation 2 for oxygen (%) selected effects 134

Figure 8.7: Pareto chart for experimentation 2 for oxygen (%) selected effects 135

Figure 8.8: Model graph for the effects of temperature (°C) on oxygen (%) 136

Figure 8.9: Model graph for the effects of hydrogen flow rate (Nm^3/h) on oxygen (%) 137

Figure 8.10: Model graph for the effects of belt speed (mm/min) on oxygen (%) 137

Figure 8.11: Model graph for the effects of temperature (°C) and belt speed (mm/min) on oxygen (%) 138

Figure 8.12: The design trend between fsss and oxygen for experimentation 3 143

Figure 8.13: Normal plot vs. residual for fsss 147

Figure 8.14: 3D surface Model for fsss vs. temperature and hydrogen gas flow rate interaction 147

Figure 8.15: Normal plot vs. residual for oxygen 151

Figure 8.16: 3D surface model for oxygen vs. temperature and hydrogen gas flow rate interaction 151

Figure 8.17: 3D surface model for oxygen vs. temperature and belt speed interaction 152

Figure 8.18: The design trend between psd and milling time for experimentation 2 156

Figure 8.19: Normal plot vs. residual for psd 159

Figure 8.20: Normal plot vs. residual for milling time 162

Figure 8.21: 3D surface Model for psd vs. classifier speed and grinding gas pressure interaction 163

Figure 8.22: 3D surface Model for milling time vs. classifier speed and grinding gas pressure interaction 163

LIST OF TABLES

Table 2.1:	A detailed overview of where cobalt is mined and refined in the world	8
Table 2.2:	Physical properties of cobalt	13
Table 2.3:	Mechanical properties of cobalt	14
Table 2.4:	The chemical composition of cobalt oxalate	16
Table 2.5:	The chemical composition of cobalt (II) hydroxide	19
Table 2.6:	The chemical composition for cobalt carbonate	21
Table 2.7:	The effects of process factors on sub-micron cobalt powder production	23
Table 2.8:	A factorial design matrix	37
Table 3.1:	Visual observations on the quality of sub-micron cobalt powder	51
Table 4.1:	The furnace operation limitation on factors	58
Table 4.2:	The jet mill operation limitation on factors	59
Table 4.3:	Reference table for the jet mill process	60
Table 4.4:	Reference table for the fisher sub-sieve sizer	63
Table 4.5:	Requirements during oxygen analysis	64
Table 4.6:	Furnace experimental parameters for design matrix 1	67
Table 4.7:	A 2^4 factor design matrix	68
Table 4.8:	Jet mill experimental parameters for design matrix 1	69
Table 4.9:	A 2^3 factor design matrix	70
Table 5.1:	Analytical data of factors and response variables for furnace experimentation 1	73
Table 5.2:	Anova of fsss for furnace experimentation 1	77

Table 5.3:	Model applicability and precision for fsss (µm)	77
Table 5.4:	Anova of oxygen for furnace experimentation 1	82
Table 5.5:	Model applicability and precision for oxygen (%)	83
Table 5.6:	Design range for the central composite design to optimize conditions for cobalt powder production	87
Table 5.7:	Design summary for furnace experimentation 4	87
Table 5.8:	Analytical data of factors and response variables for furnace experimentation 4	88
Table 5.9:	Model summary statistics for fsss	90
Table 5.10:	Lack of fit tests for fsss	90
Table 5.11:	Anova of fsss for furnace experimentation 4	91
Table 5.12:	Model applicability and precision for fsss (experimentation 4)	91
Table 5.13:	Model summary statistics for oxygen	93
Table 5.14:	Lack of fit test oxygen	93
Table 5.15:	Anova of oxygen for furnace experimentation 4	94
Table 5.16:	Model applicability and precision for oxygen (experimentation 4)	94
Table 5.17:	The design range for jet mill experimentation 1	99
Table 5.18:	Design summary for jet mill experimentation 1	99
Table 5.19:	Analytical data of factors and response variables for jet mill experimentation 1	100
Table 5.20:	Model summary statistics for particle size distribution	102

Table 5.21:	Lack of fit tests for particle size distribution	102
Table 5.22:	Anova of particle size distribution for experimentation 1	103
Table 5.23:	Model applicability and precision for psd design matrix 1	103
Table 5.24:	Model summary statistics for milling time	105
Table 5.25:	Lack of fit tests for milling time	105
Table 5.26:	Anova of milling time for experimentation 1	106
Table 5.27:	Model applicability and precision for milling time design matrix 1	106
Table 5.28:	Jet mill experimental parameters for design matrix 3	109
Table 5.29:	The design range for jet mill experimentation 3	110
Table 5.30:	Design summary for jet mill experimentation 3	110
Table 5.31:	Analytical data of factors and response variables for jet mill experimentation 3	111
Table 5.32:	Model summary statistics for particle size distribution	113
Table 5.33:	Lack of fit tests for particle size distribution	113
Table 5.34:	Anova of particle size distribution for experimentation 3	114
Table 5.35:	Model applicability and precision for psd design matrix 3	114
Table 5.36:	Model summary statistics for milling time	116
Table 5.37:	Lack of fit tests for milling time	116
Table 5.38:	Anova of milling time for experimentation 3	117
Table 5.39:	Model applicability and precision for milling time design matrix 3	117
Table 8.1:	Furnace experimental parameters for design matrix 2	128

Table 8.2: Analytical data of factors and response variables for furnace experimentation 2 129

Table 8.3: Anova of fsss for furnace experimentation 2 131

Table 8.4: Model applicability and precision for fsss (µm) 132

Table 8.5: Anova of oxygen for furnace experimentation 2 135

Table 8.6: Model applicability and precision for oxygen (%) 136

Table 8.7: Furnace experimental parameters for design matrix 3 140

Table 8.8: The design range for experimentation 3 140

Table 8.9: Design summary for furnace experimentation 3 141

Table 8.10: Analytical data of factors and response variables for furnace experimentation 3 142

Table 8.11: Model summary statistics for fsss – experimentation 3 144

Table 8.12: Lack of fit tests for fsss – experimentation 3 144

Table 8.13: Anova of fsss for furnace experimentation 3 145

Table 8.14: Model applicability and precision for fsss (experimentation 3) 146

Table 8.15: Model summary statistics for oxygen – experimentation 3 148

Table 8.16: Lack of fit tests for oxygen – experimentation 3 148

Table 8.17: Anova of oxygen for furnace experimentation 3 149

Table 8.18: Model applicability and precision for oxygen (experimentation 3) 150

Table 8.19: Jet mill experimental parameters for design matrix 2 154

Table 8.20: The design range for jet mill experimentation 2 154

Table 8.21: Design summary for jet mill experimentation 2 154

Table 8.22: Analytical data of factors and response variables for jet mill experimentation 2 155

Table 8.23: Model summary statistics for particle size distribution 157

Table 8.24: Lack of fit tests for particle size distribution 157

Table 8.25: Anova of particle size distribution for experimentation 2 158

Table 8.26: Model applicability and precision for psd design matrix 2 158

Table 8.27: Model summary statistics for milling time 160

Table 8.28: Lack of fit tests for milling time 160

Table 8.29: Anova of milling time for experimentation 2 161

Table 8.30: Model applicability and precision for milling time design matrix 2 161

Table 8.31: Meaning of terms in Anova 172

Table 9.1: Reference mass required for particle size analysis 176

LIST OF EQUATIONS

Equation 1: $CoCl_2 + C_2O_4H_2 \rightarrow CoC_2O_4 + 2HCL$ 16

Equation 2: $CoCl_2 + C_2O_4(NH_4)_2 \rightarrow CoC_2O_4 + 2(NH_4)Cl$ 16

Equation 3: $Co(CO_2)_2(H_2O)_2 \rightarrow Co + 2CO_2 + 2H_2O$ 18

Equation 4: $Co + CO_2 \rightarrow CoO + CO$ 18

Equation 5: $Co + H_2O \rightarrow CoO + H_2$ 18

Equation 6: $CoO + H_2 \rightarrow Co + H_2O$ 18

Equation 7: $CoCl_2 + 2NaOH \rightarrow Co(OH)_2 + 2H_2O$ 19

Equation 8: $Co(OH)_2 + H_2 \rightarrow Co + 2H_2O$ 19

Equation 9: $CoSO_4 + 2NaHCO_3 \rightarrow CoCO_3 + Na_2SO_4 + H_2O + CO_2$ 20

Equation 10: $CoSO_4 + 2NH_4HCO_3 \rightarrow CoCO_3 + (NH_4)_2SO_4 + H_2O + CO_2$ 20

Equation 11: $CoCl_2 + 2NaHCO_3 \rightarrow CoCO_3 + 2NaCl + H_2O + CO_2$ 20

Equation 12: $CoCl_2 + 2NH_4HCO_3 \rightarrow CoCO_3 + 2NH_4Cl + H_2O + CO_2$ 20

Equation 13: $CoCO_3 + H_2 \rightarrow Co + H_2O + CO_2$ 22

Equation 14: $CoCO_3 \rightarrow CoO + CO_2$ 22

Equation 15: $CoO + H_2 \longrightarrow Co + H_2O$ 22

Equation 16: $d_{VS} = (6 \times 10^4) \times \sqrt{k \times \frac{(1-\varepsilon)^2}{g \times \varepsilon^3} \times \frac{\eta L_U}{\Delta p}}$ 62

LIST OF ABBREVIATIONS

SEM	-	Scanning electron microscope
PSD	-	Particle size distribution
FSSS	-	Particle size
RSM	-	Response surface methodology
D.O.E	-	Design of experiments
Co	-	Cobalt
CoC_2O_4	-	Cobalt oxalate
$CoCl_2$	-	Cobalt chloride
$CoCO_3$	-	Cobalt carbonate
$Co(OH)_2$	-	Cobalt (II) hydroxide
WC	-	Tungsten carbide
OFAT	-	One factor at a time
CCD	-	Central composite design
AFG	-	Alpine fluidized bed opposed jet mill

CHAPTER 1

INTRODUCTION

1.1 Background

Cobalt is an element that mainly exists as a compound. Cobalt powder is a grey, metallic powder produced by the processing of a cobalt compound. Various processes are used to prepare cobalt powders. These processes define the nature of the cobalt powder produced.

The manufacturing facility, Shu Powders Africa based in Durban, South Africa specializes in producing cobalt powders. They produce cobalt powder by the cracking and reductive processing of cobalt carbonate. Shu Powders has successfully processed cobalt carbonate to produce normal cobalt powder using the two-step furnace (Figure 1.1).

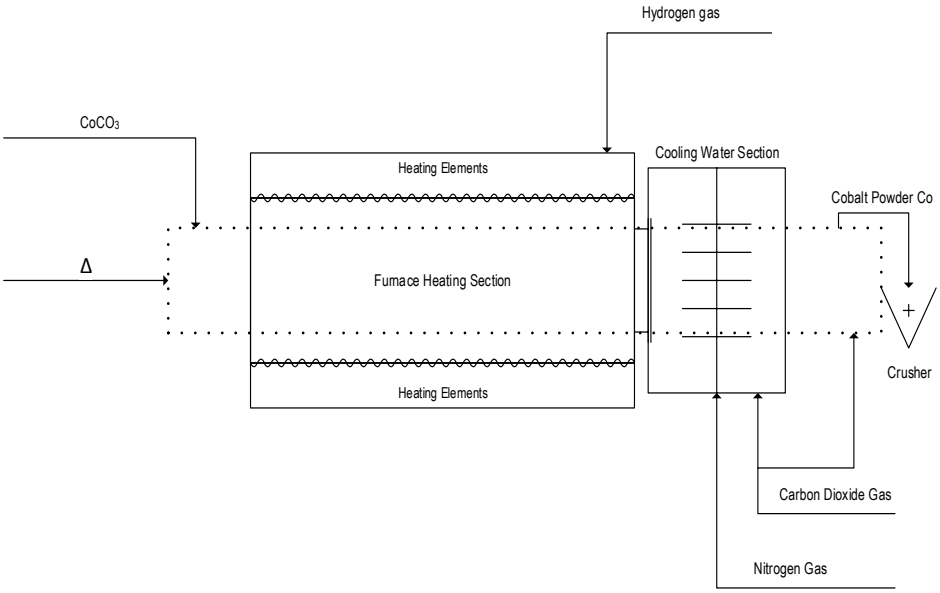

Figure 1.1 Block diagram of the two-step furnace process for the production of sub-micron cobalt powder.

A two-step furnace is essentially a unit that cracks and reduces cobalt carbonate simultaneously. There are no further processing steps for conversion. This two-step furnace was conceptualized by Shu Powders Africa and is soon to be patented. The furnace process has the capability of producing four times the amount of sub-micron powder per day than any other furnace in the cobalt industry. Processing of cobalt carbonate to produce sub-micron cobalt powder on a

continuous conveyor steel belt through a two-step furnace has never been conducted in the cobalt industry hence there were no literature in academic journals that discussed or supported the use of such a technology.

The purpose of the research was to understand the process of producing sub-micron cobalt powder by evaluating other processes used in industry to produce sub-micron cobalt powder, with the main focus being on process optimization. Sub-micron particle size (< 1.0 μm) cobalt metal powders exhibit distinct advantageous properties over larger, micron size (> 1.0 μm) powders. For example, in tungsten carbide applications, sub-micron size cobalt particles greatly improve sinter-ability and mass transport at temperatures significantly below the sintering temperatures required for micron-size cobalt powders (Singh,. 2012:300).

The aim of the research was to optimize and evaluate the process conditions affecting sub-micron cobalt powder production on both the furnace and the jet mill by:

1. Studying the effect of the various parameters on the furnace such as temperature, belt speed, hydrogen flow rate, carbon dioxide flow rate and bed depth of raw material.
2. Studying the effect of the various parameters on the jet mill such as classifier speed, grinding gas pressure, nozzle width and the AFG grinding bin.
3. Understanding the relationship between the operational parameters for both the furnace and the jet mill and their interactions with one another.

The primary function of the furnace in this process was to produce sub-micron cobalt powder that had a particle size (fsss) range of 0.60 - 0.90 μm and an oxygen range of 0.30 - 0.80%. The primary function of the jet mill was to reduce the particle size distribution with the highlight being on the d_{90} value. The d_{10} should be in the range of 2 - 3 μm, d_{50} in the range of 4.5 - 5.5 μm and d_{90} in the range of 7-10 μm (Moodlier., 2011:10).

1.2 Scope

This research investigates processing of sub-micron cobalt powder through a furnace which allows for the two steps of the chemical reaction to take place simultaneously hence the name two-step furnace. The research also evaluates the milling of sub-micron cobalt powder through the jet mill. The study is divided into six main sections:

1.2.1 An overview of cobalt powder and its uses.

1.2.2 An overview of the different precursors and processes used in industry to make sub-micron cobalt powder from a furnace and jet mill perspective.

1.2.3 An assessment of existing furnace and jet mill technology.

1.2.4 An understanding of the test methods for the response variables and the experimental methods applied to the research.

1.2.5 An overview of the results and discussion.

1.2.6 The conclusion and recommendations.

The experimentation was undertaken at plant scale and not on a pilot plant. The concerns were that this type of technology of a two-step furnace was not used in industry. Hence changes to be made to produce sub-micron cobalt powder on such a furnace were not established. Each furnace is unique and therefore process parameters can differ to a large degree. Process conditions can vary dramatically from furnace to furnace. A good understanding of effects on the sub-micron cobalt powder as a result of process conditions needed to be understood. An extensive literature review on journals and patents were undertaken.

Experimentation on the jet mill in relation to sub-micron cobalt powder has not been published. Based on literature and experience on milling normal cobalt powder, important process variables during this process were highlighted for the sub-micron cobalt powder milling. Literature on various jet mills was assessed to determine process parameters responsible for particle size distribution change.

1.3 Sub-micron Cobalt Production - Furnace

There are different precursors used in industry to produce cobalt powder and sub-micron cobalt powder. These precursors are cobalt oxalate, cobalt (II) hydroxide and cobalt carbonate. The proposed way of producing sub-micron cobalt powder for the experimentation was through the processing of cobalt carbonate as the precursor. The reason cobalt carbonate was selected as the precursor was due to the fact that the existing raw material supplier for Shu Powders Africa was only able to supply cobalt carbonate during this experimentation and it was more economical to purchase cobalt carbonate over cobalt oxalate as it was cheaper.

For this research, the cobalt carbonate processed had a fine particle size of < 0.40 micron and low levels of impurities. The advantage of processing cobalt carbonate was the high cobalt content in the cobalt carbonate being 47% and lower levels of impurities. This will be discussed in further detail in Chapter 2.

There were different processes used in industry to produce sub-micron cobalt powder such as solvent precipitation, the recovery process and direct decomposition and reduction. The process applied in this research was the direct decomposition and reduction of the cobalt salt, cobalt carbonate. These steps were carried out simultaneously on a single unit. Usually in industry there are two furnaces used to carry out each reaction (De Schepper,. 2006:5) . For the furnace experimentation, a single furnace was used.

For the furnace experimentation all six variables of the process, temperature - 1, belt speed - 2, carbon dioxide flow rate - 3, hydrogen flow rate - 4, nitrogen flow rate - 5, and bed depth of raw material - 6 were assessed. Variables 5 and 6 were discounted due to its lack of contribution to the response variables; particle size and oxygen content.

Raw material was loaded onto a continuous moving conveyor steel belt. Loading was controlled by a leveling system, which determined the bed depth of the raw material to be processed. The furnace consisted of heating and cooling sections. The heating sections of the furnace were electrically heated. The heating sections were divided into compartments which consisted of heating elements. These heating sections could be set at varying temperatures to one another. The cooling section was similar to that of a heat exchanger consisting of water flowing through a finned jacket and was responsible for the cooling process of the powder. The conveyor belt essentially travelled within the shell of the furnace. The shell of the furnace was ribbed to ensure better heat distribution to the powder on the belt. The heating elements and the cooling water of

the furnace were not in direct contact with powder travelling through the furnace. The furnace could efficiently produce normal micron cobalt powder (> 1.0 micron) (Hareepersad,. 2011:8).

The raw material was decomposed or cracked with heat and reduced using hydrogen gas. This process took place in the heating section of the furnace. The time that this process took was dependent on the residence time which was set by the belt speed of the conveyor belt. The dimensions of the furnace had to be taken into consideration as it also impacted on the processing time and it affected all process variables. Nitrogen and carbon dioxide gases were also used in the process. The nitrogen gas served to create a micro pressure and inert atmosphere in the furnace as well as cooling the product. The nitrogen gas was fed through the furnace at a higher pressure than the hydrogen gas. This prevented normal atmospheric gas from entering the furnace and creating an explosive situation in the presence of hydrogen gas. Carbon dioxide gas was used to surround the cobalt powder particles preventing the powder from oxidising and spontaneously igniting. This process was known as passivation of the cobalt powder particles. Both nitrogen and carbon dioxide gases did not participate in the reaction. All the gases in the existing furnace had a counter-current flow to the powder on the conveyor belt.

Sub-micron cobalt powder has stringent specification requirements whereby the particle size range should be between 0.60 - 0.90 µm, an oxygen range of 0.30 - 0.80%. Although carbon dioxide gas was produced in the process, it was not captured for its use in the process. The concept was investigated but was found to be, unfeasible due to volumes of carbon dioxide required for the passivation of sub-micron cobalt powder and the large capital investment required for installing such a recovery system. (Hareepersad., 2012:9)

1.4 Sub-micron Cobalt Production - Jet mill

The unit operation that was used to control particle size distribution was the AFG fluidized bed milling unit known as the jet mill. The AFG fluidized bed jet mill was used for the sub-micron cobalt powder experimentation. There are various milling units used in industry. This will be elaborated in chapter 2. The jet mill consists of four main components which are the AFG grinding bin, grinding gas valve, cyclone unit and dust filter unit. The AFG grinding bin contains the nozzles and classifier wheel. The grinding gas valve controls the pressure of the nitrogen gas entering the jet mill. The cyclone unit is responsible for the separation of fine powder and dust powder. Dust powder is cobalt powder that has a particle size less than 0.70 µm. The dust filter collects the dust cobalt powder and sends this powder into a dust tote. The unit has pneumatic valves and load cells which are controlled by a PLC (programmable logic controller). It essentially creates an interface in which signals are transferred and received. It controls the mechanism of the jet mill. There are two sets of load cells that are located at the point where powder from the furnace is loaded and the AFG grinding bin. These load cells control the amount of powder milled and are synchronized in their mechanism. It is an enclosed system. There is no chemical reaction that takes place in the jet mill. Sub-micron cobalt powder produced from the furnace was transferred to the jet mill using totes. These totes were given a batch number and carried a constant weight of powder of 250 kilograms (kgs). These batches were then jet milled. The jet mill is under a nitrogen gas atmosphere. The nitrogen gas has an oxygen content less than 0.01% and a dew point of less than - 50°C. The powder is milled and classified in the jet mill by high pressure nitrogen gas. The classification determined the cut of the powder in terms of particle size distribution. Classification and de-agglomeration was controlled by the nozzles, AFG grinding bin, classifier wheel and grinding gas pressure. The particle size distribution of the sub-micron cobalt powder was controlled at the jet mill stage. Hence it was imperative to ensure that the right parameters were set on the jet mill to obtain the desired particle size distribution. The d_{10} should be in the range of 2-3 µm, d_{50} in the range of 4.5-5.5 µm and d_{90} in the range of 7-9 µm (Moodlier,. 2011:10). For the jet mill experimentation, all four variables of the process, classifier speed - 1, nozzle size - 2, AFG grinding bin - 3 and grinding gas pressure - 4 were assessed. Upon investigation on the jet mill process parameters, it was found that the nozzle size was difficult to change as the housing of the nozzles would have to be modified. Due to the complexity of changing the nozzle size, the variable was eliminated from the investigation, hence only three variables were considered.

1.5 Thesis Outline

Chapter 1

The introduction gave an outline on the purpose of the study. It also provided a general understanding of the sub-micron cobalt powder production process and the units used for the experimentation which were the furnace and the jet mill.

Chapter 2

The literature review examined different process technologies to produce cobalt and sub-micron cobalt powder by assessing the precursors and their effect on the end product. The understanding of cobalt powder in terms of chemical and physical properties and its uses were also detailed in this chapter.

Chapter 3

This chapter represented information on the existing technology used to produce sub-micron cobalt powder to attain the required specifications.

Chapter 4

This chapters demonstrated the experimental procedures used in the research to determine optimum process variable conditions and the optimum output response variables.

Chapter 5

This chapter contained the results and discussion obtained from:

- The sub-micron cobalt process experimentation through the furnace.
- The sub-micron particle size distribution change through the jet mill.

Chapter 6

This chapter listed the conclusion and recommendations post the research conducted.

CHAPTER 2

LITERATURE REVIEW

2.1 History of Cobalt

Cobalt was discovered in 1735 and is the 27th element on the periodic table. It is only found in a chemically combined form meaning, it is usually found in a compound and not as a singular element. The German word for cobalt is kobalt which means evil spirit in English. The reason for the name was that, it was poisonous and degraded other mined elements (Enghag,. 2008:670). Cobalt has been reported to be found around the world in small concentrations in the earth's crust (Table 2.1).

Table 2.1 A detailed overview of cobalt mining and refining locations in the world according to the (CDI, 2013:55)

Country	Mined	Refined	Approx. Refined Qty
Australia	√	√	4,800
Belgium		√	4,200
Botswana	√		
Brazil	√	√	1,750
Canada	√	√	5,600
China	√	√	30,000
Cuba	√		See Canada
Finland		√	10,500
France		√	320
India			600
Japan		√	2,500
Morocco	√	√	1,300
New Caledonia	√		
Norway		√	3,000
Russia	√	√	2,100
South Africa	√	√	1,100
D.R. of Congo	√	√	3,250
Uganda		√	550
Zambia	√	√	5,400
			≈ 77,000 (tonnes)

Cobalt has been found to be extracted from a variety of ores such as iron. Cobalt is also known to have occurred in cobalt bearing minerals such as erythrite, skutterudite etc., (Figure 2.2). Cobalt is a hard metal with excellent resistance to oxidation, demonstrates high-tensile strength, and usually has a very fine particle size in the powder form. Cobalt has been widely used in the manufacture of precision cutting tools and has become an important metal strategically. It has also been used in the commercial, industrial, and military applications (Figure 2.1). The use of cobalt has also extended into the rechargeable battery industry. The uses of pure cobalt is limited, however it is extensively used as an alloy metal. Cobalt is valued for its ability to produce super alloys. These super alloys have good magnetic properties and resistance to high temperature.

2.1.1 Refined Cobalt

Refined cobalt powder has a cobalt content of 98 - 99% cobalt. It usually contains nickel, iron and copper as impurities.

2.1.2 Cobalt Matte, alloys and chemicals

Cobalt matte is an intermediate product of smelting usually used for the refining of cobalt. The composition of cobalt matte is known to contain cobalt, nickel, copper and iron sulphides. The cobalt matte usually exists as black granules or a consolidated mass. The cobalt content in the matte is 1.5 - 2.0%. Cobalt alloys are a mixture of metals whereby cobalt is the dominant metal by weight. There are various types of cobalt alloys as per point 2.1.5. There are various cobalt chemicals such as oxides, hydroxides, carbonates and sulphates.

2.1.3 Super Alloys

Super alloys are produced when cobalt is mixed with other metals. They are termed super alloys as they have the ability to withstand severe mechanical stresses and temperatures. An example of a cobalt super alloy is a nickel-cobalt based alloy. Usually when cobalt is mixed with a nickel alloy, the molecular structure of the alloy changes. The cobalt nickel alloy combination has an enhanced resistance to high temperature and chemical corrosion. Super alloys are used in jet mill engines and turbines, which require high temperature resistance. Some super alloys are

used in chemical applications where resistance to corrosion is critical (Hannis and Bide. 2009:9).

2.1.4 Magnetic Alloys

A cobalt based magnetic alloy has been produced when cobalt is mixed with several other metals. These magnetic alloys have been used in high performance electrical equipment. Cobalt has been shown to improve the magnetic properties of iron. Cobalt has been demonstrated to have the highest known curie point of 1121°C. The Curie point is the temperature at which magnetic fields become lost. A versatile magnetic alloy has been found to be an aluminum-nickel-cobalt alloy. These alloys have high mechanical strengths and operating temperatures (Hannis and Bide. 2009:9).

2.1.5 Other cobalt based alloys

There are a variety of cobalt alloys used in industry. These are high speed steels, hard facing materials, prosthetic limbs, low expansion alloys, and mar-aging steel.

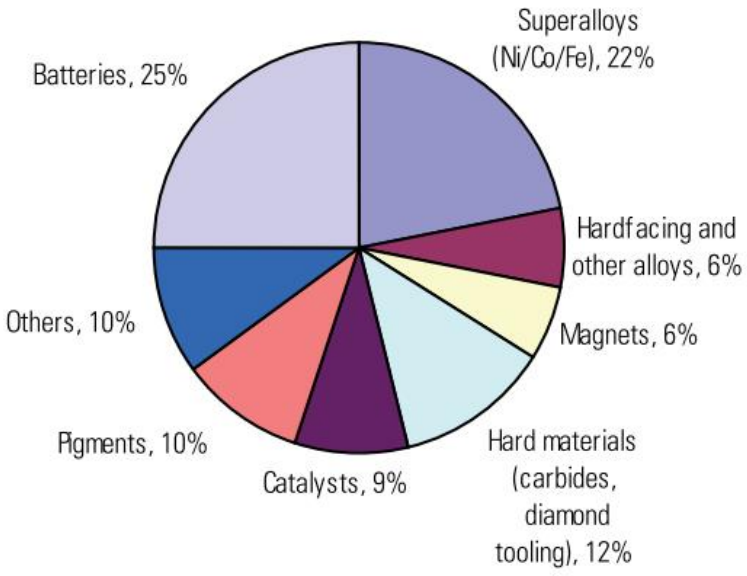

Figure 2.1 The global end use of cobalt powder (Hannis and Bide. 2009:8).

Cobalt metal has a silvery appearance with a bluish tinge. It is known to be considerably harder than iron.

Figure 2.2 A cobalt-nickel arsenide (Hannis and Bide. 2009:1).

The stages of production of cobalt (Figure 2.3) are quiet straightforward. Cobalt ore is extracted from the ground, concentrated, and refined to the metallic form. Metallic cobalt in various forms may be used directly as an alloying constituent of high speed and other steel magnet alloys, super-alloys, hard facing rods, concentrated carbides or may be used to produce cobalt oxides and salts.

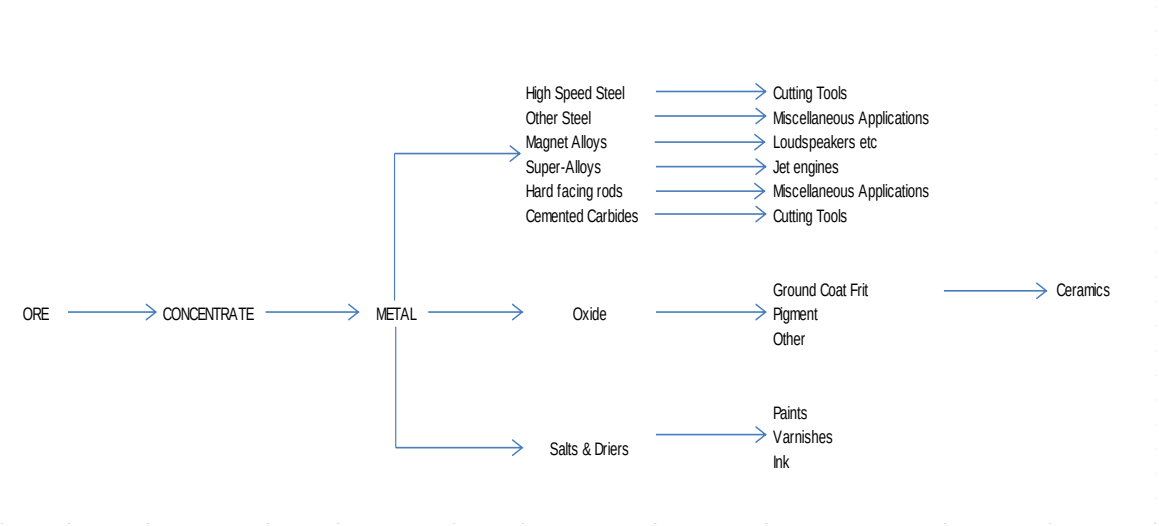

Figure 2.3 Uses of cobalt powder (Burrows and River Associates, 1971:5).

The Democratic Republic of Congo accounts for 60 percent of the world cobalt production. Cobalt occurs in copper and nickel minerals (Figure 2.4).

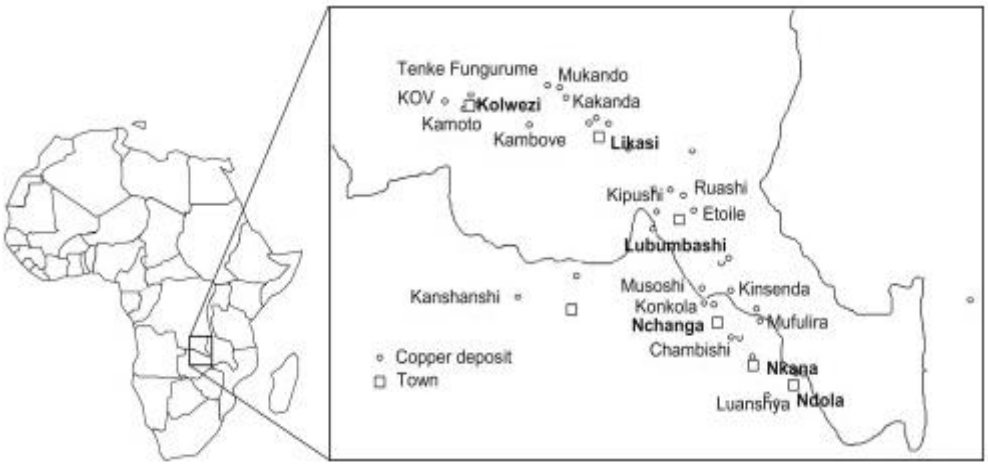

Figure 2.4 The location of the main deposits of the central African Copper belt (Crundwell *et al.*, 2011:377).

The main source of cobalt has been shown to be from copper and nickel mining in the Congo (Figure 2.5) where it is produced as a by-product (Enghag,. 2008:675).

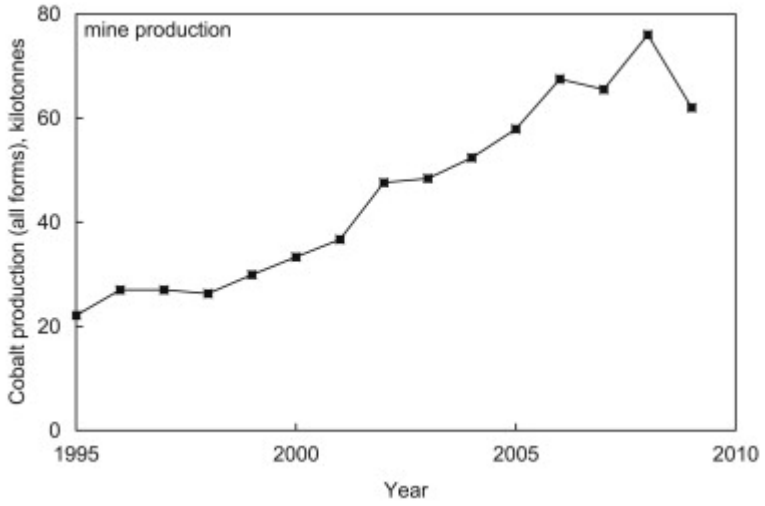

Figure 2.5 World production of primary cobalt (Crundwell *et al*., 2011:379).

2.2 Cobalt Properties

2.2.1 Physical Properties

Cobalt does not occur as a pure metal. It has been found as a component of more than one hundred minerals. Cobalt is brittle and resembles iron and nickel in appearance. The physical properties of cobalt define why it has become such a sort after metal (Table 2.2).

Table 2.2 Physical Properties of Cobalt (Chong, 2012:150)

Physical Properties	Values
Symbol	Co
Colour	Silver-grey
Atomic number	27
Atomic weight	58.933195
Element category	Transition metal
Electron configuration	$4s^3d^7$
Density	8.9 g/cm^{-3}
Liquid density at melting point temperature	7.75 g/cm^{-3}
Melting point	1768 K, 1495 °C, 2723 °F
Boiling point	3200 K, 2927 °C, 5301 °F
Heat of fusion	16.06 kJ/mol
Heat of vaporization	377 kJ/mol
Molar heat capacity	24.81 J/(mol•K)

2.2.2 Mechanical Properties

Table 2.3 Mechanical Properties of Cobalt (Chong, 2012:151)

Mechanical Properties	Crystal Structures	
	hcp	fcc
Electrical resistivity (Ω.m)	6.24×10^{-8} at 20 °C	-
Thermal expansion (/K)	13.36×10^{-6} at 25 °C	-
Thermal conductivity (W/m.K)	100	-
Young's modulus (GPa)	209	<hcp - Co
Shear modulus (GPa)	75	<hcp - Co
Bulk modulus (GPa)	180	<hcp - Co
Poisson ratio	0.31	-
Vickers hardness (MPa)	1043	<hcp - Co

Metallic cobalt occurs in two crystallographic states which are HCP (hexagonal closed packing) and FCC (face centered cubic). Cobalt in the HCP state demonstrates higher strength and hardness compared to cobalt in a FCC state (Chong, 2012:151) (Table 2.3).

2.2.3 Chemical Properties

Pure cobalt powder does not dissolve in water and soil. Cobalt extra fine powder is generally produced in a hydrogen reductive atmosphere. This powder has been found to easily oxidize and therefore has to be preserved in a vacuum or in an inert gas container. Since cobalt is such a weak reducing metal it is easily attacked by halogens and sulfur (Chong, 2012:151).

2.3 Cobalt Processes

Cobalt metal is usually refined to form a cobalt compound. The cobalt metal has to undergo a pre-treatment either a pyro-metallurgical process or a hydro-metallurgical process. These processes purify the cobalt metal and precipitates the cobalt as CoC_2O_4 or $CoCO_3$ or $Co(OH)_2$. These compounds are known as cobalt salts. These cobalt salts are used as the precursors for the production of cobalt powders. The type of cobalt salt will determine the nature of the cobalt powder produced in terms of particle size, morphology, and mechanical properties. Hence when choosing the precursor, the cobalt salt, one needs to understand the process used to produce the precursor. The process of producing the precursor will have many contributing factors that can impact the final product being the cobalt powder.

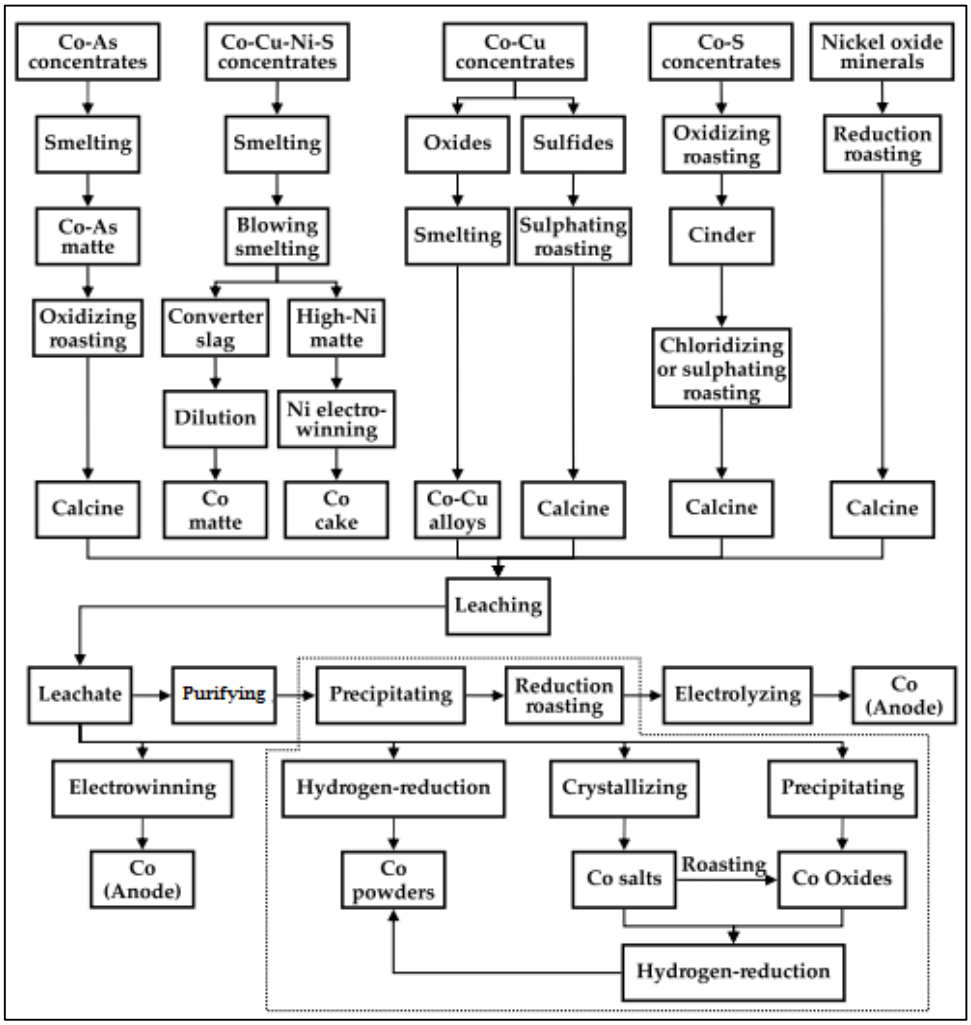

Figure 2.6 Overview of different cobalt ore and salt production processes (Chong, 2012:153).

There are various steps and stages that the cobalt ore undergoes (Figure 2.6). Cobalt ore is processed to produce different cobalt minerals also known as cobalt salts. Each salt will have different cobalt contents and different concentrations of impurities.

2.3.1 Production of Cobalt powder from Cobalt Oxalate - CoC_2O_4

Cobalt oxalate is commonly used for the production of cobalt powder and sub-micron cobalt powder. The production of CoC_2O_4 is mainly realized by the precipitation of a $CoCl_2$ solution. By adding oxalic acid $C_2O_4H_2$ or a salt of mainly ammonium oxalate $C_2O_4(NH_4)_2$, one produces CoC_2O_4 (Eq. 1 and 2).

$$CoCl_2 + C_2O_4H_2 \rightarrow CoC_2O_4 + 2HCL \qquad \textbf{Eq. 1}$$

$$CoCl_2 + C_2O_4(NH_4)_2 \rightarrow CoC_2O_4 + 2(NH_4)Cl \qquad \textbf{Eq. 2}$$

The precipitated cobalt oxalate is separated by filtering the liquid. The material is washed several times to remove traces of impurities that may exist in the material. This material is then dried to produce a cobalt oxalate that meets customer specification (Table 2.4).

Table 2.4 The chemical composition of cobalt oxalate (Moodlier, 2010:5)

CoC_2O_4			**PPM**			
Co	**Al**	**Ni**	**Fe**	**Cl^-**	**K**	**Na**
32 %	20	15	20	300	20	20
P	**As**	**S**	**Si**	**Mg**	**Mn**	**Cu**
10	5	15	20	10	10	10
Cd	**Ag**	**NH_4**	**Zn**	**Mo**	**Ca**	**Cr**
10	30	0.30 %	10	20	20	10
d10	**d50**	**d90**	**Ap**	**Fsss**	**H_2O**	**Colour**
1-3 µm	5-7 µm	12-15 µm	0.3-0.4 g/cc	0.80-1.60 µm	3 %	Pink

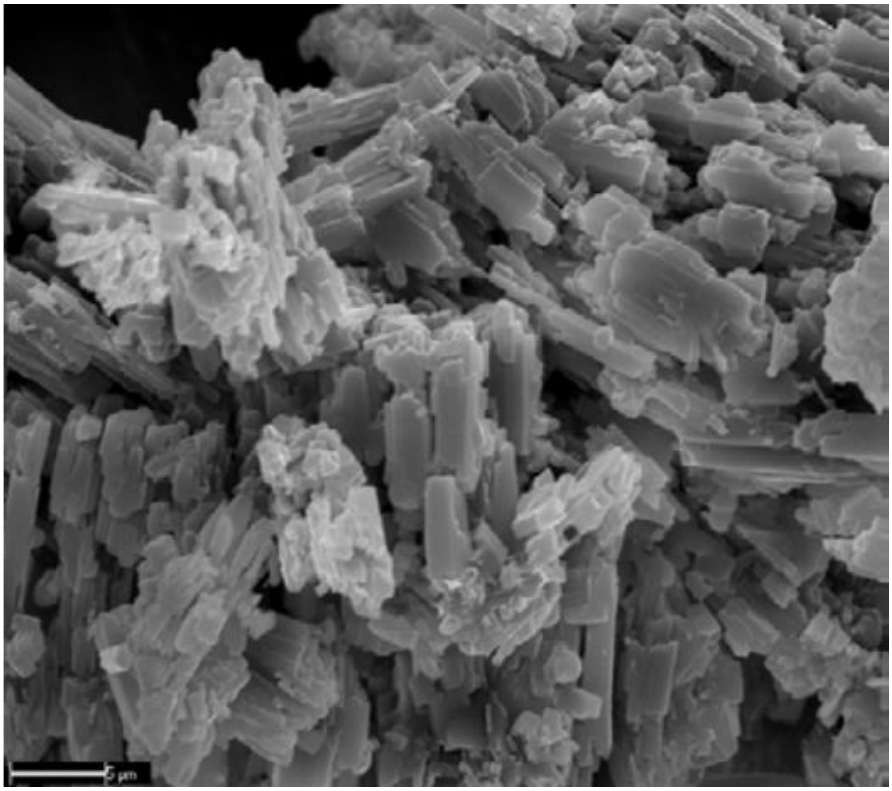

Figure 2.7 Scanning electron micrograph of Cobalt Oxalate (Bhasker *et al*., 2012:25).

Cobalt oxalate under scanning electronic microscope depicts an elongated morphology (Figure 2.7). The chemical impurities originate in the raw materials used. Hence it was crucial to ensure that the raw materials being used are of constant quality. It is of absolute importance that the final product of CoC_2O_4 is well washed in order to get rid of ammonium ($NH4^+$) and particularly chlorine (Cl^-), sodium (Na) and potassium (K) in order to avoid burning effects of the final cobalt powder. The washing process takes place at the raw material manufacturing plant. If this process is not adhered to, the raw material will contain a high content of impurities.

Carbon content is also crucial in the final product. The final carbon content is dependent on processing conditions during cobalt oxalate conversion to sub-micron cobalt powder. At higher temperatures carbon content of the powder reduces due to the decomposition process that takes place on the raw material in the furnace. As lower temperatures are applied in sub-micron cobalt powder production, the amount of carbon driven off through the process is much lower; therefore the carbon content is higher in the end product. The cobalt content is usually 65-70% higher than in the final product of normal cobalt powder production.

Particle size is dependent on both temperature and residence time of the type of furnace being used. Even if temperatures are low, if the residence time is great, the particle size of the powder will increase. Therefore it is crucial to understand the relationship between these two operating variables. The disadvantage of processing cobalt oxalate as the precursor for both normal cobalt powder and sub-micron cobalt powder are:

a. The high operating costs

b. The cobalt hardness reduces at higher temperatures.

Cobalt oxalate is decomposed in a reducing atmosphere (Eq. 3).

$$Co(CO_2)_2(H_2O)_2 \rightarrow Co + 2CO_2 + 2H_2O \qquad \textbf{Eq. 3}$$

The intermediate steps to the above reaction are:

$$Co + CO_2 \rightarrow CoO + CO \qquad \textbf{Eq. 4}$$

$$Co + H_2O \rightarrow CoO + H_2 \qquad \textbf{Eq. 5}$$

$$CoO + H_2 \rightarrow Co + H_2O \qquad \textbf{Eq. 6}$$

The cobalt oxalate is decomposed at high temperatures. The process is known to be endothermic. The required energy input is of the order of magnitude as that to evaporate the required amounts of H_2O and CO_2. The intermediate steps in the production of cobalt oxalate are highlighted in three stages (Eq. 4, 5 and 6). For each 10 kg of Cobalt powder produced one forms 7.1 m^3 CO_2 and 5.7 liters of steam. The higher the temperature of the furnace, the faster the energy will penetrate the powder. Higher temperature allows for a larger volume of powder to be decomposed at a time. However, if the temperature is too high, the powder already decomposed, will start to sinter and the powder will get coarse. The temperature required to decompose the cobalt oxalate will depend on the type of furnace being used. It is also directly related to the retention time in the furnace. Usually the temperature is situated between 500°C and 560°C in order to obtain a cobalt powder with a particle size between 1.20 µm and 1.80 µm.

To produce a sub-micron cobalt powder, the cobalt oxalate has to be cracked and reduced at a temperature of 490°C. The retention time for the decomposition of cobalt oxalate is critical when producing sub-micron cobalt powder.

2.3.2 Production of Cobalt powder from Cobalt Hydroxide - $Co(OH)_2$

Cobalt (II) hydroxide is often used as a precursor for cobalt powder production and sub-micron cobalt powder production. The production of $Co(OH)_2$ is usually produced by the precipitation of an alkaline hydroxide when reacted with a cobalt chloride (Eq.7).

$$CoCl_2 + 2NaOH \rightarrow Co(OH)_2 + 2H_2O \qquad \textbf{Eq. 7}$$

The problems experienced with cobalt hydroxide is that this material sometimes has a high content of sodium (Na) which makes the end product unstable resulting in spontaneous ignition of the cobalt powder produced. Hence it is imperative to ensure that the cobalt carbonate has low impurities (Table 2.5).

Table 2.5 The chemical composition of cobalt (II) hydroxide (Moodlier, 2010:7)

$Co(OH)_2$			**PPM**			
Co 54 %	**Al** 20	**Ni** 20	**Fe** 20	**Cl^-** 300	**K** 20	**Na** 50
P 10	**As** 5	**S** 30	**Si** 20	**Mg** 20	**Mn** 20	**Cu** 10
Cd 10	**Ag** 30	**NH_4** 0.30 %	**Zn** 10	**Mo** 20	**Ca** 20	**Cr** 10
d10 1-3 µm	**d50** 5-7 µm	**d90** 12-16 µm	**Ap** 0.3-0.4 g/cc	**Fsss** 0.80-1.60 µm	**H_2O** 5 %	**Colour** Red

$$Co(OH)_2 + H_2 \rightarrow Co + 2H_2O \qquad \textbf{Eq. 8}$$

The cobalt content in cobalt hydroxide is 54%. The reaction of cobalt (II) hydroxide takes place at temperatures of 620°C. Hydrogen gas (Eq. 8) reduces the cobalt hydroxide at temperatures between 300 - 500°C to produce sub-micron cobalt powder. It requires a larger consumption of hydrogen gas and higher energy input than cobalt oxalate. The main difference is the higher thermal stability of the cobalt powder, produced from cobalt hydrate. This means that the hardness of sintered cobalt powder remains constant at even higher temperatures (900°C), while the hardness of cobalt powder, produced from cobalt oxalate decreases at higher temperatures. It is not quite clear what might be the reason for this phenomenon.

2.3.3 Production of Cobalt powder from Cobalt Carbonate - $CoCO_3$

Cobalt carbonate is commonly used as a precursor to produce sub-micron cobalt powder. It can be produced by two processes. This can be achieved by the precipitation of a cobalt chloride or cobalt sulphate by the use of either sodium bicarbonate or ammonium bicarbonate (Eq. 9, 10, 11, 12).

$$CoSO_4 + 2NaHCO_3 \rightarrow CoCO_3 + Na_2SO_4 + H_2O + CO_2 \quad \textbf{Eq. 9}$$

$$CoSO_4 + 2NH_4HCO_3 \rightarrow CoCO_3 + (NH_4)_2SO_4 + H_2O + CO_2 \quad \textbf{Eq. 10}$$

$$CoCl_2 + 2NaHCO_3 \rightarrow CoCO_3 + 2NaCl + H_2O + CO_2 \quad \textbf{Eq. 11}$$

$$CoCl_2 + 2NH_4HCO_3 \rightarrow CoCO_3 + 2NH_4Cl + H_2O + CO_2 \quad \textbf{Eq. 12}$$

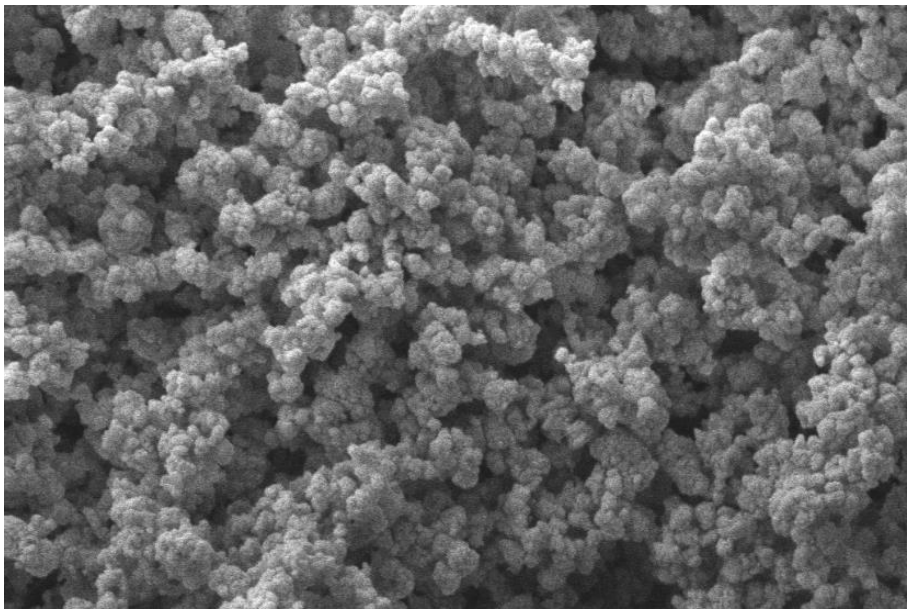

Figure 2.8 Scanning electron micrograph of Cobalt Carbonate (Moodlier, 2012:3).

Table 2.6 The chemical composition for cobalt carbonate (Moodlier, 2010:9)

$CoCo_3$			PPM			
Co 47 %	**Al** 20	**Ni** 15	**Fe** 20	**Cl^-** 250	**K** 20	**Na** 20
P 10	**Sn** 20	**S** 15	**Si** 20	**Mg** 10	**Mn** 10	**Cu** 10
Cd 10	**Ag** 30	**NH_4** 0.30 %	**Zn** 10	**Mo** 20	**Ca** 20	**Cr** 10
d10 0.1-0.3 µm	**d50** 0.8-1.2 µm	**d90** 2-4 µm	**Ap** 0.3-0.5 g/cc	**Fsss** 0.30-0.50 µm	**H_2O** 2 %	**Colour** Pink

The scanning electronic microscope image of cobalt carbonate (Figure 2.8) illustrated the spherical morphology of this type of powder. In the production stages of cobalt carbonate, it was important to take into consideration the application of the final product produced. It was imperative that the chemical and physical aspects were assessed (Table 2.6). Usually the cobalt ore is reacted with an acid which could be HCL or H_2SO_4 to produce a cobalt salt. The cobalt salt is reacted with a bicarbonate compound which could be either NH_4HCO_3 or $NaHCO_3$. The acid and bicarbonate compound have been found to have varying effects on the end product (De Schepper, 2008:5).

When the cobalt ore was precipitated by H_2SO_4 the final product contained a high content of sulphur. Although sulphur disappears during the decomposition of cobalt carbonate, the complete removal was not guaranteed. High levels of sulphur in sub-micron cobalt powder have resulted in pitting in the end product (De Schepper, 2008:7).

When the cobalt salt was precipitated by the use of $NaHCO_3$, the final product contained a high content of sodium. During the decomposition of $CoCO_3$ and the reduction with H_2, sodium did not disappear and remained in the finished product. In the final cobalt powder, the sodium content must be below 50 ppm. Sodium caused problems during the production of sub-micron cobalt powder resulting in spontaneous ignition of the powder. Therefore for the production of sub-micron cobalt powder an ammonium bicarbonate was preferred over a sodium bicarbonate and similarly HCL was preferred over H_2SO_4. The cobalt content in the finished product must be very close to 46.5% (De Schepper, 2008:7).

For the experimentation, the cobalt carbonate used was produced from an ammonium bicarbonate compound and hydrochloric acid.

Initially the cobalt carbonate would be decomposed by increasing the temperature. In order to reduce the cobalt carbonate to cobalt powder, identical conditions for the treatment of $Co(OH)_2$ would be applied which are high gas flow rates of hydrogen gas (Eq. 13).

The overall reaction is:

$$CoCO_3 + H_2 \rightarrow Co + H_2O + CO_2 \qquad \textbf{Eq. 13}$$

Intermediate steps are illustrated by (Eq. 14 and 15):

$$CoCO_3 \rightarrow CoO + CO_2 \qquad \textbf{Eq. 14}$$

$$CoO + H_2 \rightarrow Co + H_2O \qquad \textbf{Eq. 15}$$

Cobalt powder produced from cobalt carbonate has a higher thermal stability than cobalt oxalate. Hydrogen consumption is high but energy requirements are lower. At temperatures of 400-500°C, good quality sub-micron cobalt will be produced.

From the above mentioned precursors, it was found from research that cobalt carbonate was the most cost effective to produce and the energy requirements to process the cobalt salt into a sub-micron cobalt powder was lower. Cobalt carbonate was used in the research as the existing raw material supplier could only supply this feed to Shu Powders.

According to (Table 2.7) shows experimental data obtained for the production of sub-micron cobalt powder by the cracking and reduction of cobalt carbonate conducted in industry. Factors such as residence time, hydrogen flow rate and temperature were considered important for this process. For the experimentation below only particle size was considered. SCFH stands for standard cubic feet per hour.

Table 2.7 Effects of process factors on sub-micron cobalt powder production. (Singh, 2012:301)

Run	Time (Hr)	Temperature (°C)	H_2 Flow rate (cu.ft/hr)	Fsss (µm)
1	1	375	10	0.55
2	0.5	325	15	0.35
3	1	375	10	0.64
4	1.5	325	15	0.40
5	0.5	425	15	0.76
6	1.5	425	15	0.94
7	1.5	325	5	0.42
8	1.5	425	5	0.75
9	0.5	425	5	1.05
10	0.5	325	5	0.33
11	1	375	10	0.68

The experimentation was conducted using design of experiments. Process factors taken into consideration were residence time, temperature and hydrogen flow rate. There was only one response variable investigated which was particle size. The above experimental data did not take oxygen content of the final product into consideration. The particle size and oxygen content of sub-micron cobalt powder share an inverse relationship. Therefore lower temperatures would give lower particle sizes but higher oxygen readings. The information was not comprehensive as the requirements of sub-micron cobalt powder is not only particle size but oxygen content as well. Both response variables particle size and oxygen content have to be evaluated during the experimentation. Process parameters in the research conducted at Shu Powders concluded that

hydrogen gas had a minimal effect on particle size. However runs 5 and 9 in (Table 2.7), indicated that a change in hydrogen flow rate had decreased the particle size by 30% which was quite significant. Hence this made the validations made in the above experimentation questionable (Hareepersad et al., 2013:1005).

2.3.4 Other Processes

There are other processes used in industry to produce sub-micron cobalt powder. It is known, as described in U.S. Pat. Nos. 2,734,821, 2,744,003 and 2,805,149 to produce cobalt powders by direct reduction from aqueous solutions and slurries at elevated temperatures and pressures. This was termed to be a hydrometallurgical process (Figure 2.9). The hydrometallurgical powders contain more carbon and oxygen from organic additives than thermal decomposition / reduction powders. These organics form a protective layer on the individual cobalt grains and prevent cobalt from oxidizing (Oehlers *et al*., 2000:3). The cobalt powder produced in these processes show high product stability in spite of their large surface area.

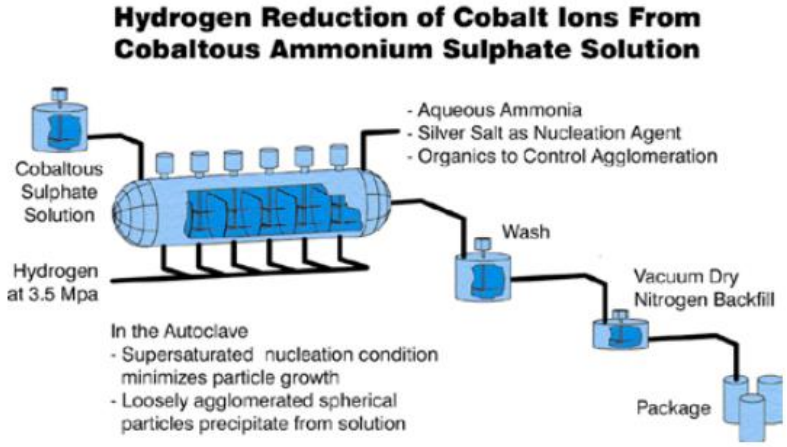

Figure 2.9 An example of a hydrometallurgical process (Oehlers *et al*., 2000:3).

While these and other similar direct reduction processes permit practical and economic production of a variety of cobalt powders, difficulties are encountered in adapting these processes for the production of ultra-fine cobalt powders having a particle size of 1 micron and less. Also, contamination of the product by impurities, particularly carbon and oxygen, is a problem with these prior processes. The other disadvantage of dissolution processes are the formation of undesirable gases such as hydrogen, chlorine and nitrous oxide. Generally there are

no purification steps in the dissolution processes; hence the starting source must be relatively pure.

Another process to produce sub-micron cobalt powder is through a recovery process. Sub-micron cobalt powder is recovered from cemented carbide scrap powder. Cemented carbide scrap (hard metal WC-Co) is treated by nitric acidic leaching. This is followed by the precipitation of cobalt hydroxide. A sub-micron size pure cobalt metal powder is then produced by the thermal breakdown and the reduction of cobalt hydroxide in a horizontal tube furnace using hydrogen gas (Gurmen et al., 2005:10).

Other direct reduction processes, such as those described in U.S. Pat. Nos. 3,494,760 and 3,669,643, for example, have been proposed for making very fine cobalt powders adapted particularly for magnetic applications. However, these processes lack the flexibility required to produce fine cobalt powders for other applications. In addition, these processes are technically difficult and expensive to carry out on a commercial scale with the result that the products are generally too expensive for wide scale industrial use (Zhang et al., 2000:555).

2.3.5 Uses of Sub-micron cobalt powder

The main application of sub-micron cobalt powder is in the hard metal and the diamond tool industry. The two industries place different demands on the quality of the sub-micron cobalt powder. In both applications cobalt and sometimes other metals is blended with hard particles like diamonds or tungsten carbide (WC). The cobalt is used as a binding agent to hold substrates firmly in place (Honhe et al., 2002:3).

In the hard metals industry, the crucial factor bearing on the sub-micron cobalt powder is the impurities such as sodium, sulphur and calcium. Particle size becomes the secondary factor. In the hard metals production, mixtures of mainly tungsten carbide and 6-15% of cobalt powder are sintered at temperatures between 1350-1450°C. Cobalt has the remarkable effect that the material maintains a good mechanical strength even at high temperatures. At these temperatures, the sintering is known as liquid phase sintering, during which the tungsten carbide dissolves in the cobalt powder. On cooling, the re-crystallization process takes place. During this time, impurities such as sodium, sulphur etc. contained in the starting materials deposit itself on the grain boundaries of the tungsten carbide crystals. This results in a reduction of the bending strength, which in the case of tools; result in the tools readily breaking at the positions of decreased strength. Oxygen and carbon contents are very important and need to be monitored.

Elevated levels of oxygen and carbon contents will influence the carbon balance during the sintering process. This results in porosity and weakness of the end product (Honhe et al., 2002:3).

In the diamond tools industry, cobalt mixed with diamonds (Figure 2.10) is considered as a very good substance to manufacture saws to cut marble stone or granite. Cobalt with tungsten carbide is considered as a very good substance to manufacture drills to penetrate concrete etc. Cobalt powder is predominantly present with other metals such as nickel, copper, iron and tin etc. Impurities give rise to micro-porosity and have the similar effect as above for hard metals. Finer particle size of cobalt powder increases the hardness of the cobalt segments. Increased hardness results in a longer life for the tools and hence it is very important. It is therefore crucial that one produces a fine sub-micron cobalt powder which has a good particle size, particle size distribution and low impurity levels. This enables the use of the powder in various applications. The finer cobalt powders usually enable better porosity in sub-micron carbides as compared to standard extra fine cobalt grades (Oehlers *et al*., 2000:1). However, very little has been published on the impact of sub-micron grain cobalt powders on hard metal processing and properties (Oehlers *et al*., 2000:1). It has been often questioned why cobalt is not simply melted and either diamonds or tungsten carbide are added in the melting process. It must be noted that the melting temperature of Co metal is 1500°C. At these temperatures diamonds and tungsten carbide will start to burn. Therefore fine cobalt powder is desired as it can be sintered at lower temperatures (De Schepper., 2009:7).

In order to obtain a large piece of metal which is desired at a lower temperature, one has to sinter the cobalt and therefore one needs fine cobalt powder. In a sintering process, the borders and the edges of powder particles start to melt. The cobalt particles grow together in such a way that it finally produces a massive block, with some pores. With fine cobalt powder one gets much more borders and edges, which allow sintering at <1500°C. The next advantage of sintered powder is that the end product has precise end forms and post treatment is seriously reduced. Tungsten carbide particles are very fine (< 1.0 μm) and therefore one needs very fine cobalt powder for binding (De Schepper., 2009:8).

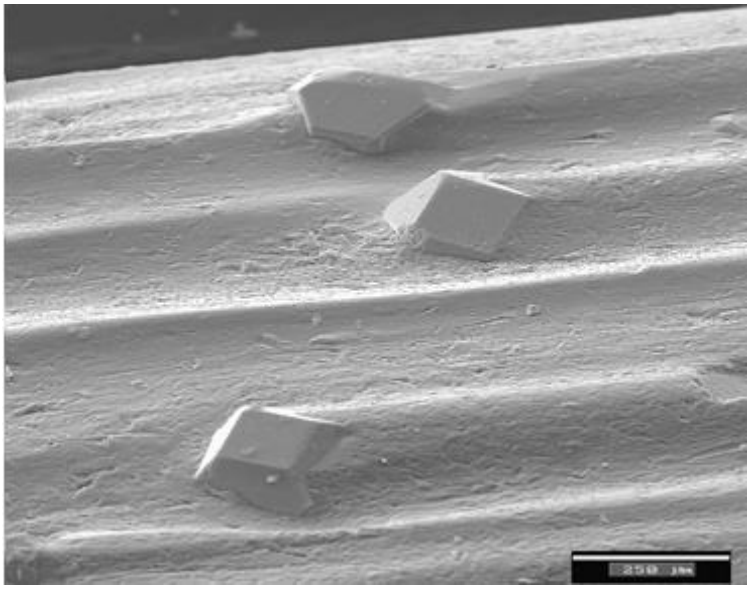

Figure 2.10 Diamonds in a cobalt metal for a diamond saw (De Schepper., 2009:10).

2.4 Milling Processes for Cobalt Powder

There are various milling processes that are used in industry such as an air classifying mill, hammer mill, pin mill, spiral jet mill, and a fluidized bed jet mill. Each mill de-agglomerates the product and some classify the product. Each mill was evaluated to assess the process parameters that were imperative to change in order to de-agglomerate powder and classify it. Furthermore it was assessed on the basis of its use in changing particle size distribution for sub-micron cobalt powder application. It was important to take note of what hardness of material each mill process could effectively de-agglomerate and classify. Cobalt powder has a Mohs hardness of 5 (Samsonov., 1968:390).

2.4.1 Air Classifier Mills

The air classifying mill (Figure 2.11) is similar to a hammer mill however it contains an internal classifier wheel. It also contains grinding media which assists in de-agglomerating the powder. The classify wheel determines the cut of the powder. Important parameters that are controlled on the air classifier mill are the air flow rate and the classifier speed. The air flow rate is used to control the rate of grinding and the rate at which powder is passed through to the classifier. Higher flow rates result in coarser powder and vice versa. High classifier speeds result in lower particle size distribution. As the name suggests this mill uses air as the medium required to mill and de-agglomerate the product. However this would be detrimental to cobalt powder as air would oxidize the product. Furthermore the mill can only classify powder to 400 mesh which is a d_{90} of 37 microns. This was not suitable for sub-micron cobalt powder particle size distribution requirements.

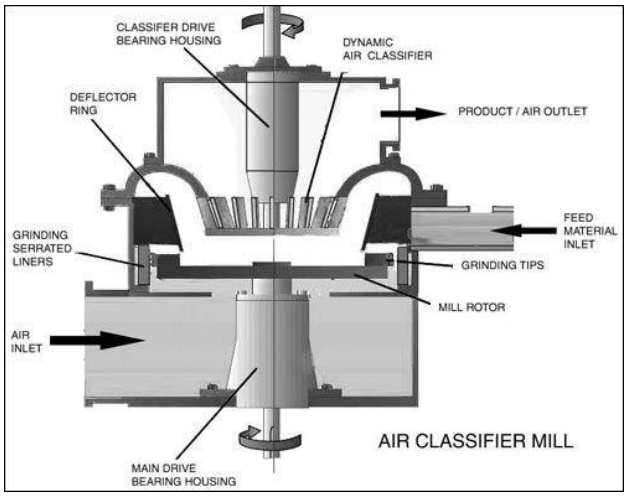

Figure 2.11 Air classifier mill (De Schepper., 2007:20).

2.4.2 Hammer Mills

Hammer mills do not contain an internal classifier wheel hence there primary function is grinding of the powder and not classification. With hammer mills, grinding is controlled by milling the powder against rigid surfaces such as the hammer mill housing, the hammer arms and passing through the powder through a screen (known also as a grate) (Figure 2.12). Process variables that are used to control the grinding process are the screen aperture size, screen shape and speed of the hammer. The output particle size distribution varies from 90 microns to 850 microns which is extremely coarse for the desired quality specification of sub-micron cobalt powder. Another disadvantage was the high energy consumption and the resultant heat generation. Heat generation is not good for sub-micron cobalt powder as temperatures higher than ambient temperature (>25°C) will result in the cobalt powder oxidizing.

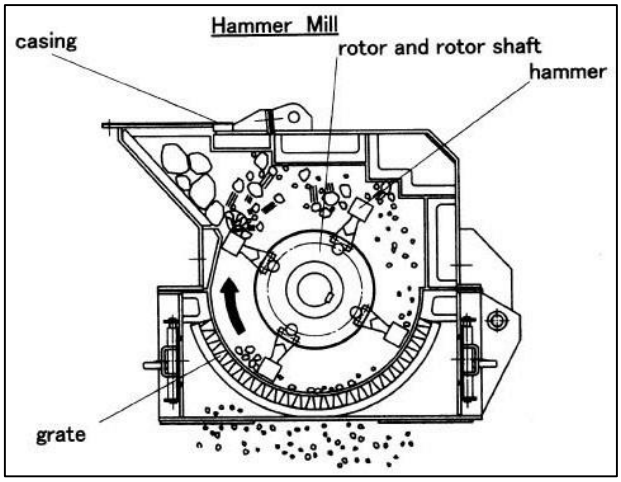

Figure 2.12 Hammer Mill Operation (De Schepper., 2007:23).

2.4.3 Pin Mills

A pin mill is also known as an impact mill (Figure 2.13). The pin mill uses different media to mill powder. The material of the grinding media is dependent on the powder to be milled. The grinding media could be either pin discs or milling balls. The material of construction for the milling balls is ceramic. Particle size reduction occurs by impacting the product with the grinding media and inert-particle attrition. Powder is accelerated by centrifugal force against the grinding media. The grind media is also in motion. Process variables that impact on particle size distribution are the speed of the grinding media and speed of the air flow rate. Particle size distribution of 10 microns or less can be achieved. This mill does not generate heat and does not have high energy requirements. The problem with using grinding media is the risk of

contamination with sub-micron cobalt powder. Depending on the grinding media, impurities such as iron or nickel can increase and result in the powder being out of specification. Another disadvantage was that this mill is effective with materials that have a Mohs hardness of <3 (De Schepper., 2007:25).

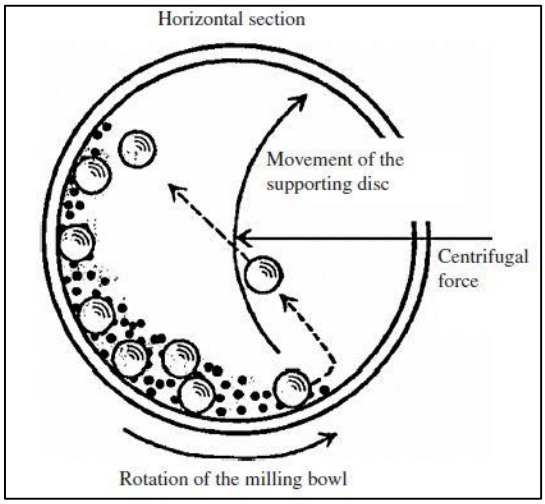

Figure 2.13 Pin Mill Configuration (De Schepper., 2007:25).

2.4.4 Spiral Jet Mills

The spiral jet mill consists of a grinding bin with several nozzles (Figure 2.14). It is a fluidized bed mill that does not have a classifier wheel. The powder enters the grinding bin of the jet mill and is subjected to a drag force and a free vortex. The drag force is created by the air flow in the mill. The free vortex is created by the centrifugal force. Large particles are affected the most by the centrifugal force. These large particles circulate around the wall and nozzles of the mill colliding with other particles. When particles become finer the drag force draws these particles with the air stream to the outlet of the mill where it is collected by the product trolley. The spiral jet mill controls only particle size and not particle size distribution which is a serious limitation when producing sub-micron cobalt powder. Furthermore this mill has limitations on the feed inlet injector allowing powder to pass throw fairly slowly, and with powder leaving the furnace not fully de-agglomerated, it creates a lot of blockages. The spiral jet mill cannot effectively mill powder with a Mohs hardness >3 hence it was not suitable for milling cobalt powder (De Schepper., 2007:27).

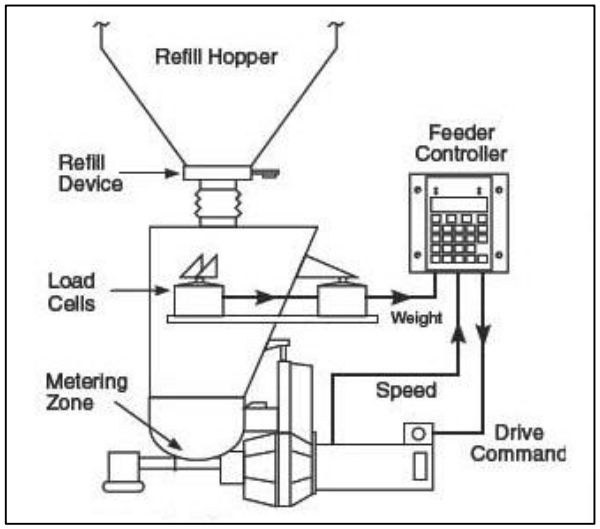

Figure 2.14 Spiral Jet Mill (De Schepper., 2007:27).

2.4.5 Fluidized Bed Jet mills

The fluidized bed jet mill consists of a grinding section and an upper classification section (Figure 2.15). The grinding section consists of a grinding chamber with several nozzles. The classification section contains a centrifugal vortex nitrogen classifier. High velocity nitrogen gas is created by the nozzles. Nozzle width can impact on the velocity of the gas flow rates. The high velocity nitrogen gas creates a vortex in which the particles collide with one another. The high velocity of the gas stream accelerates particle collisions. There are different nozzle sizes that can be applied. The nozzle sizes will impact on the gas velocity rates. The fluidized bed jet mill allows for micronization which is where the processing of powder will result in a particle size distribution of < 10 µm. The expanded gas flow conveys the ground particles toward the classifier wheel. The classifier speed is set depending on the type of cut required. The material of construction for the classifier wheel can be ceramic or steel. The steel classifier wheel allows for better throughputs than the ceramic wheel as the number of vanes in each wheel is different. The ceramic classifier wheel has 40 vanes whilst the steel classifier wheel has 30 vanes. The difference with the fluidized bed jet mill and the spiral jet mill is the spiral jet mill does not contain a classifier wheel. Furthermore the interaction of particle to particle collision is different. The spiral jet mill uses the mass and drag force which results in the grinding. The mass force is exerted on the particles due to the acceleration of the particles in motion. The drag force is exerted also on the particles due to the surrounding media. In the operation of the fluidized bed jet mill the mass force is exerted on the particles by the peripheral velocity of the classifier wheel. This results in a narrower particle size distribution and constant results

produced from this jet mill. The fluidized jet mill does not have the limitations that the spiral jet mill or the other jet mills mentioned above have. It requires low energy input and does not generate heat in the process. It controls particle size distribution by changing the rotational velocity of the classifier wheel, changing the volume of gas which is controlled by the grinding gas valve, changing the velocity of the gas which is controlled by width of the nozzles, and varying the weight in the AFG grinding bin. The only problem experienced with this type of jet mill was, it cannot mill small quantities of material at a time. It requires a minimal amount of powder fed into the system for the process to initiate (De Schepper., 2007:29).

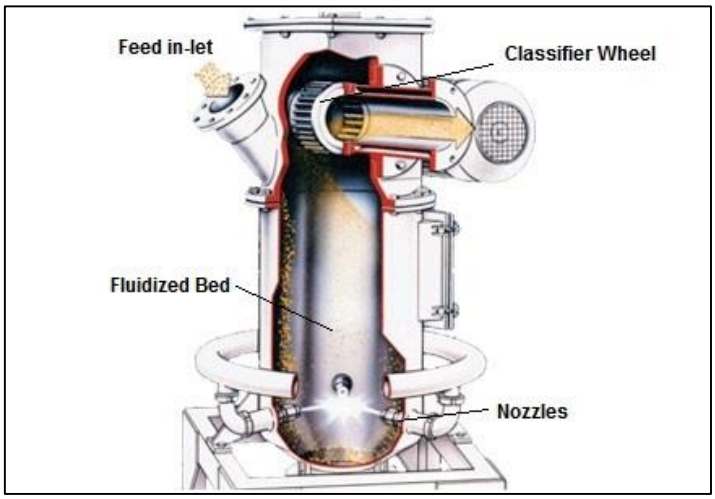

Figure 2.15 Fluidized Bed Jet mill (De Schepper., 2007:29).

2.5 Design of Experiments

Design of experiments (DOE) is a planned approach for determining cause and effect relationships. It can be applied to any process with measurable inputs and outputs (Anderson and Whitcomb 2007:ix). The following guidelines are used when using design of experiments:

2.5.1 Pre-experimental planning

Pre-experimental planning recognizes the problem, identifies the response variable, and assists in the selection of variables. Selecting process variables includes defining the range and the level. This step is crucial at the start of experimentation. The experimenter needs to understand if the work to be conducted is on an existing system. There are studies that can be conducted on the system which are confirmation studies or optimization studies. Screening and characterization is important. Good objectives must be set and understood. In some experimental studies the response variable can be clearly defined and in others it has to be defined. When the response variable needs to be defined, the question must be raised if the response variable provides useful information. Hence it is important to understand the objective of the experiment. There can be more than one response variable in a process. During the selection of variables, all variables of the system must be assessed. There are some variables that are defined as design variables, constant variables and varying variables. The design variables are those that are selected for the experimentation. The constant variables exhibit two conditions. These variables may exert an effect but it is of no interest to the objective of the research. The second condition is when the variables do not affect the response variable. Varying variables are experimental units on which the design variables are applied. These units are non-homogenous. Both constant and varying variables are assumed to have very little effect on the response variable. There also exists nuisance variable's, which have large effects that must be accounted for but is of little interest to the experimentation. These nuisance variables are classified as controlled, uncontrolled and noise variables. The controlled nuisance variable is a variable whose level can be set by the experimenter. An uncontrolled nuisance variable cannot have their level set, however the analysis of covariance can be used which compensates for the effect. Analysis of covariance is a method of comparing a variable in two or more groups taking into account variability of all variables which are called covariates. A noise variable is a variable that varies uncontrollably or naturally but it is a variable that can be controlled for purposes of the experimentation.

Noise variables are common in most experimentation's. It is of utmost importance that the design variables are set at a level which minimizes the variability as a result of the noise variables. In the planning process, the fishbone diagram was applied (Figure 4.1).

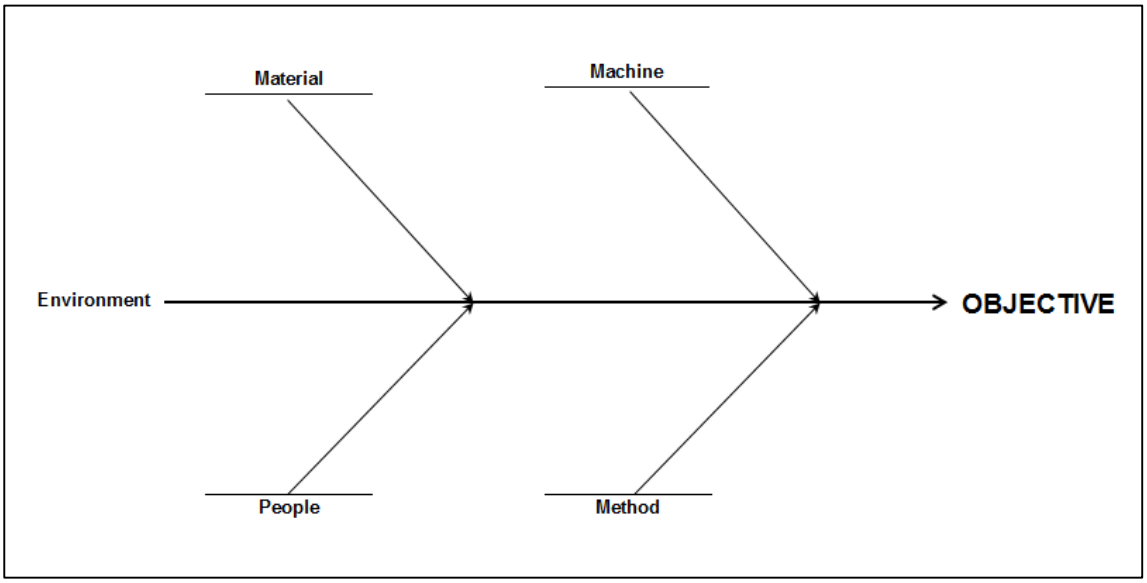

Figure 2.16 Fishbone diagram for brainstorm of factors (Anderson and Whitcomb, 2007:172).

2.5.2 Type of experimental design

The type of experimental design will be dependent on the process under experimentation. The number of variables, the number of levels, and whether blocking or randomization is involved, will determine what design will be selected. Statistical software packages assist in this decision. Design Expert was the chosen software used for the analysis of the experimentation. Essentially the experimenter will input the number of variables, ranges, and levels into the software. The software gives options on the type of design to proceed with. As the experimenter, it is crucial to always take into account the objective of the experimentation.

2.5.3 Conducting the experiment

Usually a few trial runs or pilot runs are conducted to help the experimenter understand the process if there is no prior knowledge. The reason for this approach is to highlight the consistency of the experimental material, evaluate the measurement system, to understand what the standard error is and to practice the experimentation. Based on this trial run, questions may be raised on the pre-experimental planning, if there was important information omitted etc. When the actual experimentation is conducted it is crucial to monitor the process and ensure that the plan is being adhered to. If the plan is not being adhered to it destroys experimental validity. Planning is the key tool to ensure success in conducting experimentation.

2.5.4 Performing the statistical analysis on the data

Statistical methods of analyzing data ensure that the results and recommendations are objective. The software package used in this experimentation was Design Expert. It is important to take note that the accuracy of the results is dependent on the information put into the system. The advantage of this system is that it adds objectivity into decision making.

2.5.5 Conclusion and recommendation

When conducting experimentation it is crucial to ensure that there are follow up experimental runs and confirmation testing. It is imperative to have knowledge of the process prior to commencement of the experimentation. This includes operational parameters, constraints in the existing system and the units of measurement. The experimentation must be carried out sequentially.

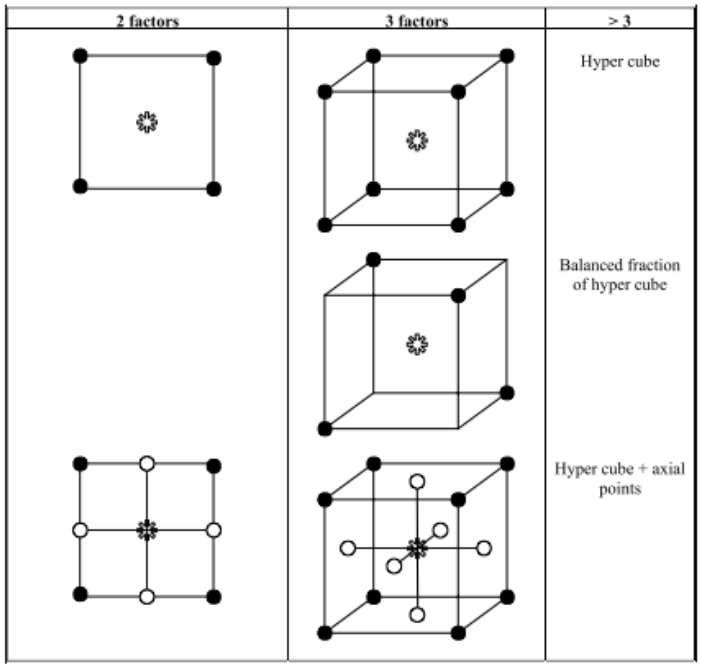

Figure 2.17 Examples of factorial, fractional factorial and composite design (Eriksson et al., 2008).

The design of experiments method, formulates the approach of any experimentation. Based on the number of variables and the levels of these variables, a design matrix is generated (Figure 2.17). The benefit of design of experiments is that it provides an organized approach when analyzing a problem or a start of a new project. This experimental method improves process yields. There is greater conformance to reaching the goal. The experimenter finds that with the use of design of experiments there are fewer experiments that have to be conducted to reach the desired result. This in turn reduces the overall costs for the experimentation (Montgomery 2009:8).

2.6 Full Factorial experiment

A full factorial experiment is a design that consists of two or more factors. The design takes into consideration all possible combinations of the factors across different levels (Table 2.8). This design allows for the experimenter to study the effects of each factor on the response variable as well as the effects of interactions between each factor on the response variable. The effect is defined to be the change in response produced by a change in the level of the factor (Montgomery 2009:162).

Table 2.8 A factorial design matrix

Run	Factor (x_1)	Factor (x_2)	Response (Y)
1	-	-	Y_1
2	-	+	Y_2
3	+	-	Y_3
4	+	+	Y_4

The disadvantage of such a design is the number of different treatment conditions that each factor must go through. The large number of treatments can be time consuming especially if there are more than 3 factors. The advantage of such a design is that the design matrix ensures that each factor interacts with each other in different conditions which enable the experimenter to evaluate the analysis taking into account the response variable and interactions between specific factors. Interactions between factors are crucial to determine how their respective combination impacts on the response variable (Montgomery 2009:10).

Design of experiments was selected over OFAT (Figure 2.18), which is the one factor at a time approach. The OFAT approach is an experimental strategy that changes one factor at a time. It evaluates the output response for the associated change in factor. This form of experimentation is inefficient as it requires a lot of runs which is time consuming and expensive. This experimentation can also miss important interactions which can lead to optimal settings (Montgomery 2009:10).

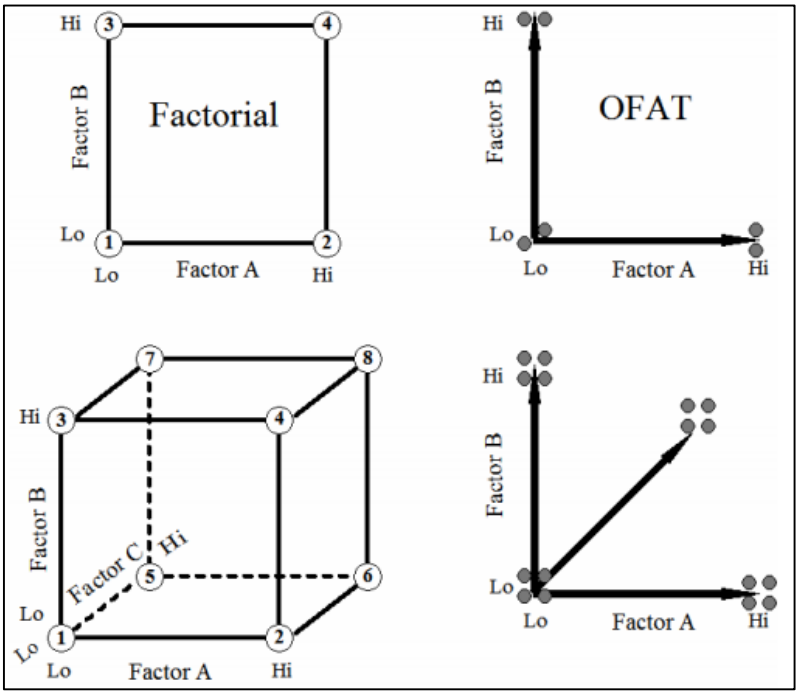

Figure 2.18 Two-level factorial vs. one factor at a time (Anderson and Whitcomb, 2007:42).

The objectives for the full factorial experimentation are:

4.2.1 To understand the process by a few runs carried out.

4.2.2 To identify factors that have an impact on the mean, variation, both or no effect.

4.2.3 To model the process with predictive equations.

4.2.4 Optimization of factors to obtain desired response variables.

4.2.5 Validating the results through confirmation tests.

2.7 Response Surface Method

The Response Surface Methodology (RSM) is a collection of mathematical and statistical techniques useful for the modeling and analysis of problems in which a response of interest is influenced by several variables and the objective is to optimize this response (Montgomery 2009:418). The development of response surface method began with the publication of an article by Box and Wilson (1951) titled "On the experimental attainment of optimum conditions". The strategy of experimentation grew and tools such as DOE were developed. Response surface methodology evaluates the relationship among the measured responses and input factors (Figure 2.19).

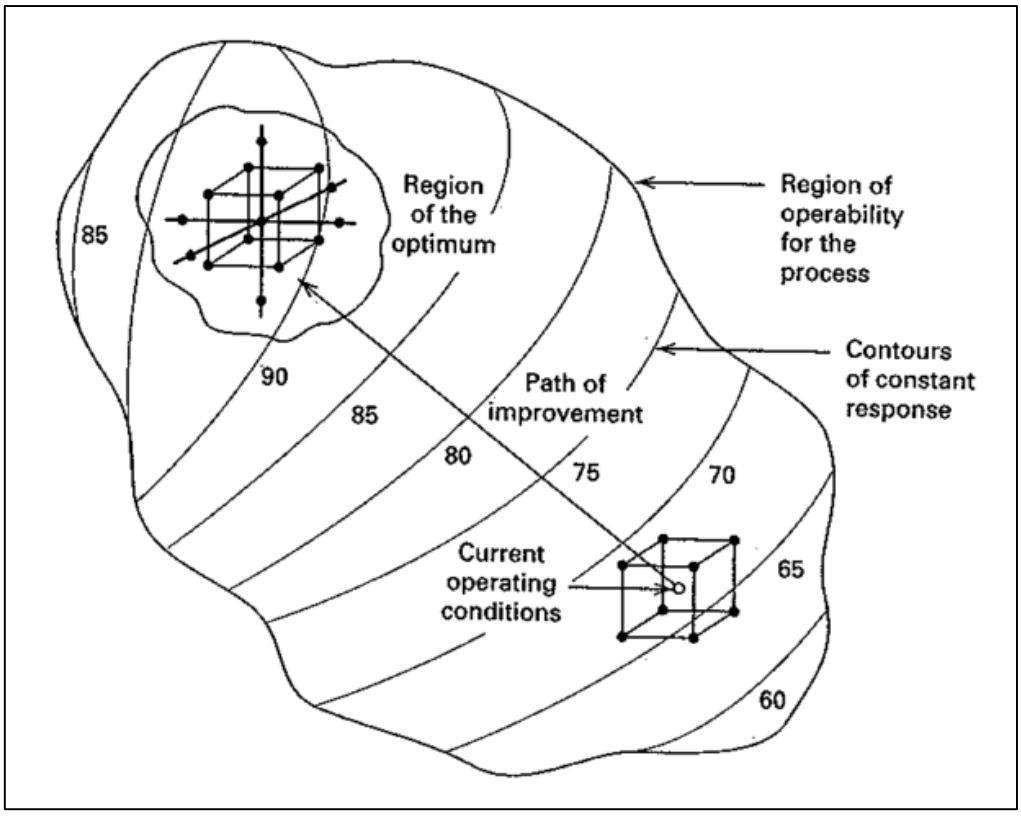

Figure 2.19 The sequential nature of response surface methodology (Montgomery, 2009:419).

The objective of response surface methodology is to determine the optimum operating conditions for the system or to determine a region of the factor space in which operating requirements are satisfied (Montgomery 2009:419).

Response surface methodology has various design routes that can be selected to evaluate results which are:

1. One factor
2. Pentagonal and Hexagonal
3. Three-level factorial
4. Central composite
5. Hybrid
6. Box Behnken
7. D-optimal, Distance-based, Modified distance
8. User defined

Response surface methodology can only be applied once design of experiments has been applied. The design of experiment's method used is the two level factorial design. The goal of response surface methodology is to generate a map of response. This map is in the form of contour plots or 3D plots. This graphical demonstration of data instantly gives the user an idea of the effect of each variable on the response variable. Generally with two level factorial designs, they don't fit surfaces, hence center points are added which aid in detecting curvature. When significant curvature is detected in a two level factorial design, more center points are added hence augmenting into a central composite design (Figure 2.20). The design route used for response surface methodology was a central composite design.

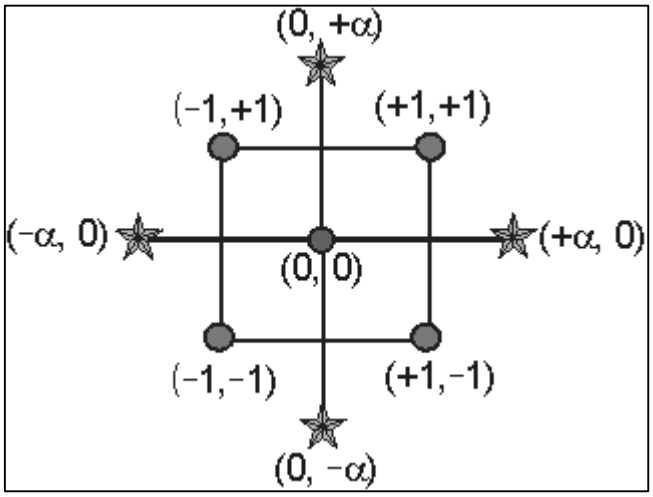

Figure 2.20 Central Composite Design Example (Anderson and Whitcomb, 2005:171).

2.7.1 Central Composite Design

Central composite design applied to a 2^4 or 2^3 level design results in the addition of axial runs. Usually center points in the experimentation duplicate operating parameters that were used in the production process prior to the experimentation. This gives the experimenter an opportunity to check if there were unusual occurrences during the experiment. It also provides a check to determine if there is process stability. When selecting central composite design as the design route there are fundamental concepts that needed to be understood. These concepts assist in determining the way the experimental run would precede by determining the number of runs and whether or not there would be replication of experimental runs. In (Figure 2.20) each corner of the square represents the factorial design points. The factorial points have different combinations. In the case of a two level design the combinations are as follows (+1, +1) (-1, -1) (+1, -1) (-1, +1). The four star points represent the axial design points. Axial points have all factors set at zero also known as the mid-point except for combination values such as (+1, -1) or (-1, +1). Axial points are in combination with alpha values as follows (0, -α) (0, +α) (-α, 0) (+α, 0). Alpha values determine the location of the axial points in the central composite design.

2.7.1.1 Factorial replicates

A factorial replicate is the number of times each factorial run will be performed. One is the default.

2.7.1.2 Axial Replicates

This is the number of times each axial run will be performed. One is the default. If there are concerns that an accurate value will not be achieved, then select two axial replicates.

2.7.1.3 Center point replicates

Design expert usually recommends the number of center points to be used. What must be noted is that the central composite design usually looks at the optimum of the design; hence more center points give better prediction at the center. These points also provide an accurate lack of fit test.

2.7.1.4 Alpha values

Alpha values determine the position of the axial runs.

2.7.1.5 Rotatable (k<6)

The rotatable option is selected for up to five factors as the default setting. The design created has a standard error of predictions equal at points equidistant from the center of the design.

2.7.1.6 Spherical

The spherical option places all factorial and axial points on the surface of a sphere of a radius. This is equal to the square root of k. The symbol k represents the number of factors.

2.7.1.7 Orthogonal quadratic

The orthogonal quadratic provides alpha values that allow quadratic terms to be independently estimated from the other terms.

2.7.1.8 Practical (k>5)

The practical option is usually selected for designs that have six or more factors. The alpha value is the 4^{th} root of the number of factors. This has been shown to produce axial values that can practically be run, and yet the design still has sound statistical properties.

2.7.1.9 Face centered

The face centered option pulls the axial points into the faces of the cube - at +/- 1 levels. This produces a design where each factor only has three levels.

2.7.1.10 Other option

The option other allows the user to specify any alpha value that is desired. When the practical alpha is too large, the option called other is selected with a value less than 1.5. This alpha distance will provide a more realistic range for the experiment than practical alpha option while providing better estimating properties than a face centered option.

2.7.2 The Three Types of RSM

There are three types of response surface methodology, the first-order, the second-order, and three-level fractional factorial. When the response in the experimentation can be defined as a linear function of independent variables then the function is a first order model. A second order model is when there is curvature in the response. Generally a higher degree polynomial is used. The first order and second order model are usually used when applying response surface methods. In both models, the factor levels are independent of each other. The three-level fractional factorial model is a modified full factorial model, where fewer runs than a full factorial design are conducted to determine the main effects and low order interactions of an experiment. The objectives of response surface methodology are to understand the topography of the response surface (local maximum, local minimum, ridge lines). It also determines the region where the optimal response occurs. The first goal for response surface method is to find the optimum response. When there is more than one response then it is important to find the compromise optimum that does not optimize only one response (Oehlert 2000:520). When there are constraints on the design data, then the experimental design has to meet requirements of the constraints. The second goal is to understand how the response changes in a given direction by adjusting the design variables. In general, the response surface can be visualized graphically by the shape of the response. The shape of the response could be a hill, saddle or a valley etc.

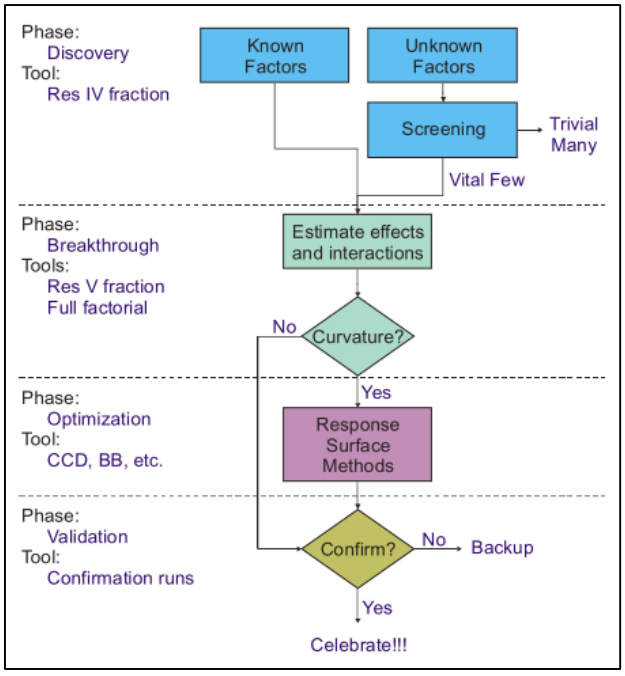

Figure 2.21 Strategy of Experimentation (Anderson and Whitcomb 2005:4)

Note that in the experimental design to attain particle size, oxygen content and particle size distribution the method of response surface methodology applied is steepest descent. The reason for this is, for the above response variables, the minimum values is desired.

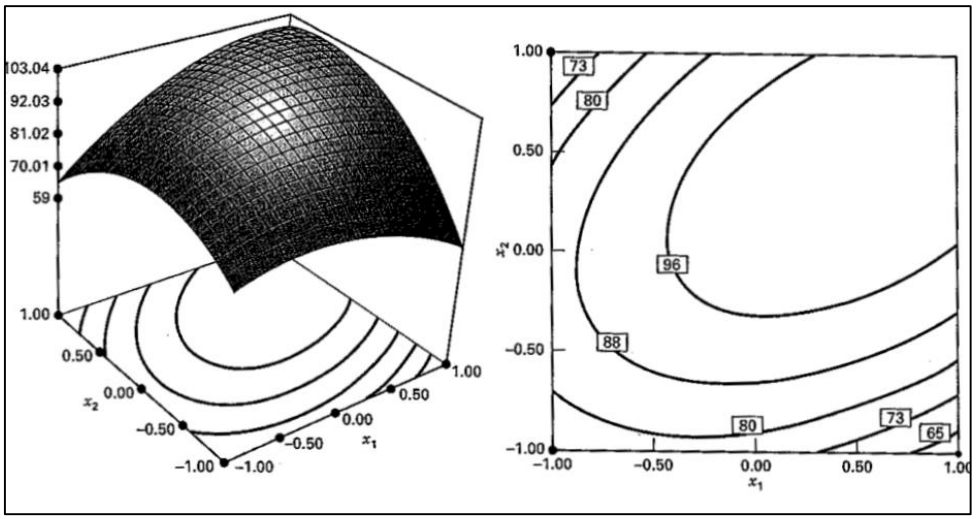

Figure 2.22 Response surface and contour plot illustrating a surface with a maximum (Montgomery 2009:425)

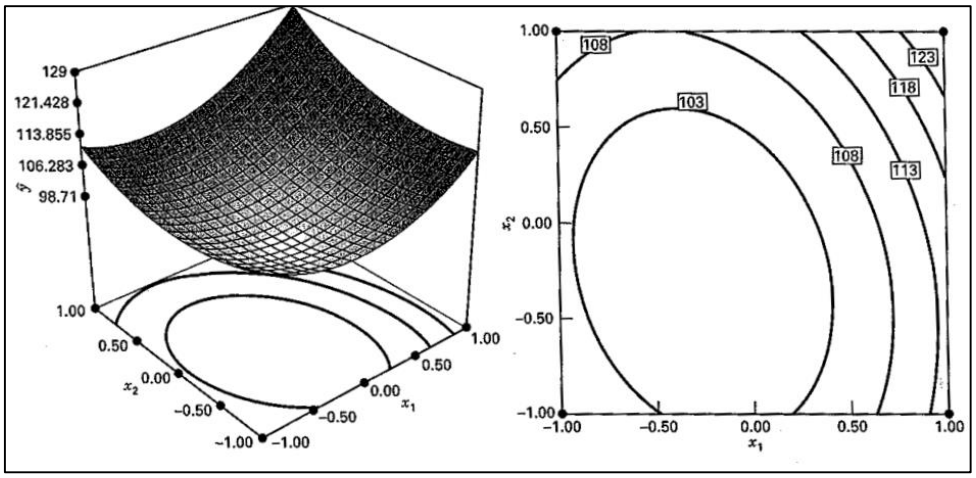

Figure 2.23 Response surface and contour plot illustrating a surface with a minimum (Montgomery 2009:426)

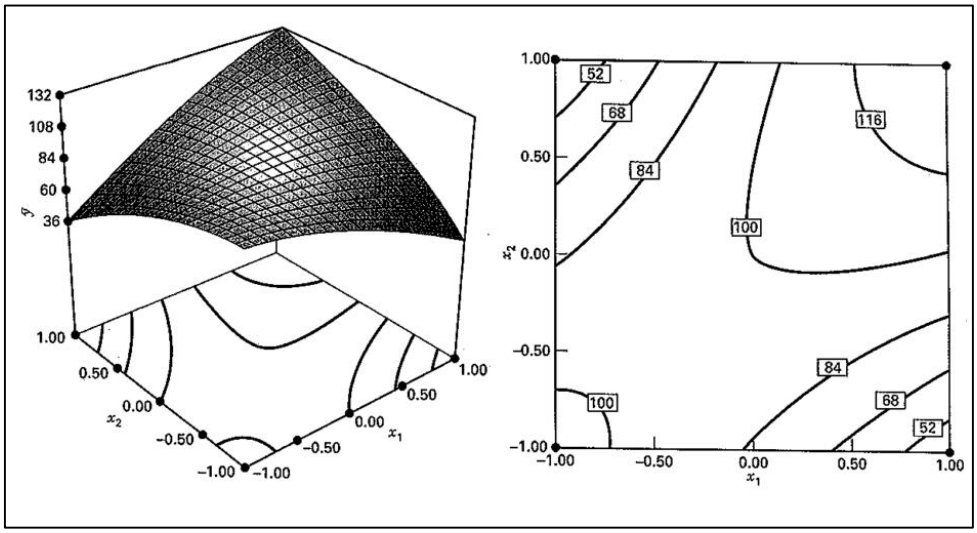

Figure 2.24 Response surface and contour plot illustrating a saddle point (mini-max) (Montgomery 2009:426)

CHAPTER 3

FURNACE AND JET MILL TECHNOLOGY

3.1 The Furnace process

The research trials were conducted on a plant scale on the new production line, Furnace 2 (Figure 3.1). Prior to the commencement of the trials, all equipment was checked by maintenance to ensure its correct functioning. All production staff were briefed on the requirements of the experimentation and were made aware that they would be actively involved in all changes made to the process. The precursor used to produce the sub-micron cobalt powder was cobalt carbonate. The process was a direct decomposition and reduction of cobalt carbonate in the presence of hydrogen gas. Essentially this process was applied to produce sub-micron cobalt powder, as it had successfully been tried and tested to produce normal cobalt powder. The draw backs of the two-step furnace was that the system was not free of external interference meaning, any interruptions in gas flows such as nitrogen gas would result in normal atmosphere entering the furnace. This would negatively impact on the product quality of the powder. Conveyor belts used in high temperature processes are known to carry off a lot of heat from the process (Chong, 2012:156). In the two-step furnace, the conveyor belt presented the same challenge which was the loss of heat. The two-step furnace required higher energy consumption in order to accommodate the heat loss as a result of the conveyor belt as compared to a standard tube furnace (Chong, 2012:156). The advantage of the system was that it was inexpensive and the precursor had very minimal amounts of impurities. The system could be easily adapted to have process variables changed. The two-step furnace had the added advantage of larger throughput, which reduced process costs as it was demonstrated at Shu Powders Africa when processing normal cobalt powder (fsss > 1.0 μm).

The process variables are:

a. Temperature
b. Hydrogen gas flow rate
c. Carbon Dioxide gas flow rate
d. Belt speed - Retention time of powder for processing
e. Nitrogen gas flow rate
f. Bed depth of raw material

All variables could easily be measured as they were electronically controlled. These variables needed to be understood by evaluating their effect on the powder and their interaction with one another. The furnace heating section was electrically heated. The furnace heating section consisted of elements and insulation which were not in contact with the powder. The powder passed through the furnace in a ribbed inner stainless steel shell. The heat from the elements, penetrated through the shell which in turn heated the powder up. The diameter of the shell was 100 mm. The furnace heating section was fundamentally split into three heating sections. These heat sections had temperature probes which measure the temperature. A good understanding of this process was required in order for one to control temperatures in the heating zones of the furnace.

Hydrogen gas flow rate was produced by the decomposition of ammonia. The ammonia decomposer was electrically heated and contained a nickel catalyst. The hydrogen gas was purified by the activated alumina. This was to ensure the purity and dew point of the gas was within range. The gas stream had a purity of <5 ppm of ammonia residue and a dew point temperature of -50°C as per the gas quality standard at Shu Powders Africa.

Nitrogen gas was produced by the swing absorber towers. This system used atmospheric air and drew this into a pre-filter unit to remove dust from the air stream. The air was then compressed to 7 bar and sent through to the swing absorber towers. The coarse air was sent through to air driers and filters. The air drier served to remove moisture from the air stream and the filters were used to remove oil residue which was imparted to the air stream at the air compressor stage. These towers contained activated carbon and activated alumina. The coarse air was passed through these towers and reacted with hydrogen to remove the excess oxygen in the form of water. The nitrogen gas produced had a purity level of < 5 ppm of oxygen. Quality of gases used was analyzed digitally using oxygen analyzers and dew point analyzers.

Shu Powders produced the hydrogen and nitrogen gas on site which was advantageous as the gas quality was monitored very closely and there was a large volume of gas at our disposal. If dew points were not within specification with these gases it would negatively impact on the quality of the powder.

Carbon dioxide gas was stored on site. The CO_2 gas was obtained from Air Liquide. All carbon dioxide deliveries had an certificate of analysis sheets which comply with the requirements for our system.

The belt speed was the rate at which the steel conveyor belt travelled through the furnace which was known as residence time. It was measured in mm/min. This could be controlled electronically as well.

The bed depth of the raw material was the thickness of the powder on the belt. This was controlled by a level system.

Based on actual and theoretical knowledge it was found that the nitrogen gas flow rate had little or no effect on sub-micron cobalt powder production. The main purpose of the nitrogen gas was primarily to create an inert atmosphere and cool the product leaving the heated section of the furnace. It also prevented the back flow of hydrogen gas in the furnace. The level system that controlled the bed depth of the raw material was kept constant to ensure that there was a constant amount of powder that was being processed. If there was any change in the bed depth, all process parameters would be impacted. Both the nitrogen gas flow rate and the bed depth were kept constant throughout the experimentation.

In order to obtain an objective conclusion an experimenter needed to plan and design the experiment, and analyze the results. Two methods were applied in this work; these were design of experiments and response surface methodology.

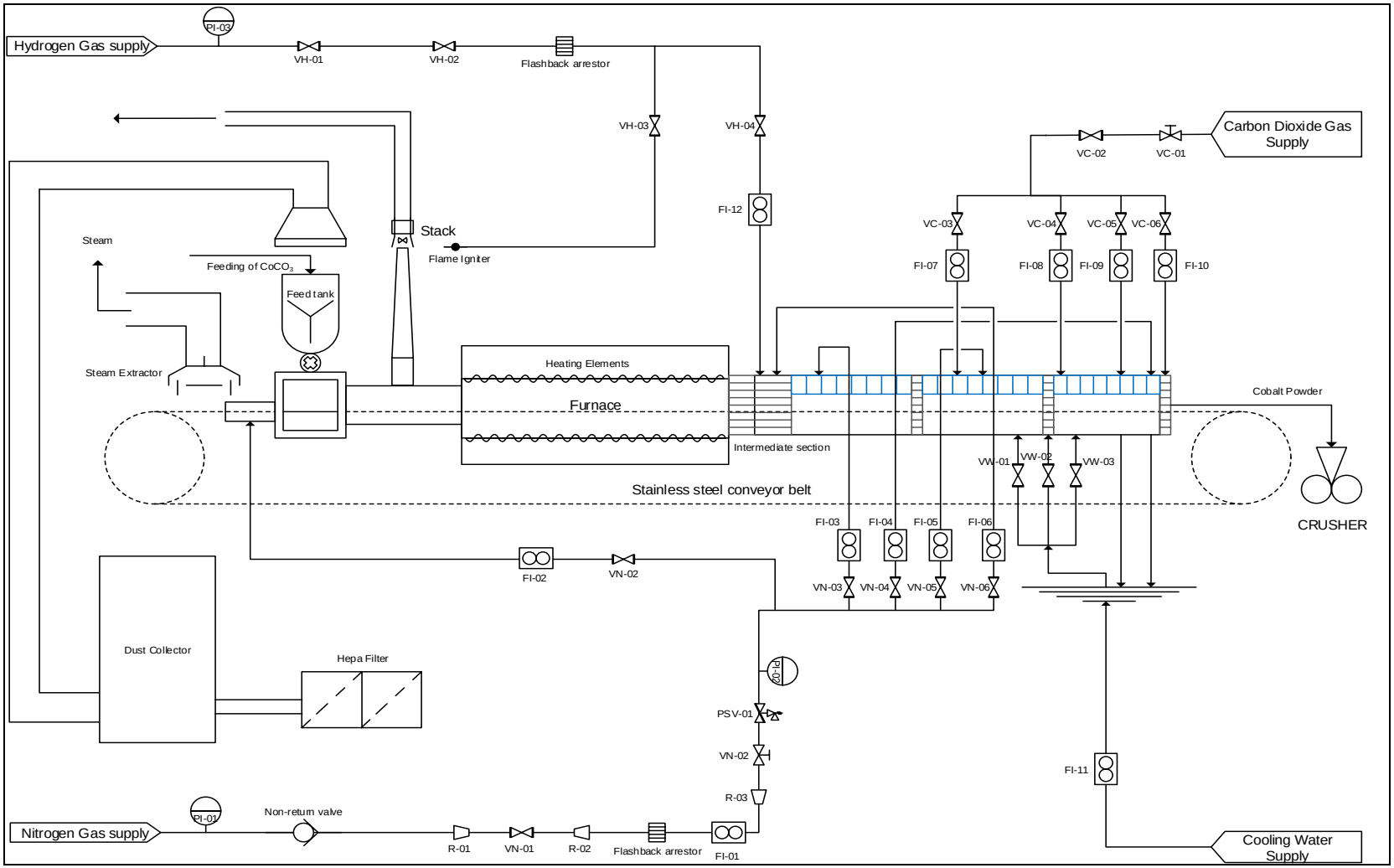

Figure 3.1 Process flow diagram of the furnace.

The furnace was electrically heated over three days to operating temperature range set out by the experiment. The furnace usually expands and retracts during the heating phase. Hence three days was required for the heating phase to ensure that this did not interfere with the residence time in the furnace. If the furnace was heated to set point temperature over a short period of time, the furnace underwent sudden expansion. This sudden expansion would result in the stainless steel belt stretching and warping which would impact on the function of the belt. The belt speed controlled residence time. Residence time was a crucial factor which could impact on product quality. Hence the start-up procedure for the furnace during sub-micron cobalt powder production had be adhered to. The furnace temperature could be set electronically.

All gases were electronically tested to ensure that the dew point temperature for all gases, hydrogen, nitrogen and carbon dioxide were between -25°C to -50°C. Dew point is the measurement of the temperature at which the gas will start to produce moisture. Gases used in the process had to be dry as any moisture in the gas would increase the oxygen content of the product which was detrimental to the quality of cobalt. The oxygen content in cobalt was measured and had to be within the range 0.30 - 0.80%. All flow meters were also calibrated to ensure that the flow rates set were an accurate reflection of what was really going into the furnace. The furnace was purged using nitrogen gas to ensure that an inert atmosphere was created and to remove any oxygen gas pockets that could exist in the furnace. This was required from a safety point of view. If the concentration of hydrogen was between 4% - 75% in the furnace an explosion could occur.

The raw material, cobalt carbonate, used in the experimentation was selected on the basis of particle size and apparent density. These batches used in the experimentation had a particle size range of (0.40 µm - 0.50 µm) and an average apparent density of 0.40 g/cm^3. The reason why batches of raw material were selected on the basis of particle size (fsss) and apparent density were, to minimize the number of variables in the process that required to be investigated. These factors on the cobalt carbonate were easy to keep constant. All raw material fed into the process was documented. The raw material was fed onto the steel belt. The bed depth of the raw material on the steel belt was kept constant. The height of the level system controlling the powder height on the furnace was set to 25 mm. The powder passes through the heating section of the furnace where powder comes into contact with the high temperature and the hydrogen gas. This was where the cracking by the heat of the furnace and the reduction by the hydrogen gas stream took place. The nitrogen gas stream was fed through the cooling section of the furnace only. The nitrogen gas created an inert atmosphere in the cooling section. Carbon

dioxide gas was fed into the last section of the cooling section and the area where the powder entered the crusher unit.

The sub-micron cobalt powder produced was cooled by the water and nitrogen gas in the cooling section. The temperature of the powder had to be below ambient temperatures as temperatures higher than 25°C would result in the sub-micron cobalt powder spontaneously igniting as sub-micron cobalt is highly flammable. The sub-micron cobalt powder was passivized by carbon dioxide gas. Samples were taken at the point where the product left the cooling section. Visual inspection was also conducted through a site glass on the furnace. The following observations were made (Table 3.1):

Table 3.1 Visual observations on the quality of sub-micron cobalt powder

Visual Observations:	Reason:
Yellow/Brown traces on powder	Powder not reduced efficiently, less H_2 gas
Black lines (in the center of powder)	Sintering due to high temperature
Black patches (surface of powder)	Oxidation state. Powder usually begins to burn
Pink/Purple traces on powder	Not properly cracked containing traces of the raw material. Due to low temperature

The sample taken at the furnace stage was analyzed for particle size and oxygen content. For the experimentation, 3 samples were taken randomly at the same section to confirm accuracy of the test results. An average of 36 samples was taken off the belt of the furnace per a day. The settings on the furnace were based on the operational limits of the system and the design matrix generated by design of experiments. The settings on the furnace were changed every 3 days. The reason for this was to obtain an overview and understanding on the effects of the process changes. All external interferences if any were documented.

3.2 The Jet Mill Process

The main purpose of a jet mill was to de-agglomerate the cobalt powder which was responsible for the control of particle size distribution.

3.2.1 Jet mill description

The jet mill uses pressurized nitrogen gas. This gas serves two functions, one was to create an inert atmosphere, and the other was to create the tornado effect in the grinding bin. Product from the furnace was conveyed onto the jet mill via the feed opening into the grinding bin, which was known as the alpine fluidized bed. The alpine fluidized bed contains load cells which measure two weights. These weights are selected by the user. There was the target weight and the off-set weight (figure 3.2). The set weight determines the level at which the powder will sit in AFG. The off-set weight controls the amount of powder milled at 2 minute intervals. Through design of experiments the optimal level of powder was determined (Hareepersad., 2014:5).

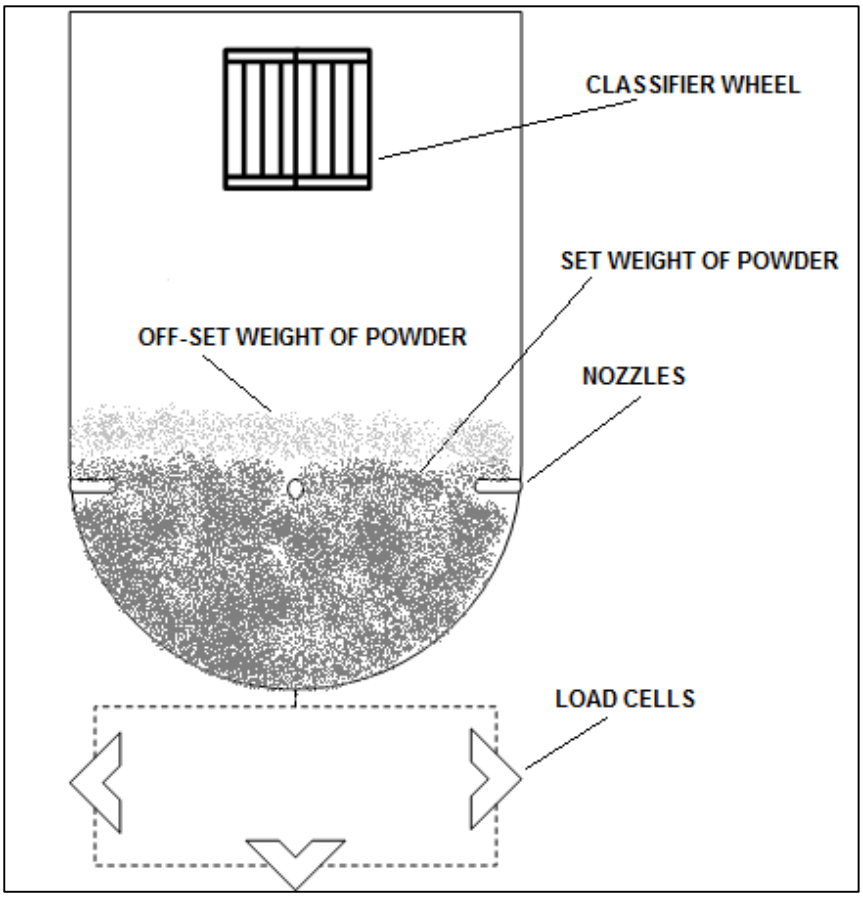

Figure 3.2 Schematic diagram of the AFG (jet mill grinding bin) Unit (Hareepersad., 2014:5).

The powder was de-agglomerated by the nitrogen jets leaving the nozzles. Pressurized nitrogen gas was injected into the jet mill through three nozzles, right into the milling zone. The gas flows from each nozzle and contact each other in the middle of the jet mill (milling zone). As the powder entered the milling zone, the nitrogen gas from the nozzles accelerated the powder allowing for collision. During this process the cobalt particles bounce against each other with a high force and become very fine as more individual particles collided. The pressure was set by adjusting the grinding gas pressure. The jet stream was used to take the powder up with the gas stream. The grinding gas pressure impacts on particle size. Similarly the nozzle width determined the flow rate of the nitrogen gas which in turn impacted the particle size of the powder. The gas stream leaving the jet mill carried the milled particles through the classifier. The classifier allowed only fine particles to pass through and the coarse particles to fall back into the grinding bin hence controlling the particle size distribution of the powder. The fine powder was extracted in accordance with the set point speed set on the classifier. This powder was transferred through a discharge outlet into the cyclone or filter unit where it was removed as final product (Figure 3.3). Essentially the classifier wheel controlled the particle size distribution of the powder (Hareepersad., 2014:7).

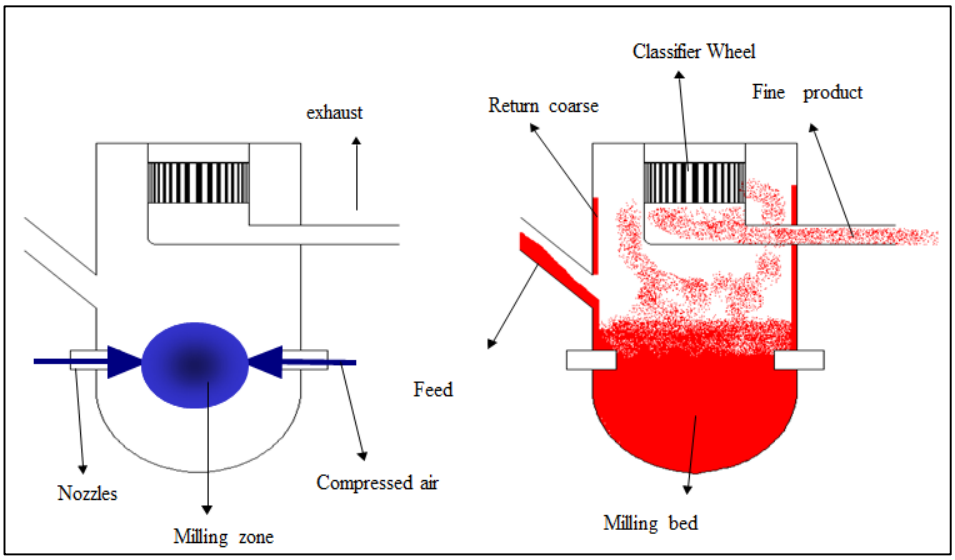

Figure 3.3 Process flow diagram of the jet mill (Hareepersad., 2014:7).

The jet mill operates automatically and was controlled by a PLC. There are sensors with alarms that ring off to indicate to the operator that product from the cyclone or filter unit was at 500 kgs in weight, to signal that an empty trolley of powder should be loaded onto the unit. Important

variables for the jet mill process are the classifier speed, nozzle width, AFG grinding bin and grinding gas pressure.

3.2.2 Important variables - jet mill process

The jet mill has 4 important variables that govern the jet mill process. There are process limitations on the jet mill that has to be considered prior to the experimentation.

3.2.2.1 Classifier speed

The classifier wheel is responsible for particle size cut. The classifier wheel is 200 mm in diameter. The material of construction is either ceramic or steel. The maximum speeds for both classifier wheel types are 6000 rpm. The range varies between 1000-6000 rpm. The throughput of the steel classifier wheel is greater than the ceramic classifier wheel. A ceramic classifier wheel was selected for the experimentation. The reason was that the steel classifier wheel, during the milling of cobalt powder, resulted in an increase of impurities such as iron and nickel content. The problem is that these impurities can only be removed if the product is sent back through the furnace as rework. This costs money to re-process the powder and re-work material cannot be converted to sub-micron cobalt powder. This had occurred in previous production runs. The ceramic wheel is very sensitive and precaution must be taken during installation. For the experimentation changes in classifier speed were made. The changes in the speed of the classifier wheel must be made when the jet mill is switched off electronically. From past operation on the jet mill, it has been noted that higher classifier speeds results in a higher residence time for powder milling however the advantage is that the particle size distribution is narrowed. After each experimental run the classifier wheel must be inspected to ensure that there is no process material stuck in the groves of the ceramic wheel. This blockage usually occurs when processing sub-micron cobalt powder, as the powder has a higher viscosity meaning lower ability to flow and hence the powder tends to block the groves of the classifier wheel (Hareepersad., 2014:9).

3.2.2.2 Nozzle width

The nozzles are situated in the grinding unit of the jet mill. The grinding unit contains three nozzles. The nozzle width varies from 6.3-10 mm. The narrower the width of the nozzle the higher the jet gas flow rates and effect on a high energy size reduction. The wider the nozzle width the lower the jet gas flow rates. Lower grinding gas flow rates mean gentle grinding. The material of construction for the nozzles is ceramic. The nozzle changes on the mill are a difficult

parameter to change. Different diameter nozzles require different nozzle housing. These changes require a change in all process conditions of the mill. Therefore for the experimentation changes to the nozzles was omitted. The size of nozzles used in the jet mill was the standard size of 8 mm (Hareepersad., 2014:10).

3.2.2.3 AFG grinding bin

The AFG grinding bin sets the weight of the cobalt powder that would be filled in the grinding bin. The difference between the off-set weight and the set weight of powder is the amount of powder to be milled. This weight is crucial as it would determine the grinding efficiency. The AFG grinding bin contains the nozzles and the classifier wheel.

3.2.2.4 Grinding gas pressure

The grinding gas pressure is controlled by the grind gas valve. The grind gas valve is electronically controlled and can be set by the operator. The grinding gas pressure also impacts the grinding gas flow rate. Higher grinding gas pressure would result in high grinding gas flow rates and lower grinding gas pressures would result in lower grinding gas pressures. Changes to grinding gas pressure would impact on the milling time of the product. Note although lower grinding gas pressure mean gentle grinding, it also means that powder would be milled for a longer period of time and therefore more desirable to reduce particle size distribution. The grinding gas pressure varies from 1.0 - 7.0 bar. Note the grinding gas valve was calibrated after every change in pressure settings. This was to ensure accuracy in the experimentation.

CHAPTER 4

EXPERIMENTAL METHODS

4.1 Approach for Experimentation

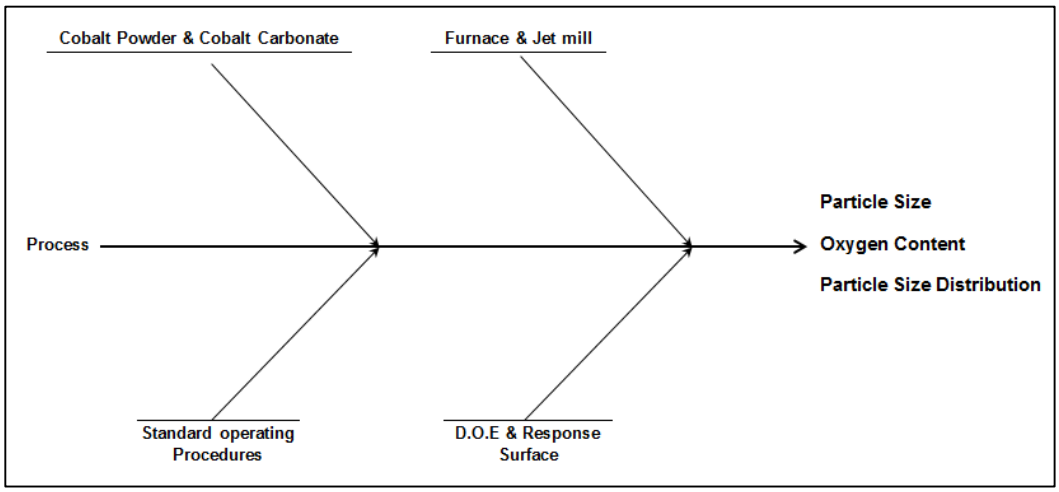

Figure 4.1 Experimental brainstorming for the research.

4.1.1 Process

The experimentation was carried out in a single furnace. All equipment such as elements and flow meters to the furnace were all checked and calibrated, to remove any room for error or source of disturbance. Each step from (Figure 4.1) is defined below.

4.1.2 Cobalt powder & cobalt carbonate

A good understanding of the raw material and the end product was required. In terms of the raw material for the experimentation, batches used were required to be of uniform particle size. This created a constant feed and allowed the experimenter to reduce the number of variables to be considered. The reason for this was particle size of the raw material could have an effect on the process conditions required such as temperature. In terms of the end product, process conditions suitable for sub-micron production had to be understood. The process conditions were confirmed by looking at literature.

4.1.3 Standard operating procedures

There needed to be a well-defined set of operating conditions that all shop floor staff understood for the experimentation. All process conditions were monitored every 30 minutes to ensure that there was little or no fluctuation.

4.1.4 Design of experiments and response surface methodology

The experimentation needed to be carried out in a systematic way. Design of experiments essentially developed the design matrix in which the experimentation would be carried out. Response surface methodology took the experimental data and modelled this data. This method defined the limits of the process by evaluating the process at its peaks and dips.

4.1.5 Furnace & Jet mill

The furnace and the jet mill were the unit operations used in the experimentation. These units needed to be understood and the capabilities defined. This assessment guided the choice of the process conditions.

4.1.6 Particle size, oxygen content & particle size distribution

The above factors also known as response variables were the objectives required to be achieved during the experimentation. The specifications and the ranges required needed to be well defined prior to the experimentation. By defining the requirements of the responses, targets were set. This guided the experimenter in the direction in which the experiment needed to proceed.

4.2 The Furnace Process

The use of design of experiments provided the matrix or the route in which the experimentation proceeded. The parameters were assessed on their individual limitations which could present itself in the form of a maximum or minimum value that the factor could be set at. This assessment was guided by experience in the system and if it were feasible to make such changes in the system. This came to light when looking at the value of the product to be produced. Off-spec material costs money to produce and treatment thereof, hence experimentation had to be efficient to obtain satisfactory results and be cost effective. Below (Table 4.1) was the operating range that the factors assessed on the furnace could be set to. The sequential startup of the furnace is in Chapter 9, Appendix B.

Table 4.1 The furnace operation limitation on factors

Factor	Range
Temperature	0 - 1200 °C
Hydrogen Flow rate	0 - 300 Nm^3/h
Belt Speed	0 - 110 mm/min
Carbon Dioxide Flow rate	0 - 150 Nm^3/h

4.3 The Jet mill Process

There was a sequential start-up for the jet mill during experimentation. All product produced from the jet mill was tracked to the batch of powder from the furnace and raw material. Each batch of powder from the furnace weighed 250 kgs. Two batches of these make up 1 batch of jet mill product which weighed 500 kgs as point 4 and 7 in (Figure 4.2) . This method helped to identify if there were any interruptions to the system. Once sub-micron cobalt powder was produced through the furnace by selecting the ideal process parameters, the sub-micron cobalt powder was then transferred to the jet mill to undergo jet mill experimentation. Jet mill experimentation would only proceed once sub-micron cobalt powder was produced to meet the required specification. This sub-micron cobalt powder would undergo the jet mill experimentation with the primary objective being particle size distribution. It was imperative to ensure that the nitrogen gas had an oxygen purity of < 5 ppm. The nitrogen gas was the medium which would mill the cobalt powder hence high purity of the gas was crucial. The operational parameters for the jet mill are as per Table 4.2. The sequential startup is detailed in Chapter 9, Appendix B.

Table 4.2 The jet mill operation limitation on factors

Factor	Range
Classifier speed	1000 - 6000 rpm
AFG Weight	20 - 50 kg
Grinding Gas Pressure	1.0- 7.0 bar

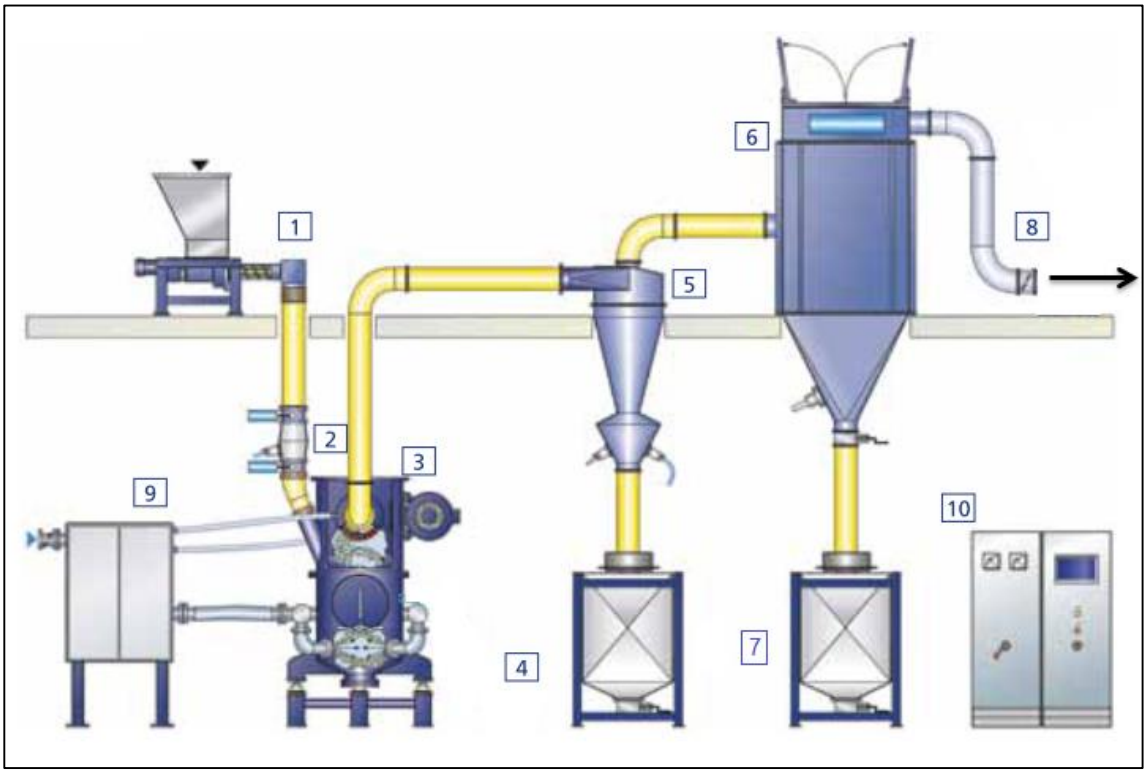

Figure 4.2 Schematic diagram for the jet mill process (Alpine fluidized bed opposed jet mill 2010).

Table 4.3 Reference table for the jet mill process

Number	Function
1	Feed metering Unit
2	Feed Flap valve
3	Fluidized bed opposed jet mill AFG
4	Product trolley
5	Cyclone
6	Automatic Filter
7	Dust trolley
8	Recycled Nitrogen
9	Nitrogen compressor
10	Control Unit

4.4 Particle size

The particle size of the sub-micron cobalt powder was tested by the Fisher sub-sieve sizer machine model WLP-208 (Figure 4.3). The fisher principle (Figure 4.4) used the air permeability method to determine the average particle size known as the fisher number. Note (Table 4.5) indicates the functions of each step for (Figure 4.4). The particle size analysis method is in Chapter 9, Appendix B.

Figure 4.3 Fisher Sub-Sieve Sizer WLP-208.

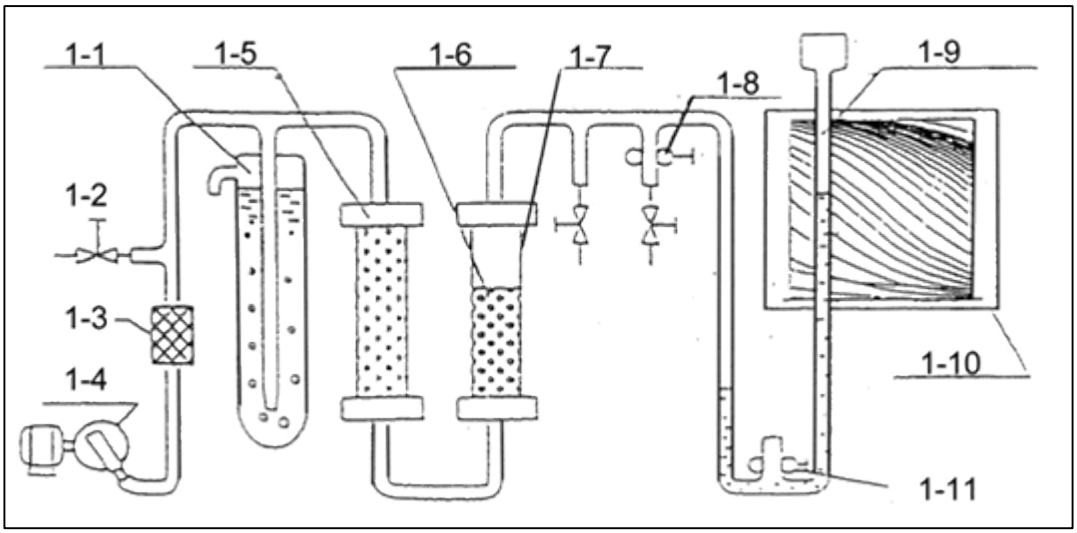

Figure 4.4 Fisher sub-sieve sizer principle (Fisher sub-sieve sizer 2012).

4.4.1 The fsss sub-sieve sizer machine process

The air pump generates compressed air and the air passes through the air filter. The function was to remove impurities. After the pressure regulator, the air goes through the drier. The drier was made up of allochroic silica gel to dehydrate the sample. Air entered the sample tube, after passing through the packed powder sample. Compressed air entered the manometer. This air created a pressure drop which resulted in the water in the manometer to rise. The level of water in the manometer was an indication of the particle size for the powder being tested. The height was read on the chart which gave the average particle size of the powder. The unit worked on the formula (Eq. 16).

$$d_{VS} = \left(6 \times 10^4\right) \times \sqrt{k \times \frac{(1-\varepsilon)^2}{g \times \varepsilon^3} \times \frac{\eta L_U}{\Delta p}} \qquad \textbf{Eq. 16}$$

d_{VS}	=	Average diameter in microns
k	=	Shape factor
g	=	Acceleration of gravity
ε	=	Powder porosity
η	=	Viscosity of air
L	=	Length or height of compacted sample in cm
$_U$	=	Flow rate passing sample layer in cm/second
Δp	=	Pressure drop

Table 4.4 Reference table for the fisher sub-sieve sizer

Number	Function
1-1	Pressure Regulator
1-2	Pressure control
1-3	Air Filter
1-4	Air Pump
1-5	Drier
1-6	Packed powder sample
1-7	Sample tube
1-8	Range control
1-9	Manometer
1-10	Calculator chart
1-11	Manometer level control

Note that a standard sample tube is run after each analysis to ensure accuracy of analysis. The procedure when analyzing the particle size is described in Chapter 9, Appendix B.

4.5 Oxygen content

Oxygen content is the measure of the amount of oxygen that exists in the cobalt powder. The oxygen content was measured in percent and was measured by a LECO RO600. Every sample of sub-micron cobalt powder was tested for oxygen content. All samples were housed in a desiccant drier to prevent further oxidation in atmosphere. This was crucial to ensure accuracy of analysis. After every oxygen analysis, a standard known as the JK-47 was tested. There were five components that were checked before and after analysis (Table 4.5). The test method for oxygen analysis is in Chapter 9, Appendix B.

Table 4.5 Requirements during oxygen analysis

Factors	Requirement
Pressure of Helium	~ 1400 kPa
Tin capsule	To hold cobalt sample
Sample Weight	0.10 grams Co
JK-47	1.09 %
Upper Electrode	Clean with bristle brush

4.6 Particle size distribution

Laser diffraction is a technique that is based on the spatial distribution of scattered light. This light distribution is directly based on the particle size of the sample analyzed. This method is known to be very good and accurate for particle size distributions of 0.1µm to 3000 µm. Also an added advantage is that small samples are required for analysis. Another commonly used technique is the sieving analysis. The advantages of such a technique are that it is cheap, simple to use and it is well adapted for bulk materials. The major disadvantage of this technique is that the particle size distribution for the sub-micron cobalt powder cannot be measured by the sieving test method. The reason for this is the d_{90} on sub-micron cobalt powder is below 10 µm and the smallest sieve in the sieve test method can only measure a d_{90} of 37 µm. Hence it is not practical to use this test method to analyze particle size distribution. The analytical method used to test the particle size distribution produced from the jet mill experimentation is laser diffraction. The particle size distribution of sub-micron cobalt powder was measured by the Malvern Master-sizer 2000. This unit uses a laser diffraction technique (Figure 4.5). Essentially the particles are passed through a focused laser beam. These particles scatter light at an angle which is inversely proportional to the particle size. The angle and the intensity of the scattered light are measured by a series of photosensitive detectors. The particle size distribution is calculated by evaluating the scattering intensity in relation to the angle of the scatter light.

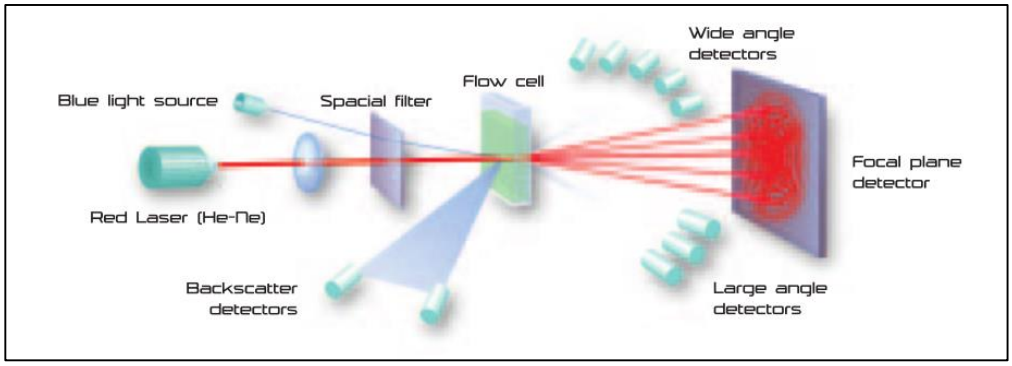

Figure 4.5 Fundamentals of the technology (A guidebook to particle size analysis 2012).

Laser diffraction results are reported as d_{10}, d_{50} and d_{90}. It also gives information on the surface weighted mean D [3,2] and the volume weighted mean D [4,3]. The particle size distribution analysis method is in Chapter 9, Appendix B.

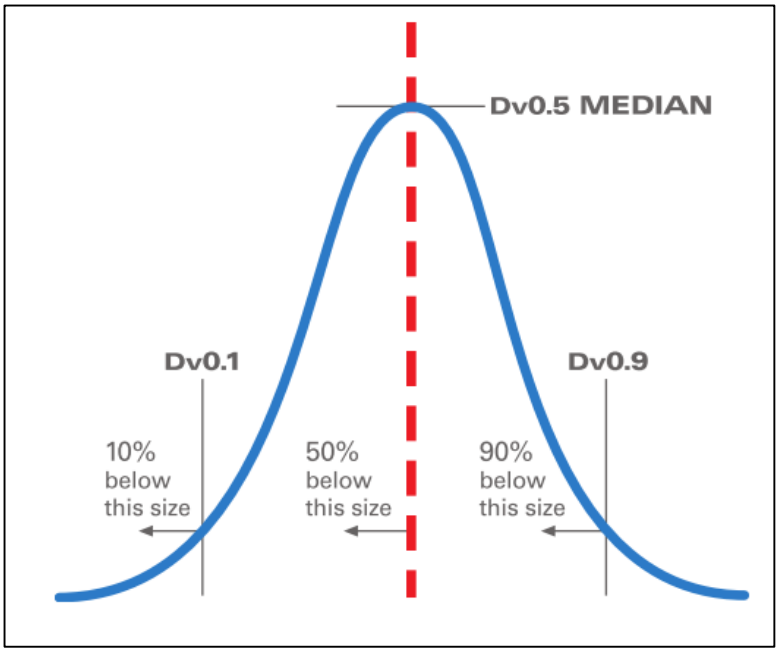

Figure 4.6 Demonstration of 3 axis values (A guidebook to particle size analysis 2012).

4.7 Design of Experiments

4.7.1 Furnace Experimentation

Design of experiments was used to formulate the matrix which defined how the experimental runs would be carried out. Each experimental run in the design matrix was carried out over three days, to determine average results yielded. For the furnace there were four design matrices generated for the experimentation on the furnace. The initial two design matrices were evaluated using the 2-level factorial analysis. These design matrices consisted of 6 center points and 22 runs each. The last two design matrixes for the furnace experimentation were evaluated using response surface central composite method and consisted of 30 and 46 runs each. In total there were 120 runs that were conducted on the furnace experimentation. Note six center points were selected for all the experimentations as the rule of thumb was a minimum of five center points should be selected in a design (Anderson and Whitcomb 2005:171). The objectives of the experimentation were to attain a particle size fsss range of 0.60 - 0.90 µm and an oxygen range of 0.3 - 0.8%. The results of the experimentation were evaluated by the use of response surface methodology. The cobalt compound used as the precursor was cobalt carbonate. Process parameter ranges for the factors were based on literature and plant experience. The reaction temperature for sub-micron cobalt powder production was assumed to take place between 300-500°C. The minimum ranges selected for hydrogen gas, carbon dioxide gas and belt speed were based on normal cobalt powder production (Fsss > 1.0 µm).

Table 4.6 Furnace Experimental parameters for design matrix 1

Factor	Range
Temperature	300 - 500 °C
Hydrogen Flow rate	100 - 200 Nm^3/h
Belt Speed	50 - 100 mm/min
Carbon Dioxide Flow rate	20 - 100 Nm^3/h

The initial experimental design matrix was based on a wide process operating range as per (Table 4.7). This approach yielded important results in determining the trend observed and the direction that the design would go in.

For the research, a two-level full factorial design was selected. A 2^4 factor full factorial design matrix (Table 4.7) was selected for the furnace experimentation.

Table 4.7 A 2^4 factor design matrix

Run	Comb.	Factors			
		A	B	C	D
1	(1)	-	-	-	-
2	a	+	-	-	-
3	b	-	+	-	-
4	ab	+	+	-	-
5	c	-	-	+	-
6	ac	+	-	+	-
7	bc	-	+	+	-
8	abc	+	+	+	-
9	d	-	-	-	+
10	ad	+	-	-	+
11	bd	-	+	-	+
12	abd	+	+	-	+
13	cd	-	-	+	+
14	acd	+	-	+	+
15	bcd	-	+	+	+
$16 = 2^4$	abcd	+	+	+	+

4.7.1 Jet mill Experimentation

The response variables studied on the jet mill were particle size distribution and milling time. The objectives of the experimentation were to attain a particle size distribution of d_{10} range of 2 - 3 µm, d_{50} in the range of 4.5 - 5.5 µm and d_{90} in the range of 7-10 µm. The main focus was on the d_{90} value. The second objective was to ensure that the time of milling was optimal to ensure that product quality was attained efficiently and effectively. Longer milling times would result in a back log of furnace product which negatively impacted productivity. Effective milling through the jet mill was important to ensure that there would be continuous production through the furnace. The operating variables assessed were classifier speeds, grinding gas pressure and AFG weight. For the jet mill there were three design matrices generated for the experimentation. The first design matrix consisted of 20 runs. A wide operating range for the operating variables was studied for the first experimentation (Table 4.8).

Table 4.8 Jet mill experimental parameters for design matrix 1

Factor	Range
Classifier speed	1000- 6000 rpm
Grinding gas pressure	2 - 7 bar
AFG weight	20 - 60 kgs

This approach yielded important results in determining the trend observed and the direction that the design would go in.

A 2^3 factor full factorial design matrix (Table 4.9) was selected for the jet mill experimentation.

Table 4.9 A 2^3 factor design matrix

Run	Comb.	Factors		
		A	B	C
1	(1)	-	-	-
2	a	+	-	-
3	b	-	+	-
4	ab	+	+	-
5	c	-	-	+
6	ac	+	-	+
7	bc	-	+	+
8	abc	+	+	+

4.8 Design Expert Software:

The design expert software was used to analyze the data generated by the experimentation. For the furnace experimentation the initial two design matrixes were generated by the use of the 2 level factorial design methods. As the response variables got closer to the optimum levels the response surface method was applied using the central composite design approach. This further modified the design matrix as there were additional experimental runs and center points and axial points. For the jet mill experimentation the response surface method was applied using the central composite design approach. The software analyzed the data produced from the experimentation and highlighted if the experimental data was adequate in determining the optimal settings for the unit under observation. The software assisted in laying out the approach of the experimentation by generating a model which graphically represented the data.

CHAPTER 5

RESULTS AND DISCUSSION

This chapter presents the experimental results for the production of sub-micron cobalt powder. Experimentation was conducted on an electrically heated furnace and a jet mill. Particle size, oxygen content and particle size distribution of sub-micron cobalt powder are the factors that define the end quality of the powder. These factors are the response variables.

5.1 Design of Experiments for Furnace experiment 1

5.1.1 Response Variable Fsss

Design of experiments 1 for the furnace experimentation was essentially a screening experiment to determine the effects of each factor on the response variables. Analytical data for process factors and response variables generated by design of experiments are represented in (Table 5.1). Response variables particle size and oxygen content was studied to determine the effects that each factor had on these response variables and the effect of their interactions. There was 6 center points that were selected for this design.

Table 5.1 Analytical data of factors and response variables for furnace experimentation 1

STD	RUN	Factor 1 - A TEMP °C	Factor 2 - B H_2 Nm^3/h	Factor 3 - C CO_2 Nm^3/h	Factor 4 - D BS mm/min	Response 1 FSSS µm	Response 2 O_2 %
19	1	400	150	60	75	0.6	1
14	2	500	100	100	100	1.08	0.59
16	3	500	200	100	100	1.13	0.42
20	4	400	150	60	75	0.62	1.01
12	5	500	200	20	100	1.15	0.48
15	6[1]	300	200	100	100	0.28	3
18	7	400	150	60	75	0.63	1.05
21	8	400	150	60	75	0.63	1.08
7	9[1]	300	200	100	50	0.45	1.5
22	10	400	150	60	75	0.61	0.99
11	11[1]	300	200	20	100	0.27	3.2
1	12[1]	300	100	20	50	0.39	2.2
13	13[1]	300	100	100	100	0.22	3.6
4	14	500	200	20	50	1.78	0.21
8	15	500	200	100	50	1.8	0.14
3	16[1]	300	200	20	50	0.46	1.75
6	17	500	100	100	50	1.7	0.33
2	18	500	100	20	50	1.69	0.41
17	19	400	150	60	75	0.6	1.02
10	20	500	100	20	100	1.06	0.49
9	21[1]	300	100	20	100	0.2	3.8
5	22[1]	300	100	100	50	0.39	2.1

For runs 6, 9, 11, 12, 13, 16, 21, and 22 experimental conditions were not sufficient to produce desired sub-micron cobalt powder. The center point experimental runs were run 1, 4, 7, 8, 10, and 19. The fsss analysis did not require a transform as the ratio between minimum and maximum response value was below 10. The effects of each factor on the response needed to be understood. The half normal plot (Figure 5.1) or Pareto chart (Figure 5.3) was used to graphically highlight the effects of the factors on the response variable.

[1] These runs generated sub-micron cobalt powder that was un-reduced and highly oxidized.

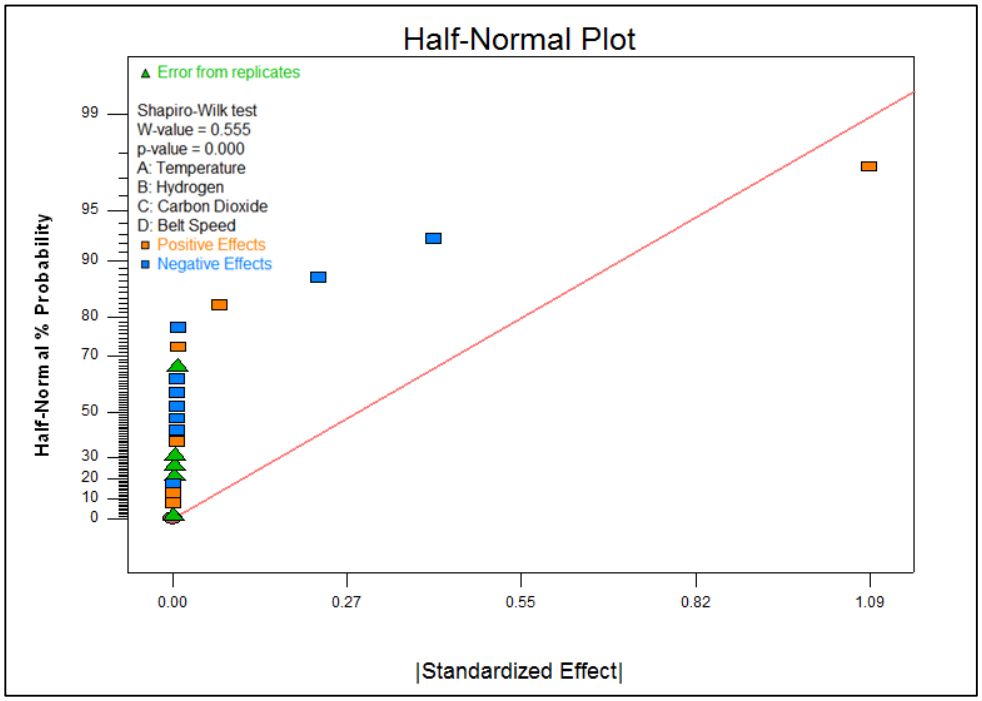

Figure 5.1 Half-normal probability for experimentation 1 for fsss (µm) un-selected effects.

The factors in the experimentation were assessed to determine if they followed a normal distribution. This assessment or test was called the Shapiro-Wilk test. The *p*-value was determined before and after selection of effects that fell of the line. The p-value was 0 when no effects were selected which indicated that the points of the design are not normally distributed. Note if the *p*-value was greater than 0.10 before selection of effects, this indicated that there were no statistically significant effects. All factors that fell below the red line and that was farther away from the red line (closer to the bottom right hand corner) was selected as significant effects. Usually effects closer to the red line are a result of noise or interference.

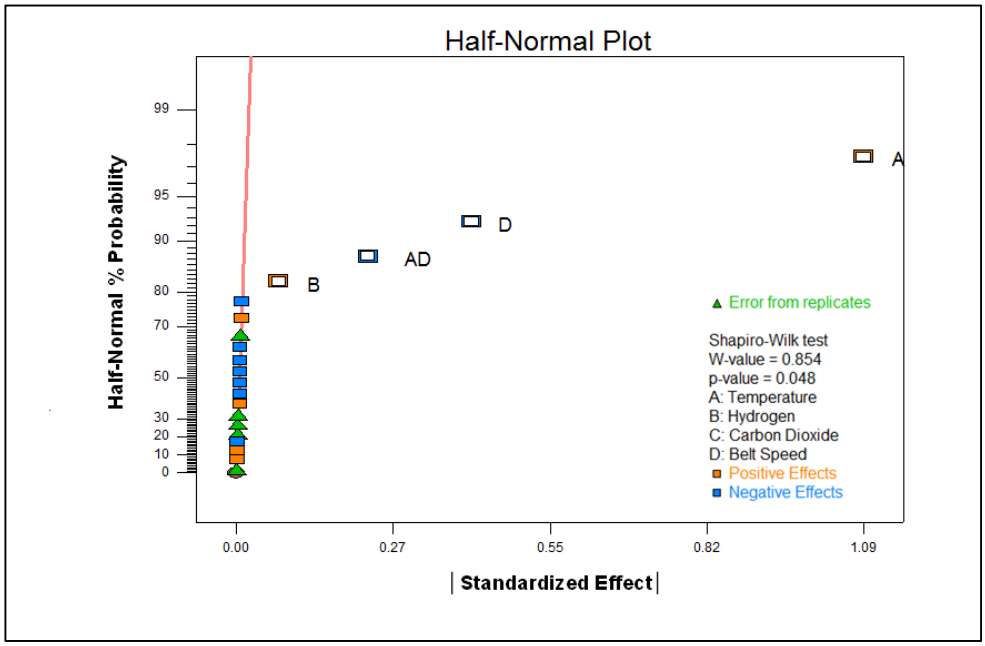

Figure 5.2 Half-normal probability for experimentation 1 for fsss (µm) selected effects.

Figure 5.2 was a replication of Figure 5.1 after effects had been selected. Factor A (temperature), D (belt speed), B (hydrogen flow rate), and the two factor interaction AD (temperature × belt speed) were selected as main effects. The *p*-value generated after the selection was 0.048. The concern here was that the *p*-value was below 0.10 which indicated that there could be deviation from the assumption of normality of non-selected effects.

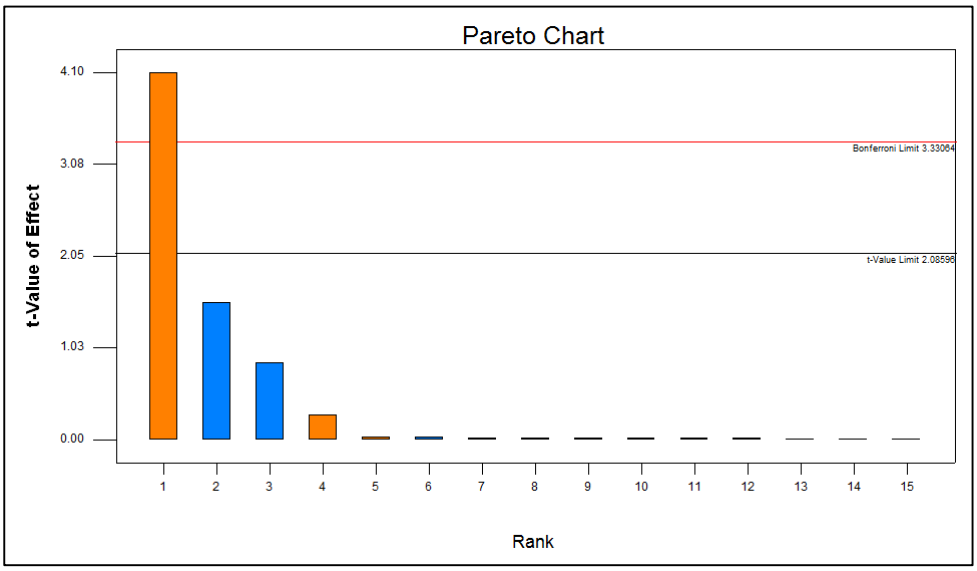

Figure 5.3 Pareto chart for experimentation 1 for fsss (µm) un-selected effects.

Figure 5.3 is the Pareto chart highlighting the magnitude of the effects in the experimentation. It is figure 5.1 represented as a Pareto chart.

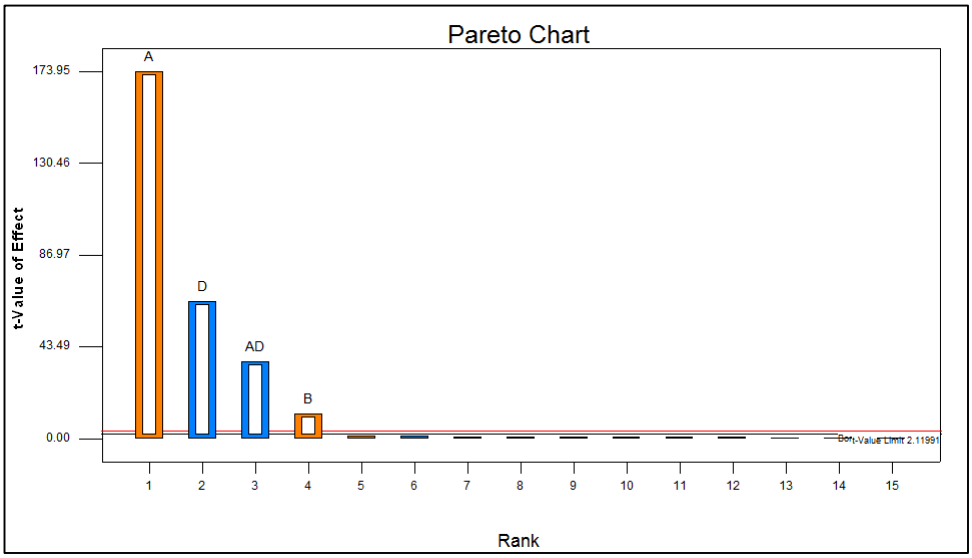

Figure 5.4 Pareto chart for experimentation 1 for fsss (µm) selected effects.

The selected effects are above the Bonferroni and t-value limit. The orange colour represents a positive effect indicating an increase effect on the response. The blue colour represents a negative effect indicating a decrease effect on the response. The chart (Figure 5.4) indicates that factor A which was temperature had the single largest positive effect on particle size (fsss). An increase in temperature (A) would result in a higher particle size. An increase in hydrogen gas flow rate (B) would have a small effect on particle size. An increase in belt speed (D) and a combination of an increase in belt speed and temperature (AD) would result in a lower particle size.

Table 5.2 Anova of fsss for furnace experimentation 1

Source	Sum of Squares	df	Mean Square	F Value	p-value Prob > F	Significance
Model	5.66	4	1.42	8992.83	< 0.0001	Significant
A-Temperature	4.76	1	4.76	30258.22	< 0.0001	Significant
B-Hydrogen	0.022	1	0.022	138.2	< 0.0001	Significant
D-Belt Speed	0.67	1	0.67	4245.32	< 0.0001	Significant
AD	0.21	1	0.21	1329.59	< 0.0001	Significant
Curvature	0.3	1	0.30	1919.14	< 0.0001	Significant
Residual	0.00252	16	0.00016	-	-	-
Lack of Fit	0.00157	11	0.00014	0.75	0.6797	Not significant
Pure Error	0.00095	5	0.00019	-	-	-
Cor Total	5.97	21	-	-	-	-

The model F value of 8992.83 in (Table 5.2) implied that the model was significant. There was only a 0.01% chance that a "Model F-value" this large could occur due to noise. When the values of Prob > F was less than 0.05 this indicated that the model terms are significant. The curvature F value of 1919.14 indicates that curvature was significant. The lack of fit F-value of 0.75 implies that this value was not significant. There is a 67.97% chance that a lack of fit F-value this large could occur due to noise.

Table 5.3 Model applicability and precision for fsss (µm)

Std. Dev.	0.013	R-Squared	0.9996
Mean	0.81	Adj R-Squared	0.9994
C.V. %	1.56	Pred R-Squared	0.9992
PRESS	0.00469	Adeq Precision	240.181

The predicted r-squared of 0.9992 in (Table 5.3) was in reasonable agreement with the adjusted r-squared of 0.9994. Adequate precision measures the signal to noise ratio. A ratio greater than 4 was desirable. The ratio of 240.181 indicates an adequate signal.

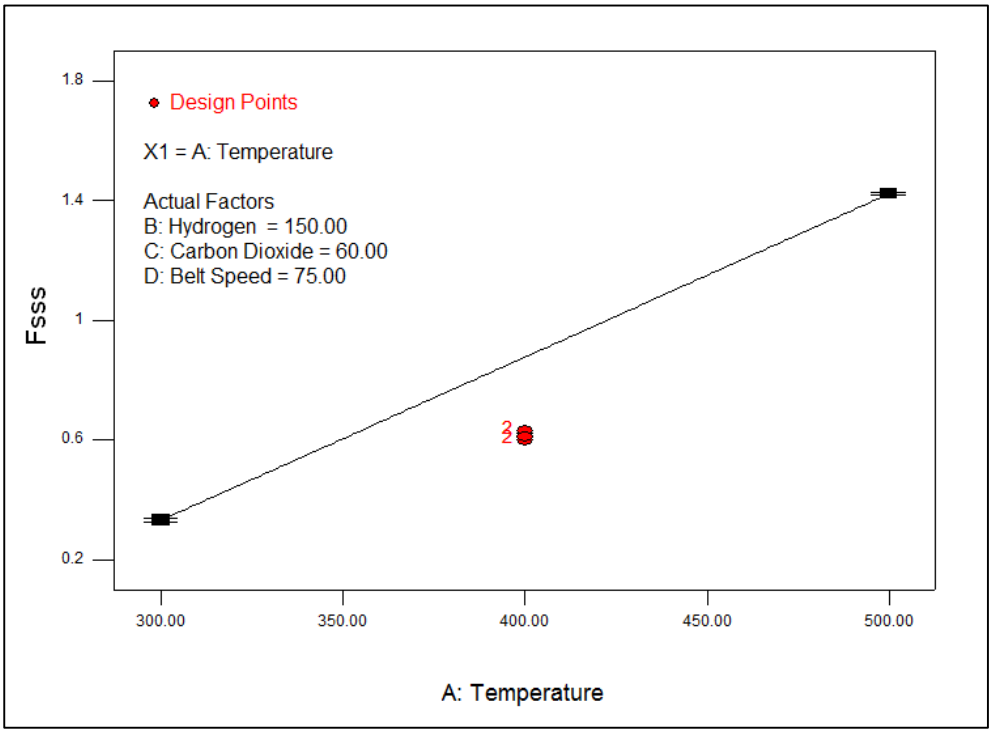

Figure 5.5 Model graph for the effects of temperature (°C) on fsss (µm).

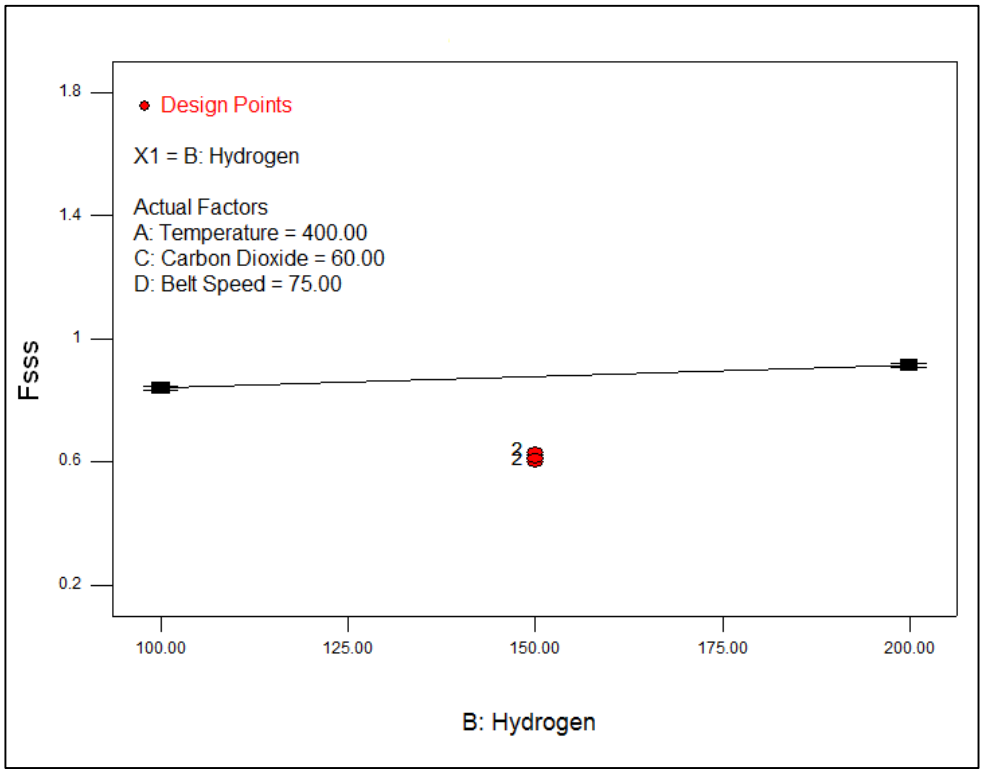

Figure 5.6 Model graph for the effects of hydrogen gas flow rate (Nm^3/h) on fsss (µm).

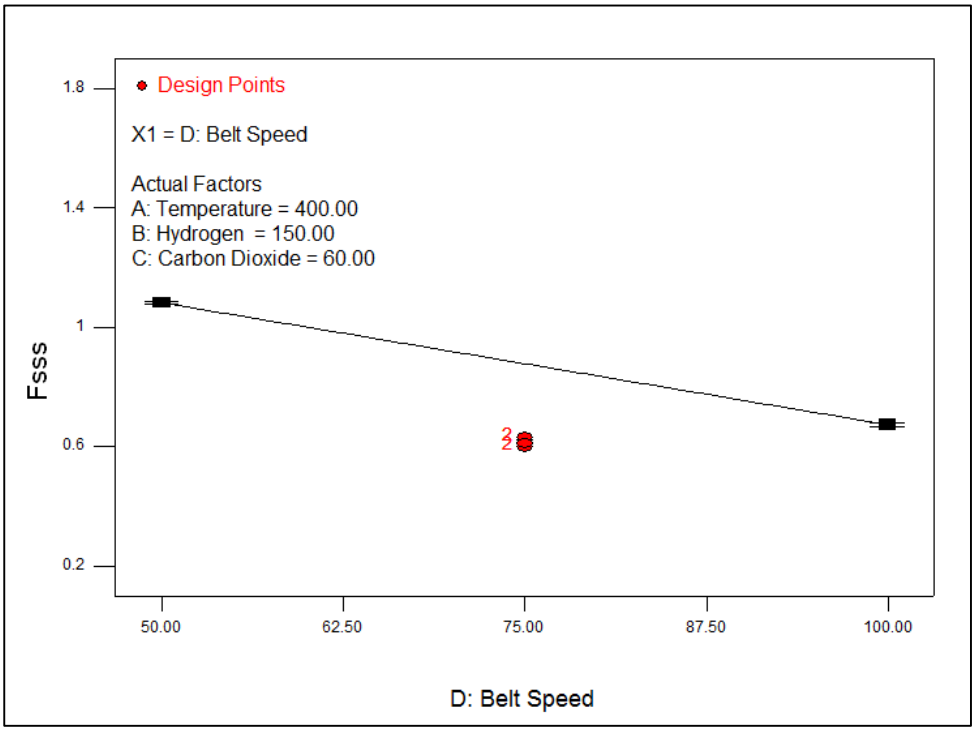

Figure 5.7 Model graph for the effects of belt speed (mm/min) on fsss (µm).

The interaction between fsss and temperature (Figure 5.5) highlights that as temperature increases, fsss on the powder increases. The interaction between fsss and hydrogen gas flow rate (Figure 5.6) highlights that at high volumes of hydrogen gas flow rate the fsss on the powder slightly increases. The interaction between fsss and belt speed (Figure 5.7) highlights that when belt speed is increased, the fsss on the powder decreases.

5.1.2 Response Variable Oxygen

The oxygen analysis required a transform as the ratio between minimum and maximum response value was above 10. The transform selected was guided by the Box-Cox power transform diagnostic tool. The suggested transformation was square root for oxygen.

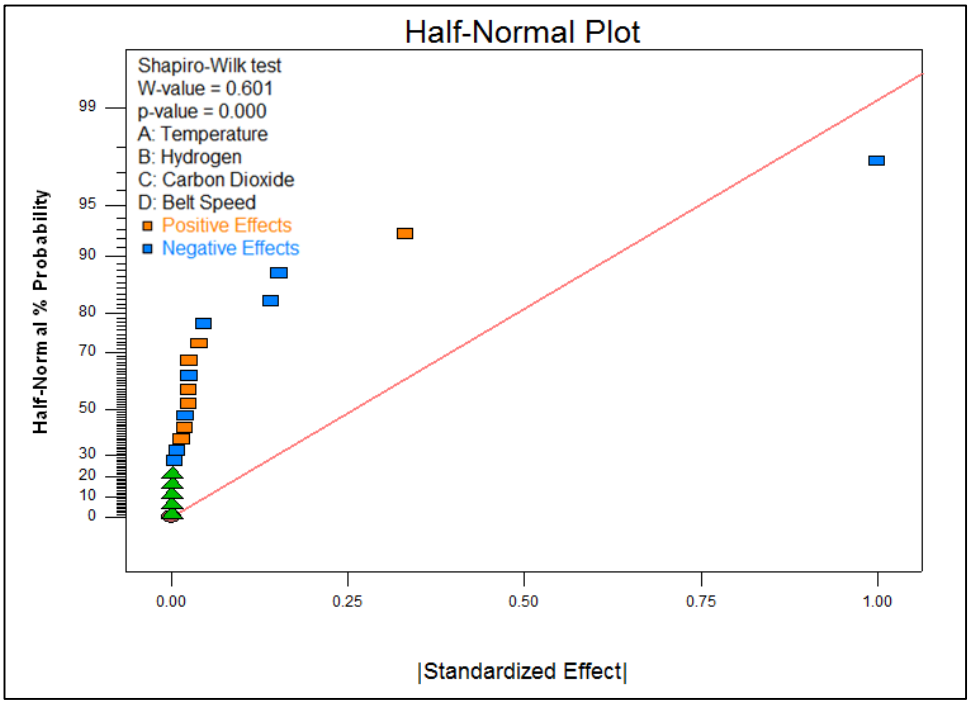

Figure 5.8 Half-normal probability for experimentation 1 for Oxygen (%) Un-selected effects.

The *p*-value is zero (Figure 5.8) when no effects are selected which indicates that the points of the design are not normally distributed.

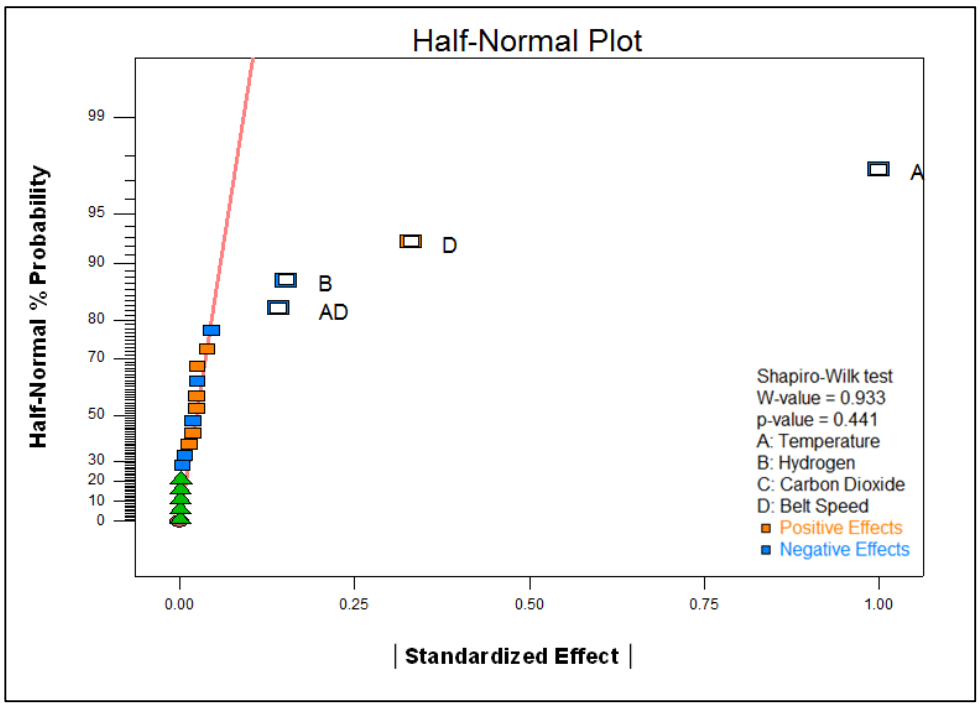

Figure 5.9 Half-normal probability for experimentation 1 for oxygen (%) selected effects.

Figure 5.9 is a replication of Figure 5.8 however it includes the selected effects. Factors A (temperature), D (belt speed), B (hydrogen flow rate), and the two factor interaction AD (temperature × belt speed) are selected as main effects in Figure 5.9. The *p*-value generated after the selection is 0.441.

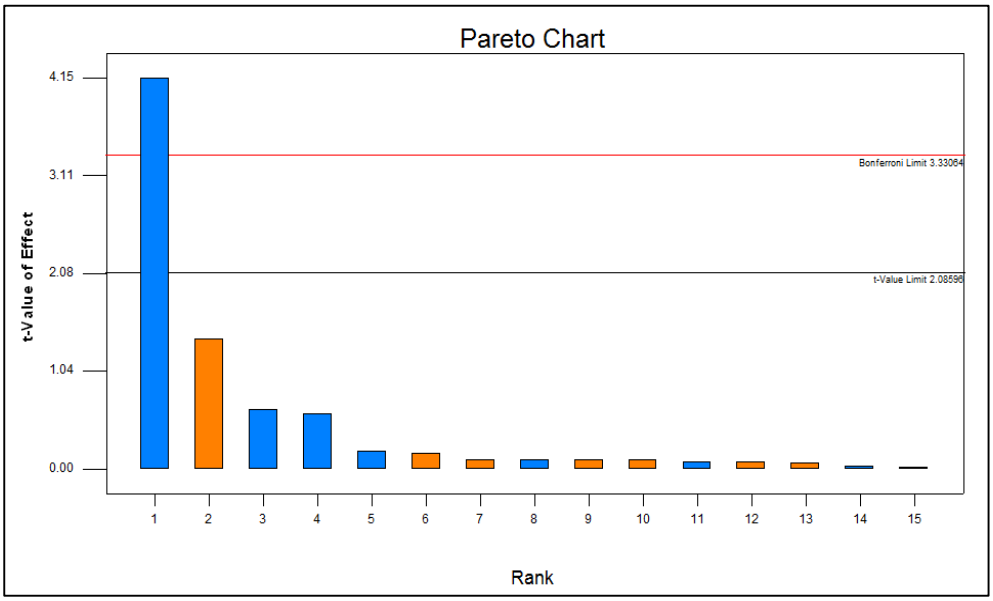

Figure 5.10 Pareto chart for experimentation 1 for oxygen (%) un-selected effects.

Pareto chart in Figure 5.10 is highlighting the magnitude of the effects in the experimentation.

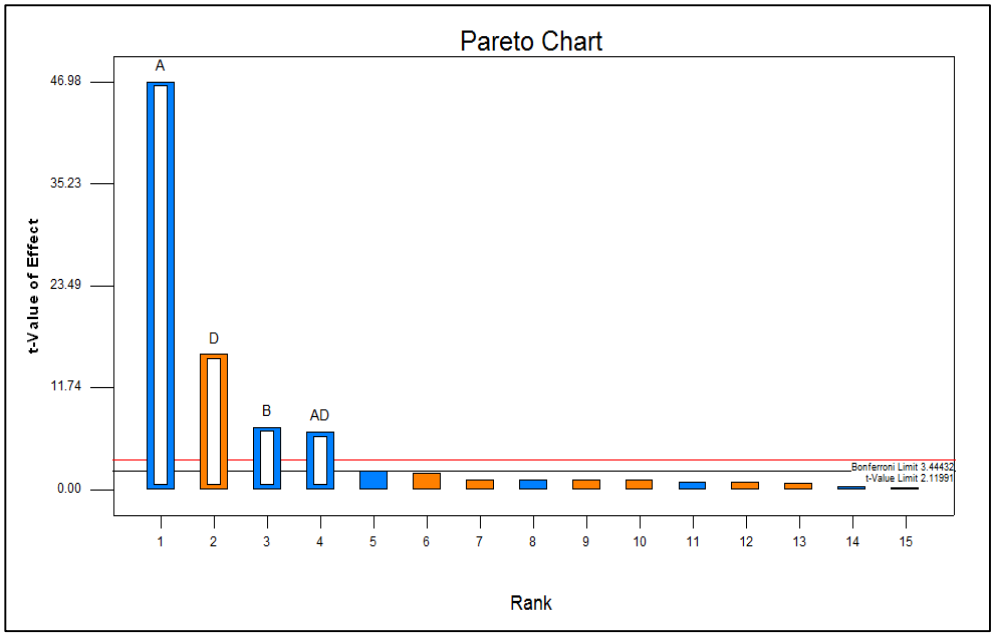

Figure 5.11 Pareto chart for experimentation 1 for oxygen (%) selected effects.

The selected effects are above the Bonferroni and t-value limit. Figure 5.11 indicates that factor A which is temperature has the single largest negative effect on particle size (fsss). An increase in temperature (A), hydrogen gas flow rate (B) and the combination of temperature and belt speed (AD) will result in lower oxygen content. An increase in belt speed (D) will result in higher oxygen content.

Table 5.4 Anova of oxygen for furnace experimentation 1

Source	Sum of Squares	df	Mean Square	F Value	p-value Prob > F	Significance
Model	4.6	4	1.15	616.31	< 0.0001	significant
A-Temperature	3.99	1	3.99	2137.96	< 0.0001	significant
B-Hydrogen	0.093	1	0.093	49.84	< 0.0001	significant
D-Belt Speed	0.44	1	0.44	235.00	< 0.0001	significant
AD	0.079	1	0.079	42.43	< 0.0001	significant
Curvature	0.39	1	0.32	20.73	< 0.0001	significant
Residual	0.030	16	0.00181	-	-	-
Lack of Fit	0.028	11	0.00259	9.32	0.0116	significant
Pure Error	0.001389	5	0.0002778	-	-	-
Cor Total	4.67	21	-	-	-	-

The model F value of 616.31 in (Table 5.4) implied that the model was significant. There was only a 0.01% chance that a "Model F-value" this large could occur due to noise. When the values of Prob > F was less than 0.05 this indicated that the model terms are significant. The curvature F value of 20.73 indicated that curvature was significant. There was only 0.03% chance of a curvature f-value this large could occur due to noise. The lack of fit F-value of 9.32 implied that this value was significant. There was a 1.16% chance that a lack of fit F-value this large could occur due to noise.

Table 5.5 Model applicability and precision for oxygen (%)

Std. Dev.	0.043	R-Squared	0.9936
Mean	1.08	Adj R-Squared	0.9919
C.V. %	4.00	Pred R-Squared	0.9867
PRESS	0.062	Adeq Precision	65.706

The predicted r-squared of 0.9867 in (Table 5.5) was in reasonable agreement with the adjusted r-squared of 0.9919. Adequate precision measures the signal to noise ratio. A ratio greater than 4 was desirable. The ratio of 65.706 indicates an adequate signal.

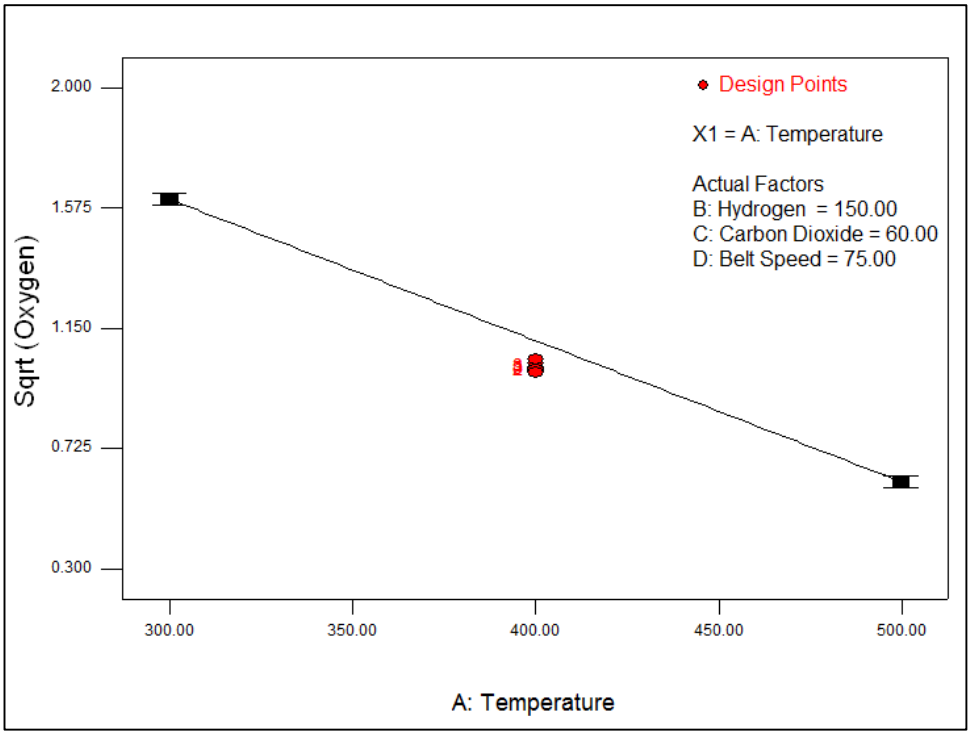

Figure 5.12 Model graph for the effects of temperature (°C) on oxygen (%).

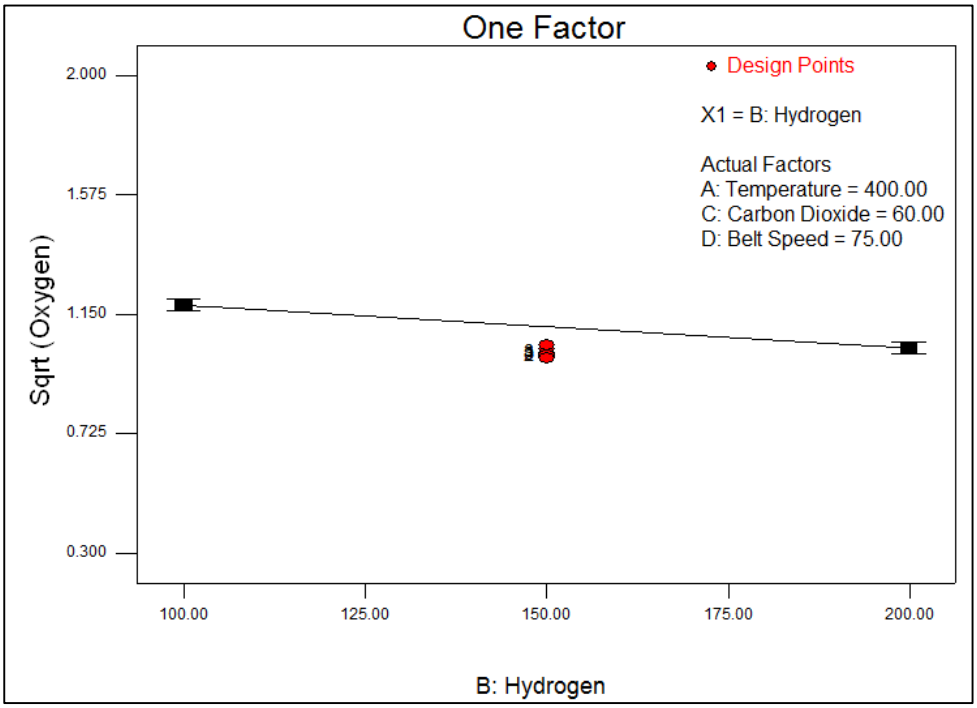

Figure 5.13 Model graph for the effects of hydrogen gas flow rate (Nm^3/h) on oxygen (%).

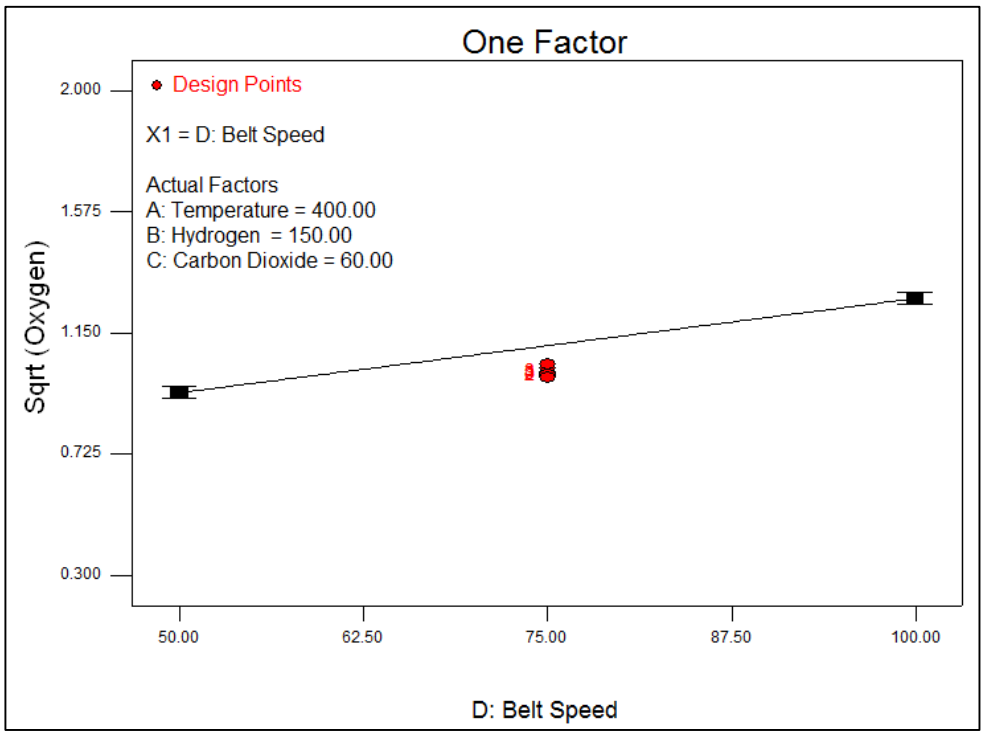

Figure 5.14 Model graph for the effects of belt speed (mm/min) on oxygen (%).

The interaction between oxygen (sqrt) and temperature (Figure 5.12) highlights that as temperature increases, oxygen content in the powder decreases. The interaction between oxygen

(sqrt) and hydrogen gas flow rate (Figure 5.13) highlights that at high volumes of hydrogen gas flow rate the oxygen content in the powder slightly decreases. The interaction between oxygen (sqrt) and belt speed (Figure 5.14) highlights that when belt speed is increased, the oxygen content in the powder increases.

5.1.3 Trends observed for furnace experimentation 1 (Particle size & Oxygen)

The first experimental design consisted of 22 runs. It defined the trends observed between individual and combined factors on the response variables. The initial trial highlighted the relationship shared between the two response variables particle size and oxygen. To attain desired value for particle size and oxygen operational parameters had to be set to accommodate both response variables. This posed the challenge as particle size and oxygen shared an inversely proportional relationship. The experimental design set out by design of experiments consisted of varying operational parameters such as temperature, hydrogen gas flow rate, and carbon dioxide flow rate and belt speed.

The trend observed for experiment 1 in relation to the response variable particle size was that temperature, belt speed and hydrogen gas affected the particle size by minimizing or maximizing the particle size. The second trend observed in relation to response variable oxygen was that temperature, hydrogen gas and belt speed affected the oxygen content by minimizing or maximizing the oxygen content. It was noted that carbon dioxide gas flow rate had no effect on particle size and very little effect on oxygen content. This operating parameter was not eliminated immediately because although it did not minimize the response variable it contributed greatly to the passivation and state of the end product. This was highlighted in experimental runs 6, 9, 13 and 22 when carbon dioxide was used in high volumes. Powder produced in these runs were not decomposed and reduced properly, however it was highly passivated by carbon dioxide and therefore it did not combust even though the powder was in an oxidized state. This was seen in the other design experiments. For experimental runs 11, 12, 16 and 21, flow rates of 20 Nm^3/h of carbon dioxide was not sufficient to prevent combustion of the powder. Hence the objective for analyzing carbon dioxide gas flow rate was to determine the efficient volume required for ideal passivation. The center point experimental runs indicated that there was repeatability with results as the response variables showed little deviation during the center point experimental runs.

This experimental design concluded that at temperatures of 300°C, the precursor is not reduced properly and therefore the cobalt powder produced was in an unstable state in which it

spontaneously combusts. Temperatures greater than and equal to 500°C yielded powder with a particle size greater than 1 micron even at maximum belt speed on the furnace. It was observed that higher volumes of hydrogen gas reduced oxygen content of the cobalt powder significantly at constant operating conditions. Similarly belt speed was observed to control particle size and oxygen content simultaneously at constant operating conditions. The challenge faced was that temperature had opposite effects on both responses. Temperature had a positive effect on particle size and a negative effect for oxygen. Therefore the combination of temperature with factors such as belt speed and hydrogen gas was crucial to investigate in order to obtain both response variables at optimum.

The analysis and trends observed for design matrix 2 which was analyzed by design of experiments are presented in Chapter 8, section 8.1. The analysis and trends observed for design matrix 3 which was analyzed by response surface central composite design are presented in Chapter 8, section 8.2.

Design matrix 4 is the final experiment that was conducted. This experimental design attained the production of sub-micron cobalt powder with the desired particle size and oxygen content.

5.2 Response surface methodology for furnace experiment 4

Design matrix 4 represented the last experiment for the furnace. The design method was response surface methodology using central composite design. There were 3 axial points and 6 center points that were selected for the design. The alpha value selected was at 1.36 which was an orthogonal quadratic alpha as it was the least extreme as compared to the other alpha values. This set the cubical portion of the central composite design. The design range was represented in (Table 5.6).

Table 5.6 Design range for the central composite design to optimize conditions for cobalt powder production

Factor	Units	-1 Level	+1 Level	(-) alpha	(+) alpha
Temperature	°C	445	475	440	480
Hydrogen gas	Nm^3/h	200	250	191	259
Carbon dioxide gas	Nm^3/h	80	100	76	104
Belt speed	mm/min	80	100	76	104

Altogether there were 46 runs for experimentation 4 of which consisted of 6 center points and 3 axial points for each factor. The range for each factor was narrowed as each experimentation was run.

Table 5.7 Design summary for furnace experimentation 4

Factor	Name	Units	Type	Low Actual	High Actual	Low Coded	High Coded	Mean	Std. Dev.
A	Temperature	°C	Numeric	445	475	-1	1	460	11.519
B	Hydrogen gas	Nm^3/h	Numeric	200	250	-1	1	225	19.199
C	Carbon Dioxide gas	Nm^3/h	Numeric	80	100	-1	1	90	7.68
D	Belt speed	mm/min	Numeric	80	100	-1	1	90	7.68

The design summary for design matrix 4 is represented in (Table 5.7).

The design matrix (Table 5.8) determined how each run would be conducted.

Table 5.8 Analytical data of factors and response variables for furnace experimentation 4

Std	Run	Factor 1 - A TEMP (°C)	Factor 2 - B H_2 (Nm_3/h)	Factor 3 - C CO_2 (Nm^3/h)	Factor 4 - D BS (mm/min)	Response - 1 Fsss (μm)	Response - 2 Oxygen (%)
25	1	460	191	90	90	0.72	0.68
17	2^2	440	225	90	90	0.4	0.99
38	3^2	460	225	90	104	0.6	0.9
23	4	460	191	90	90	0.78	0.6
39	5	460	225	90	104	0.65	0.79
22	6^2	480	225	90	90	0.95	0.5
43	7	460	225	90	90	0.7	0.6
12	8	475	250	80	100	0.8	0.6
21	9^2	480	225	90	90	1.01	0.41
42	10	460	225	90	90	0.77	0.51
18	11^2	440	225	90	90	0.38	1.1
2	12^2	475	200	80	80	0.99	0.4
13	13^2	445	200	100	100	0.4	0.9
41	14	460	225	90	90	0.8	0.49
11	15^2	445	250	80	100	0.42	0.97
15	16^2	445	250	100	100	0.35	1.09
28	17	460	259	90	90	0.82	0.45
46	18	460	225	90	90	0.75	0.58
7	19^2	445	250	100	80	0.62	0.9
9	20^2	445	200	80	100	0.47	0.92
8	21^2	475	250	100	80	1.01	0.38
1	22^2	445	200	80	80	0.65	1.01
10	23	475	200	80	100	0.75	0.78
16	24	475	250	100	100	0.7	0.65
19	25^2	440	225	90	90	0.35	1.05
5	26^2	445	200	100	80	0.68	0.95
44	27	460	225	90	90	0.71	0.6
24	28	460	191	90	90	0.78	0.71
35	29	460	225	90	76	0.9	0.4
32	30	460	225	104	90	0.77	0.85
40	31^2	460	225	90	104	0.6	1.01
31	32	460	225	76	90	0.7	0.67
34	33	460	225	104	90	0.75	0.6
33	34	460	225	104	90	0.73	0.65
4	35^2	475	250	80	80	1.15	0.35
26	36	460	259	90	90	0.87	0.45
3	37^2	445	250	80	80	0.63	0.78

Std	Run	Factor 1 - A TEMP (°C)	Factor 2 - B H_2 (Nm_3/h)	Factor 3 - C CO_2 (Nm^3/h)	Factor 4 - D BS (mm/min)	Response - 1 Fsss (µm)	Response - 2 Oxygen (%)
37	41	460	225	90	76	0.92	0.4
45	42	460	225	90	90	0.78	0.59
6	43[2]	475	200	100	80	1.09	0.5
29	44	460	225	76	90	0.78	0.68
27	45	460	259	90	90	0.72	0.62
36	46[2]	460	225	90	76	0.99	0.33

The following runs produced normal cobalt powder with a particle size > 0.95 µm, these were runs 6, 9, 12, 12, 21, 35, 43 and 46. The following runs produced cobalt powder that was unreduced and highly oxidized; these were runs 2, 3, 11, 13, 15, 16, 19, 20, 22, 25, 26, 31, and 37. The design trend between oxygen and fsss for experimentation 4 is represented in (Figure 5.15).

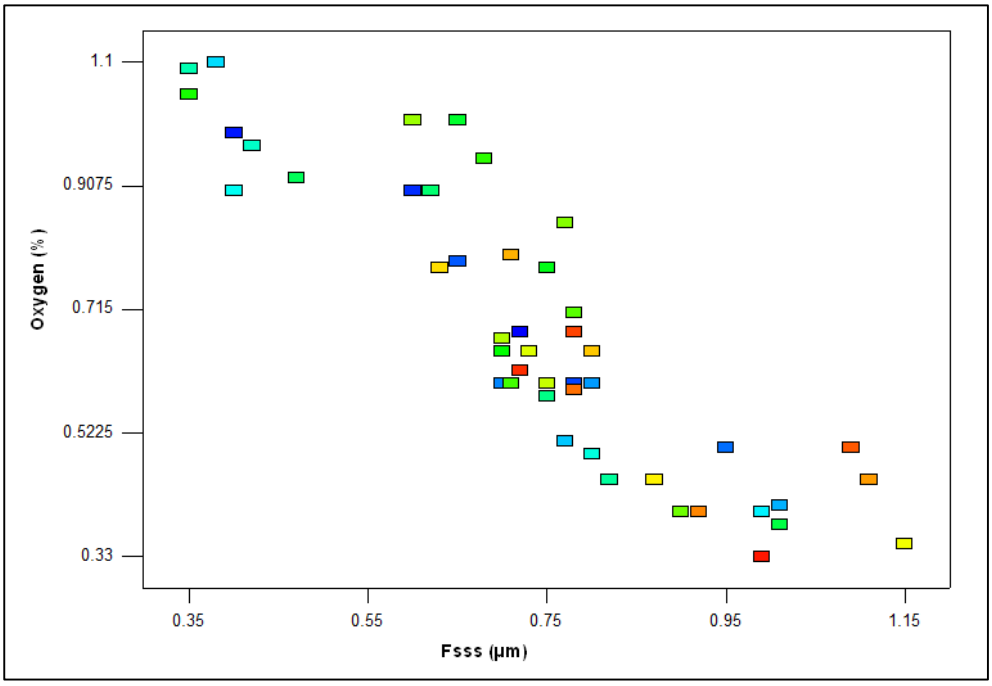

Figure 5.15: The design trend between fsss and oxygen for experimentation 4

[2] These runs consist of powder that is unreduced and highly oxidized to powder that is classified as normal cobalt powder.

5.2.1 Response Variable Fsss

The fsss analysis did not require a transform as the ratio between the minimum and maximum response value was 3.28. A transform is only required when the ratio is greater than 10.

Table 5.9 Model summary statistics for fsss

Std. Source	Adjusted Dev.	R-Squared	Adjusted R-Squared	Predicted R-Squared	PRESS
Linear	0.06	0.9168	0.9087	0.893	0.19
2FI	0.059	0.9308	0.911	0.8581	0.25
Quadratic	0.052	0.952	0.9303	0.8813	0.21
Cubic	0.048	0.9698	0.9409	0.7514	0.44

The model summary (Figure 5.9) indicated that a cubic model was aliased. When a model is aliased this means that there are not enough unique design points to estimate all the model coefficients. The model suggested was the quadratic model as this has a maximum predicted R-squared and adjusted R-squared value.

Table 5.10 Lack of fit tests for fsss

Sum of Source	Mean Squares	F (df)	p-value Square	Value	Prob > F
Linear	0.099	20	0.00495	2.13	0.0468
2FI	0.074	14	0.00530	2.28	0.0428
Quadratic	0.036	10	0.00365	1.57	0.1841
Cubic	4.82E-03	2	0.00241	1.04	0.372
Pure Error	0.049	21	0.00233		

The lack of fit tests (Table 5.10) compared residual error with pure error from replicated design points. A significant lack of fit was represented by a low Prob > F value. The quadratic model was highlighted again as the suggested model as it does not show significant lack of fit.

Table 5.11 Anova of fsss for furnace experimentation 4

Source	Sum of Squares	df	Mean Square	F Value	p-value Prob > F	Significance
Model	1.69	14	0.12	43.89	< 0.0001	Significant
A-temp	1.17	1	1.17	423.36	< 0.0001	Significant
B-hydrogen gas	5.05E-04	1	5.05E-04	0.18	0.6713	
C-carbon dioxide	4.28E-03	1	4.28E-03	1.56	0.2216	
D-belt speed	0.46	1	0.46	166.66	< 0.0001	Significant
AB	5.63E-03	1	5.63E-03	2.04	0.1628	
AC	2.25E-04	1	2.25E-04	0.082	0.7768	
AD	7.23E-03	1	7.23E-03	2.63	0.1153	
BC	7.23E-03	1	7.23E-03	2.63	0.1153	
BD	2.25E-04	1	2.25E-04	0.082	0.7768	
CD	4.23E-03	1	4.23E-03	1.54	0.2246	
A^2	0.035	1	0.035	12.64	0.0012	Significant
B^2	1.83E-04	1	1.83E-04	0.066	0.7984	
C^2	2.68E-03	1	2.68E-03	0.98	0.3311	
D^2	1.61E-06	1	1.61E-06	5.86E-04	0.9808	
Residual	0.085	31	2.75E-03			
Lack of Fit	0.036	10	3.65E-03	1.57	0.1841	Not Significant
Pure Error	0.049	21	2.33E-03			
Cor Total	1.78	45				

The model F-value of 43.89 in (Table 5.11) indicated that the model was significant. Model terms A, D and A^2 were significant. Model term A^2 had a small effect on particle in relation to model terms A and D. The lack of fit value of 1.57 indicated that there was an insignificant lack of fit which implies that the model could fit the data

Table 5.12 Model applicability and precision for fsss (experimentation 4)

Std. Dev.	0.052	R-Squared	0.952
Mean	0.74	Adj R-Squared	0.9303
C.V. %	7.1	Pred R-Squared	0.8813
PRESS	0.21	Adeq Precision	26.276

The predicted R-squared and the adjusted R-squared in (Table 5.12) were in agreement with each other. The adequate precision value of 26.276 indicated an adequate signal.

The final equation generated in terms of actual factors is:

$$\begin{aligned} FSSS = {} & (-48.67649) + (+0.18543 \times T) + (-0.015969 \times H_2) + (+0.064516 \times CO_2) + \\ & (+0.069661 \times BS) + (+5.0E^{-05} \times T \times H_2) + (-2.5E^{-05} \times T \times CO_2) + \\ & (-1.42E^{-04} \times T \times BS) + (-8.5E^{-05} \times H_2 \times CO_2) + (-1.5E^{-05} \times H_2 \times BS) + \\ & (-1.625E^{-04} \times CO_2 \times BS) + (-1.82E^{-04} \times T^2) + (+4.76E^{-06} \times H_2^{\,2}) + \\ & (-1.14E^{-04} \times CO_2^{\,2}) + (+2.79E^{-06} \times BS^2) \end{aligned}$$

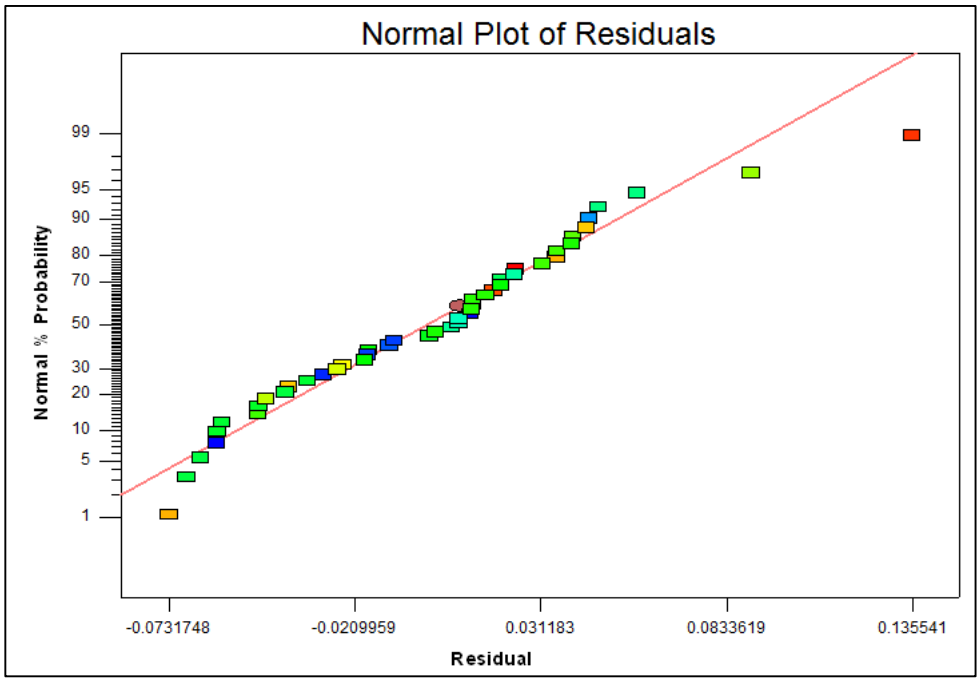

Figure 5.16 Normal Plot vs. Residual for fsss.

The data points (Figure 5.16) represent a linear pattern which was desired as a non-linear pattern indicates non-normality in the error term.

5.2.2 Response Variable Oxygen

The oxygen analysis did not require a transform as the ratio between the minimum and maximum response value was 3.33. A transform is only required when the ratio is greater than 10.

Table 5.13 Model summary statistics for oxygen

Std. Source	Adjusted Dev.	R-Squared	Adjusted R-Squared	Predicted R-Squared	PRESS
Linear	0.06	0.9168	0.9087	0.893	0.19
2FI	0.059	0.9308	0.911	0.8581	0.25
Quadratic	0.052	0.952	0.9303	0.8813	0.21
Cubic	0.048	0.9698	0.9409	0.7514	0.44

The model summary (Table 5.13) indicated that a cubic model is aliased. The model suggested is the quadratic model as this has a maximum predicted R-squared and adjusted R-squared value.

Table 5.14 Lack of fit test oxygen

Sum of Source	Mean Squares	F (df)	p-value Square	Value	Prob > F
Linear	0.45	20	0.023	4.31	0.0008
2FI	0.37	14	0.026	5.02	0.0005
Quadratic	0.12	10	0.012	2.26	0.0557
Cubic	3.63E-03	2	1.82E-03	0.34	0.7125
Pure Error	0.11	21	5.27E-03		

The lack of fit tests (Table 5.14) compared residual error with pure error from replicated design points. A significant lack of fit was represented by a low Prob > F value. The quadratic model was highlighted again as the suggested model as it did not show significant lack of fit.

Table 5.15 Anova of oxygen for furnace experimentation 4

Source	Sum of Squares	df	Mean Square	F Value	p- value Prob > F	Significance
Model	1.98	14	0.14	19.05	< 0.0001	Significant
A-temp	1.11	1	1.11	149.65	< 0.0001	Significant
B-hydrogen gas	0.051	1	0.051	6.93	0.0131	
C-carbon dioxide	9.08E-03	1	9.08E-03	1.23	0.2769	
D-belt speed	0.47	1	0.47	63.71	< 0.0001	Significant
AB	0.013	1	0.013	1.79	0.1912	
AC	1.00E-04	1	1.00E-04	0.013	0.9083	
AD	0.058	1	0.058	7.78	0.009	
BC	4.90E-03	1	4.90E-03	0.66	0.4223	
BD	8.10E-03	1	8.10E-03	1.09	0.3038	
CD	2.50E-05	1	2.50E-05	3.38E-03	0.954	
A^2	0.17	1	0.17	22.94	< 0.0001	Significant
B^2	6.57E-05	1	6.57E-05	8.86E-03	0.9256	
C^2	0.062	1	0.062	8.37	0.0069	
D^2	0.019	1	0.019	2.6	0.1171	
Residual	0.23	31	7.41E-03			
Lack of Fit	0.12	10	0.012	2.26	0.0557	Not Significant
Pure Error	0.11	21	5.27E-03			
Cor Total	2.21	45				

The model F-value of 19.05 in (Table 5.15) indicated that the model was significant. Model terms A, D and A^2 are significant. The lack of fit value of 2.26 indicated that there was an insignificant lack of fit which is good as we wanted the model to fit.

Table 5.16: Model applicability and precision for oxygen (experimentation 4)

Std. Dev.	0.086	R-Squared	0.8959
Mean	0.68	Adj R-Squared	0.8489
C.V. %	12.65	Pred R-Squared	0.7048
PRESS	0.65	Adeq Precision	17.135

The predicted R-squared and the adjusted R-squared in (Table 5.16) are in agreement with each other. The adequate precision value of 17.135 is indicates an adequate signal.

The final equation generated in terms of actual factors is:

$$Oxygen = (+110.65840) + (-0.40474 \times T) + (+0.017843 \times H_2) + (-0.11910 \times CO_2) + (-0.24490 \times BS) + (-7.67E^{-05} \times T \times H_2) + (+1.67E^{-05} \times T \times CO_2) + (+4.00E^{-04} \times T \times BS) + (+7.00E^{-05} \times H_2 \times CO_2) + (+9.00E^{-05} \times H_2 \times BS) + (-1.25E^{-05} \times CO_2 \times BS) + (+4.03E^{-04} \times T^2) + (+2.85E^{-06} \times H_2^2) + (+5.48E^{-04} \times CO_2^2) + (+3.05E^{-04} \times BS^2)$$

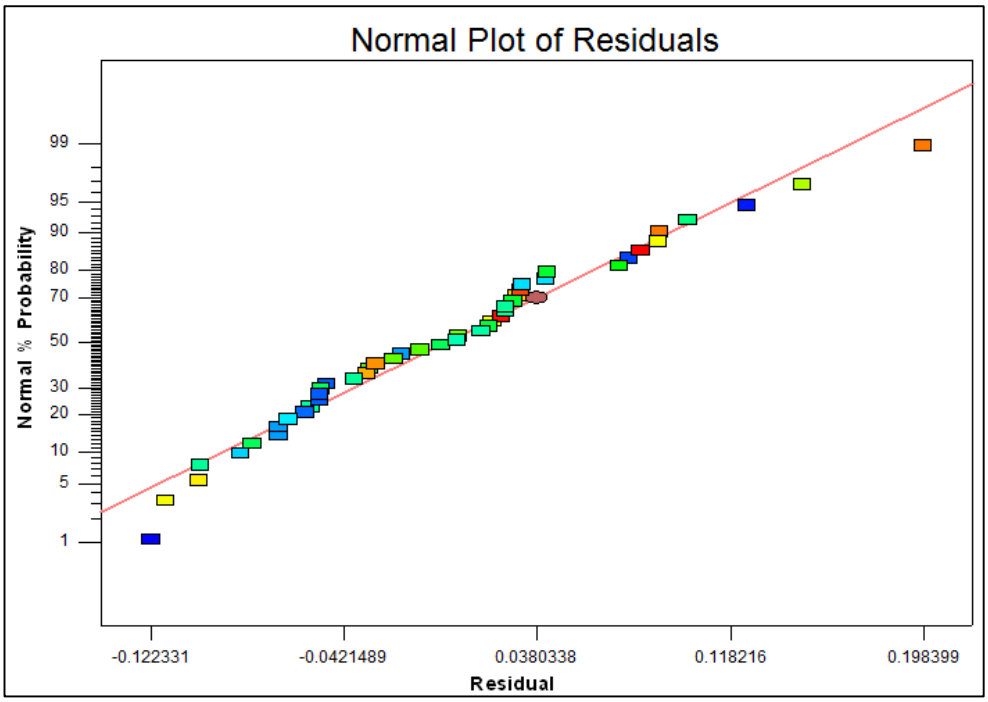

Figure 5.17 Normal Plot vs. Residual for Oxygen.

The data points (Figure 5.7) represented a linear pattern which was desired as a non-linear pattern indicates non-normality in the error term.

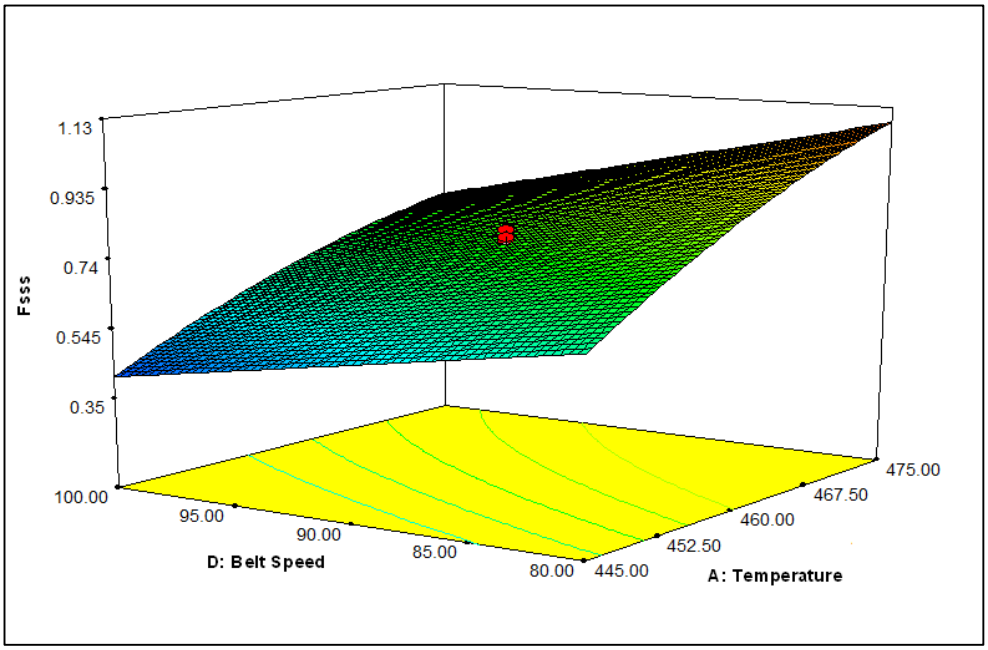

Figure 5.18 3D surface model for particle size vs. temperature and belt speed interaction.

High belt speeds and low temperature (Figure 5.18) result in lower particle size (fsss).

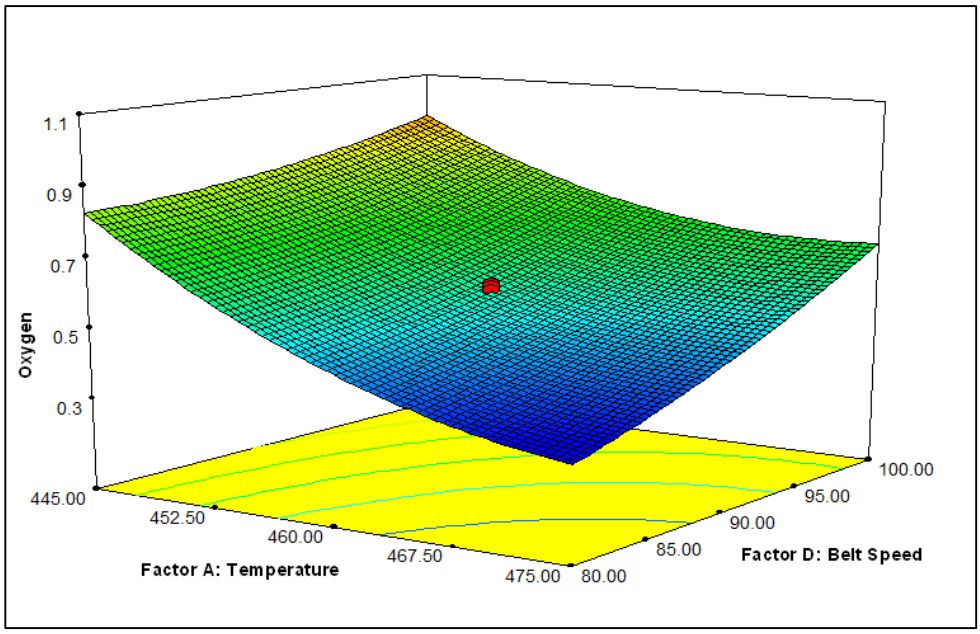

Figure 5.19 3D surface model for oxygen vs. temperature and belt speed interaction.

High temperatures and low belt speeds (Figure 5.19) result in low oxygen content.

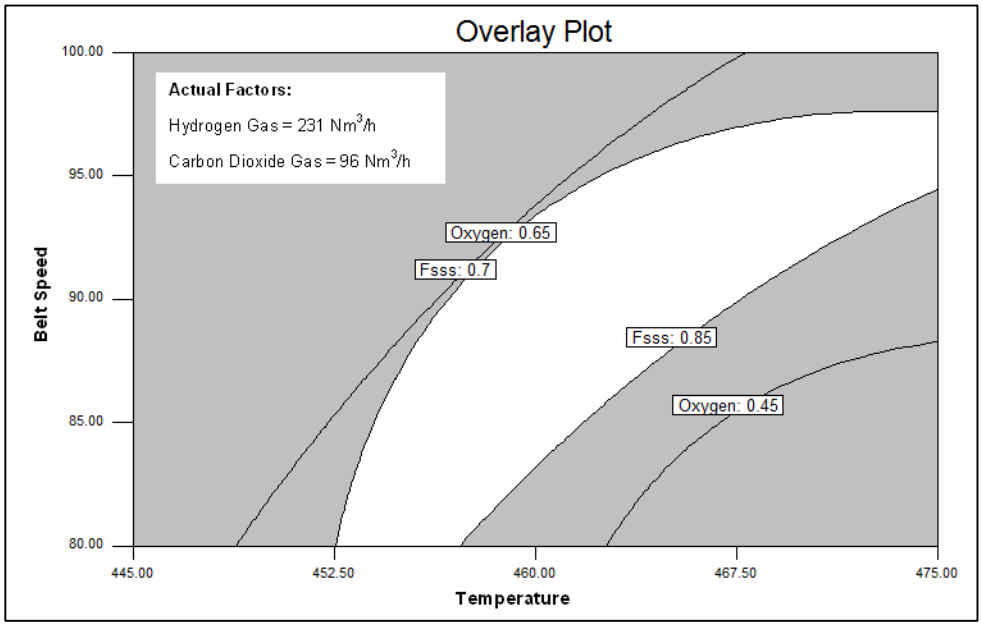

Figure 5.20 Overlay plot highlighted in white indicating the area of the optimum results.

Figure 5.20 was an overlay plot which highlighted the area which both the response values were at its optimum. The area highlighted in white was at constant hydrogen and carbon dioxide gas flow rates. This area encompasses varying combinations of both belt speed and temperature in which the responses are within optimal range. This optimal range is at fsss (0.70 - 0.85 µm) and oxygen (0.45 - 0.65%).

5.2.3 Trends Observed for Furnace Experimentation 4 (Particle size and oxygen)

The last experimental design consisted of 46 runs which included 6 center points and 3 axial points. The operating range selection for experimentation 4 was narrowed as experimentation 2 and 3 were conducted. In experimentation 4, some runs produced unreduced and highly oxidized powder whilst some runs produced normal cobalt powder with a particle size > 0.95 µm. The trends observed for experimentation 4 were that temperature and belt speed had a large impact on both responses particle size and oxygen content. The axial points randomized each variable at values above and below the maximum and minimum range in selected runs whilst maintaining all other variables at center point values. This helped to immediately highlight the effects that these variables had on the response variables. The suggested models for both responses were a quadratic model. The experimentation assisted in narrowing down 4 variables to 2 variables by maintaining a constant hydrogen and carbon dioxide gas flow rate. Both these gases helped to maintain a sufficient reductive and passivated atmosphere in the furnace. Optimum particle size

and oxygen content were obtained at operating ranges (456 - 466°C) temperature, (87 - 89 mm/min) belt speed, (96 Nm^3/h) carbon dioxide flow rate and (231 Nm^3/h) hydrogen gas flow rate.

5.3 Jet-mill Experimentation

When sub-micron cobalt powder was successfully produced with desired response variable requirements, experimentation on the jet mill had commenced.

5.4 Response Surface Methodology for Jet mill Experimentation 1

Experimental data for design matrix 1 was analyzed using response surface methodology. (Table 5.21) represents the experimental run and associated responses. The response variables studied were particle size distribution and milling time. The experimental run consisted of 6 center points and 1 axial point. The alpha value selected was 1.52 which was set by the orthogonal quadratic alpha. The design range for jet mill experiment 1 was as per (Table 5.17).

Table 5.17 The design range for jet mill experimentation 1

Factor	Units	-1 Level	+1 Level	(-) alpha	(+) alpha
Classifier speed	rpm	1000	6000	- 311.62	7311.62
Grinding gas pressure	bar	2	7	0.69	8.31
AFG weight	kg	20	60	9.5	70.49

Table 5.18 Design summary for jet mill experimentation 1

Factor	Name	Units	Type	Low Actual	High Actual	Low Coded	High Coded	Mean	Std. Dev.
A	Classifier speed	rpm	Numeric	1000	6000	-1	1	3500	1988.17
B	Grinding gas pressure	bar	Numeric	2	7	-1	1	4.5	1.988
D	AFG weight	kg	Numeric	20	60	-1	1	40	15.905

The design summary (Table 5.18) highlights the mean and standard deviation for each parameter.

Table 5.19 Analytical data of factors and response variables for jet mill experimentation 1

Std	Run	Factor A	Factor B	Factor C	Response 1	Response 2
		Classifier Speed (rpm)	Grinding Gas pressure (bar)	AFG Weight (kg)	PSD - d90 (µm)	Milling Time (hrs)
14	1	3500	4.5	70.49	17	5
10	2[3]	7311.62	4.5	40	-	-
2	3	6000	2	20	15	9
3	4	1000	7	20	25	3
17	5	3500	4.5	40	15	7
9	6[3]	-311.62	4.5	40	-	-
15	7	3500	4.5	40	16	6.5
4	8	6000	7	20	15	4
8	9	6000	7	60	20	2
20	10	3500	4.5	40	15.7	7
11	11[3]	3500	0.69	40	-	-
13	12[3]	3500	4.5	9.51	-	-
1	13	1000	2	20	20	4
12	14[3]	3500	8.31	40	-	-
16	15	3500	4.5	40	15.4	6.7
18	16	3500	4.5	40	15.9	6.5
19	17	3500	4.5	40	16	7
6	18	6000	2	60	19	6
5	19	1000	2	60	25	3
7	20	1000	7	60	28	2.5

In the experimental matrix above 5 runs could not be conducted as the experimental ranges for the operating variables were above and below the prescribed operating ranges.

[3] These experimental runs could not be conducted as the operating variables set points were either above or below the operating range.

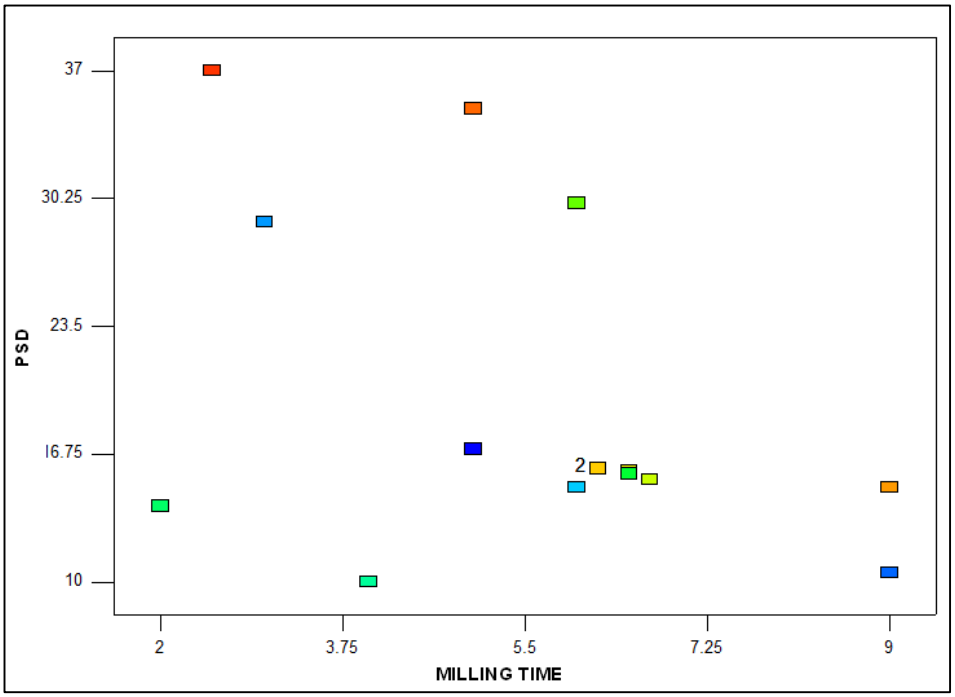

Figure 5.21 The design trend between psd and milling time for experimentation 1

The design trend was illustrated in (Figure 5.21).

5.4.1 Response Variable Particle Size Distribution

The particle size distribution analysis did not require a transform as the ratio between the minimum and maximum response value was 3.7.

Table 5.20 Model summary statistics for particle size distribution

Std. Source	Adjusted Dev.	R-Squared	Adjusted R-Squared	Predicted R-Squared	PRESS
Linear	4.29	0.8097	0.7578	0.6061	419.05
2FI	4.98	0.8135	0.6737	-1.0435	2174.08
Quadratic	0.62	0.9978	0.9949	-	+
Cubic	0.40	0.9993	0.9979	-	+

The model summary (Table 5.21) indicated that the quadratic and cubic model was aliased. The model suggested was the linear model as this had a maximum predicted R-squared and adjusted R-squared value.

Table 5.21 Lack of fit tests for particle size distribution

Sum of Source	Mean Squares	F (df)	p-value Square	Value	Prob > F
Linear	201.67	6	33.61	211.83	< 0.0001
2FI	197.57	3	65.86	415.07	< 0.0001
Quadratic	1.53	1	1.53	9.65	0.0267
Cubic	0	0	-	-	-
Pure Error	0.79	5	0.16	-	-

The lack of fit tests (Table 5.21) compared residual error with pure error from replicated design points. A significant lack of fit was represented by a low Prob > F value. The linear model was highlighted as the suggested model however the model does show a significant lack of fit.

Table 5.22 Anova of particle size distribution for experimentation 1

Source	Sum of Squares	df	Mean Square	F Value	p-value Prob > F	Significance
Model	861.43	3	287.14	15.60	0.0003	Significant
A-Classifier speed	830.28	1	830.28	45.11	< 0.0001	Significant
B-Grinding gas pressure	0.031	1	0.031	0.0169	0.9679	-
C-AFG weight	31.12	1	31.12	1.69	0.2201	-
Residual	202.46	11	18.41	-	-	-
Lack of Fit	201.67	6	33.61	211.83	< 0.0001	Significant
Pure Error	0.79	5	0.16	-	-	-
Cor Total	1063.89	14	-	-	-	-

The model F-value of 15.60 in (Table 5.22) implied that the model was significant. The above table indicated that the classifier speed had a major impact on particle size distribution. The lack of fit value of 211.83 indicated that the lack of fit was significant. The concern here was that the model does not fit.

Table 5.23: Model applicability and precision for psd design matrix 1

Std. Dev.	4.29	R-Squared	0.8097
Mean	19.43	Adj R-Squared	0.7578
C.V. %	22.08	Pred R-Squared	0.6061
PRESS	419.05	Adeq Precision	10.833

The predicted R-squared and the adjusted R-squared in (Table 5.23) are in agreement with each other. The adequate precision value of 10.833 indicated an adequate signal.

The final equation generated in terms of actual factors was:

$$PSD = (+30.13185) + (-0.04075 \times \mathrm{CS}) + (-0.025 \times GP) + (+0.087467 \times \mathrm{A}FG)$$

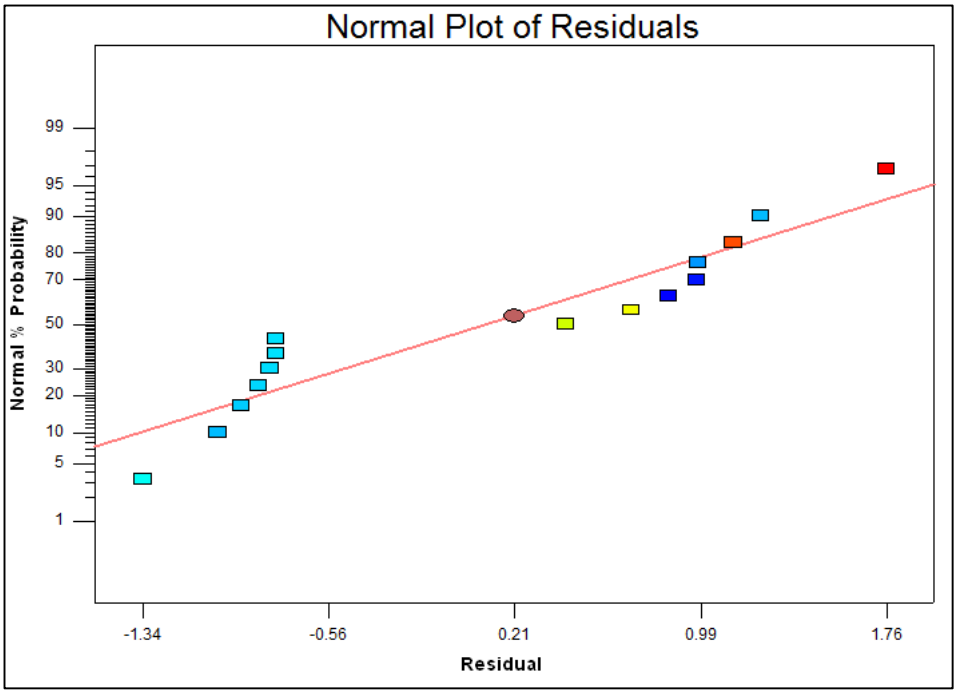

Figure 5.22 Normal plot vs. residual for PSD.

The data points in (Figure 5.22) were distributed across the linear target line. This indicated that the range selected yielded data that was not conclusive enough to highlight the main effects. Hence the range had to be evaluated and narrowed.

5.4.2 Response Variable Milling Time

Milling time analysis did not require a transform as the ratio between the minimum and maximum response value was 4.5.

Table 5.24 Model summary statistics for milling time

Std. Source	Adjusted Dev.	R-Squared	Adjusted R-Squared	Predicted R-Squared	PRESS
Linear	1.06	0.7920	0.7353	0.5089	29.27
2FI	0.92	0.8859	0.8003	-0.3442	80.10
Quadratic	0.43	0.9813	0.9563	-	+
Cubic	0.26	0.9944	0.9843	-	+

The model summary in (Table 5.24) indicated that the quadratic and cubic model was aliased. The model suggested was the linear model as this had a maximum predicted R-squared and adjusted R-squared value.

Table 5.25 Lack of fit tests for milling time

Sum of Source	Mean Squares	F (df)	p-value Square	Value	Prob > F
Linear	12.06	6	2.01	30	0.0009
2FI	6.47	3	2.16	32.17	0.0011
Quadratic	0.78	1	0.78	11.66	0.0189
Cubic	0	0	-	-	-
Pure Error	0.34	5	0.067	-	-

The lack of fit tests (Table 5.25) compared residual error with pure error from replicated design points. A significant lack of fit was represented by a low Prob > F value. The linear model was highlighted again as the suggested model however the model did show a significant lack of fit.

Table 5.26 Anova of milling time for experimentation 1

Source	Sum of Squares	df	Mean Square	F Value	p-value Prob > F	Significance
Model	47.19	3	15.73	13.96	0.0005	Significant
A-Classifier speed	7.03	1	7.03	6.24	0.0296	Significant
B-Grinding gas pressure	38.28	1	38.28	33.97	0.0001	Significant
C-AFG weight	1.88	1	1.88	1.67	0.2228	-
Residual	12.40	11	1.13	-	-	-
Lack of Fit	12.06	6	2.01	30	0.0009	Significant
Pure Error	0.34	5	0.067	-	-	-
Cor Total	59.59	14	-	-	-	-

The model F-value of 13.96 in (Table 5.26) implied that the model was significant. The above table indicated that the classifier speed and grinding gas pressure had a major impact on particle size distribution. The lack of fit value of 30 indicated that the lack of fit was significant. The concern here was that the model did not fit.

Table 5.27 Model applicability and precision for milling time design matrix 1

Std. Dev.	1.06	R-Squared	0.7920
Mean	5.57	Adj R-Squared	0.7353
C.V. %	19.05	Pred R-Squared	0.5089
PRESS	29.27	Adeq Precision	12.971

The predicted R-squared and the adjusted R-squared in (Table 5.27) were in agreement with each other. The adequate precision value of 12.971 indicated an adequate signal.

The final equation generated in terms of actual factors are:

$$MillingTime = (+9.10229) + (+0.00375 \times \mathrm{CS}) + (-0.8750 \times GP) + (-0.021506 \times \mathrm{A}FG)$$

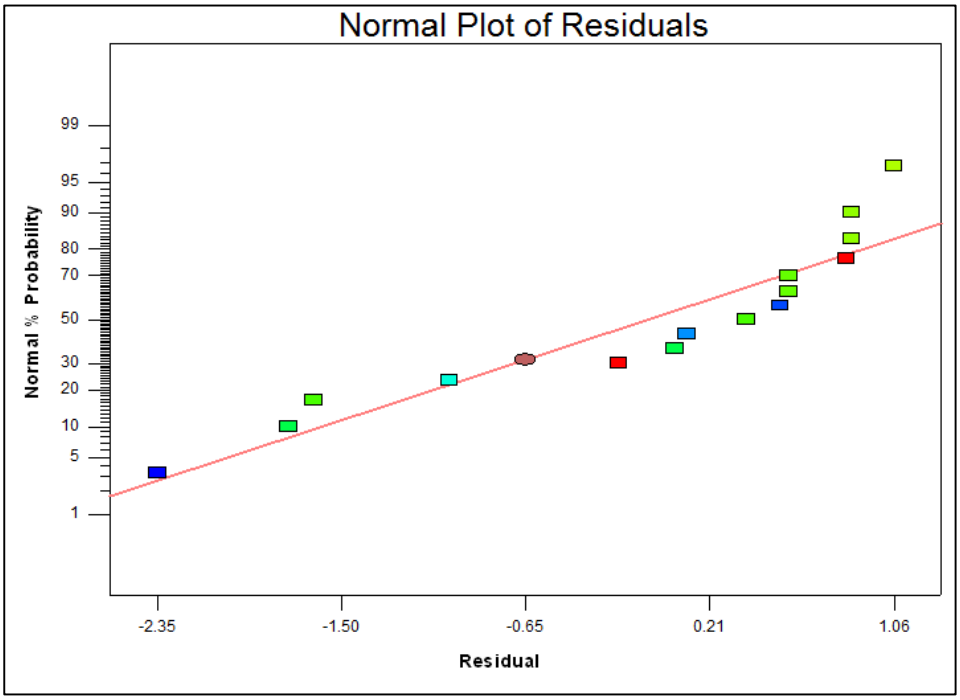

Figure 5.23 Normal plot vs. residual for milling time.

The data points in (Figure 5.23) were distributed much more evenly across the linear target line.

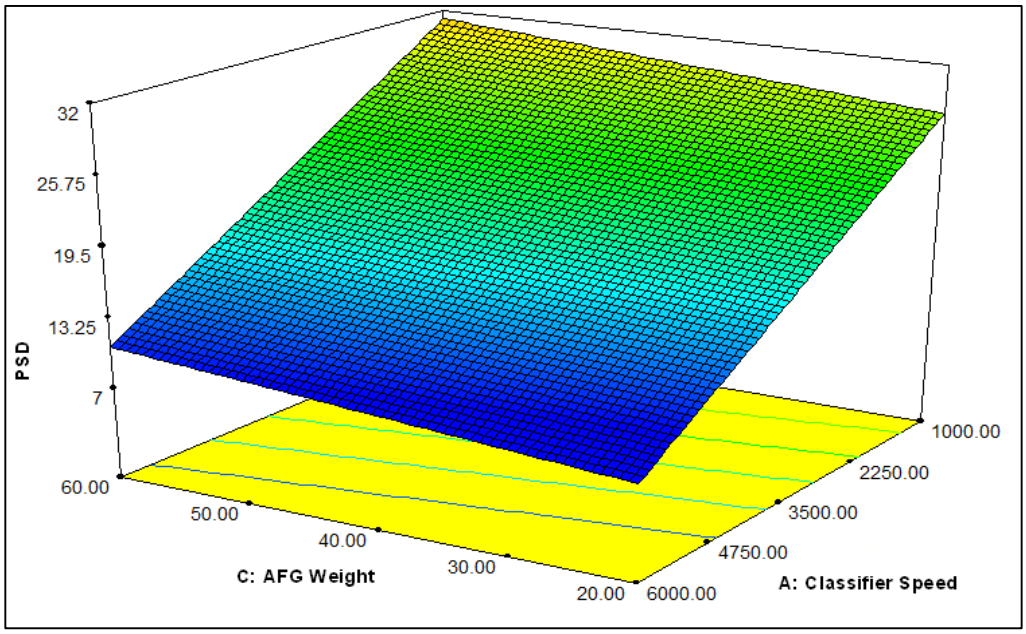

Figure 5.24 3D surface model for psd vs. AFG weight and classifier speed interaction.

High classifier speeds and low AFG weights (Figure 5.24) resulted in lower particle size distribution.

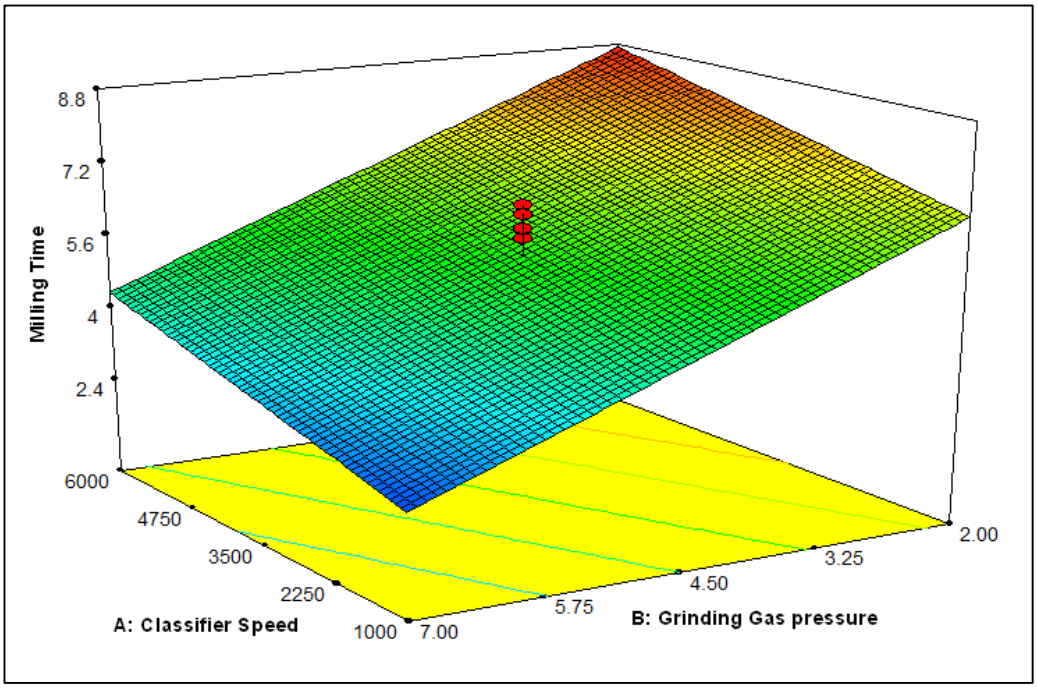

Figure 5.25 3D surface model for milling time vs. classifier speed and grinding gas pressure interaction.

High grinding gas pressure and low classifier speeds (Figure 5.25) resulted in lower milling time.

5.4.3 Trends observed for Jet mill Experimentation 1 (PSD and Milling time)

The initial experimentation highlighted the effects that each factor had on the response variables. The interaction between the response variables were also highlighted whereby milling time and particle size distribution had an inverse relationship. During the experiment it was found that as the particle size distribution reduced, milling time increased significantly. Effects of the jet mill factors highlighted that high classifier speeds reduced particle size distribution but increased milling time. Higher grinding gas pressure assisted in reducing milling time but increased particle size distribution. The AFG weight was a factor that required careful monitoring. When the afg weight was increased, the particle size distribution increased and milling time reduced. When the afg weight was decreased, the particle size distribution reduced but the milling time increased. However it was found that ideally lower weights for the afg was ideal but has to be in conjunction with factors such as classifier speed and grinding gas pressure.

5.5 Response Surface Methodology for Jet mill Experimentation 3

Design matrix 3 represents the last experiment for the jet mill. There were 3 axial points selected for the design. The alpha value selected was at 1.28 which was a rotatable alpha as it was least extreme as compared to the other alpha values. This set the cubical portion of the central composite design. The operating range for design matrix was as per (Table 5.28).

Table 5.28 Jet mill experimental parameters for design matrix 3

Factor	Range
Classifier speed	5000 - 5800 rpm
Grinding gas pressure	6 - 6.5 bar
AFG weight	40 - 45 kgs

Table 5.29 The design range for jet mill experimentation 3

Factor	Units	-1 Level	+1 Level	(-) alpha	(+) alpha
Classifier speed	rpm	5000	6000	4888	5911
Grinding gas pressure	bar	6.0	6.5	5.93	6.6
AFG weight	kg	40	45	39	46

The design range was as per (Table 5.29).

Table 5.30 Design summary for jet mill experimentation 3

Factor	Name	Units	Type	Low Actual	High Actual	Low Coded	High Coded	Mean	Std. Dev.
A	Classifier speed	rpm	Numeric	5000	5800	-1	1	5400	298.3
B	Grinding gas pressure	bar	Numeric	6.0	6.5	-1	1	6.25	0.186
D	AFG weight	kg	Numeric	40	45	-1	1	42.5	1.86

The design summary highlighted the mean and standard deviation for jet mill experimentation 3 as per (Table 5.30).

The design matrix (Table 5.31) determined how each run would be conducted.

Table 5.31 Analytical data of factors and response variables for jet mill experimentation 3

Std	Run	Factor A	Factor B	Factor C	Response 1	Response 2
		Classifier Speed (rpm)	Grinding Gas pressure (bar)	AFG Weight (kg)	PSD - d90 (µm)	Milling Time (hrs)
32	1	5400	6.25	43	7.324	2.5
26	2	5400	6.25	46	7.201	2.2
5	3[4]	5000	6	45	10.526	2.4
28	4	5400	6.25	43	7.01	2.3
10	5[4]	4889	6.25	43	12.521	2.1
18	6	5400	6.6	43	8.501	1.7
19	7	5400	6.6	43	9.752	1.76
30	8	5400	6.25	43	7.561	2.25
3	9[4]	5000	6.5	40	11.689	1.95
11	10[4]	4889	6.25	43	12.896	1.9
31	11	5400	6.25	43	7.065	2
7	12[4]	5000	6.5	45	12.514	1.87
6	13	5800	6	45	6.21	4.8
20	14	5400	6.6	43	8.878	1.75
25	15	5400	6.25	46	7.501	2.3
27	16	5400	6.25	43	7.121	2.15
13	17	5911	6.25	43	6.01	4.0
14	18	5911	6.25	43	6.021	4.2
23	19	5400	6.25	39	6.91	2.4
12	20	5911	6.25	43	6.156	4.5
21	21	5400	6.25	39	7.001	2.3
16	22	5400	5.9	43	6.651	3.0
22	23	5400	6.25	39	7.124	2.2
24	24	5400	6.25	46	7.986	2.2
9	25[4]	4889	6.25	43	13.498	1.8
29	26	5400	6.25	43	7.421	2.2
17	27	5400	5.9	43	6.781	2.9
2	28	5800	6	40	6.001	5.0
1	29[4]	5000	6	40	10.261	2.6
8	30	5800	6.5	45	6.966	2.98
4	31	5800	6.5	40	6.721	3.0
15	32	5400	5.9	43	6.891	3.0

[4] These experimental runs produced sub-micron cobalt powder with a particle size distribution greater than the specification.

Altogether there were 32 runs for experiment 3 which consisted of 6 center points and 3 axial points for each factor. The range for each factor was narrowed as each experimentation was ran. Sub-micron cobalt powder with a particle size distribution d90 < 9 µm and effective milling time < 2.6 hours were runs 1, 2, 4, 6, 7, 8, 11, 14, 15, 16, 19, 21, 23, 24 and 26.

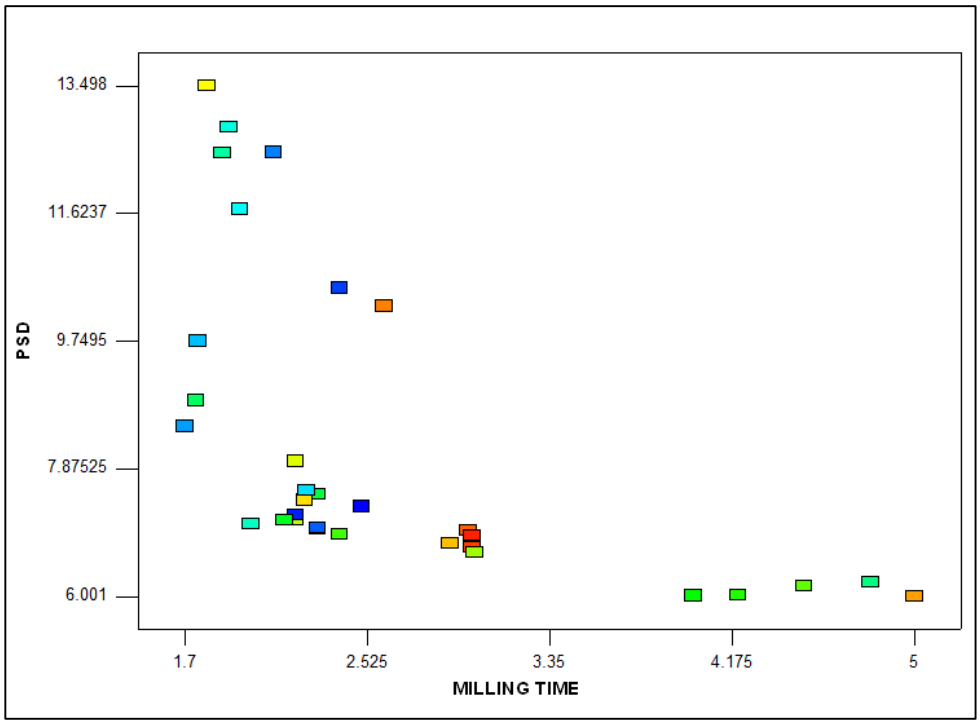

Figure 5.26 The design trend between psd and milling time for experimentation 3.

The design trend observed between milling time and psd was illustrated in (Figure 5.26).

5.5.1 Response Variable Particle size distribution

The particle size distribution analysis did not require a transform as the ratio between the minimum and maximum response value was 2.25.

Table 5.32 Model summary statistics for particle size distribution

Std. Source	Adjusted Dev.	R-Squared	Adjusted R-Squared	Predicted R-Squared	PRESS
Linear	1.00	0.8197	0.8004	0.7668	36.38
2FI	1.00	0.8233	0.7809	0.6739	50.87
Quadratic	0.36	0.9818	0.9743	0.9517	7.53
Cubic	0.34	0.9870	0.9776	0.8389	25.13

The model summary (Table 5.32) indicated that the cubic model was aliased. The model suggested was the quadratic model as this had a maximum predicted R-squared and adjusted R-squared value.

Table 5.33 Lack of fit tests for particle size distribution

Sum of Source	Mean Squares	F (df)	p-value Square	Value	Prob > F
Linear	26.20	11	2.38	21.00	< 0.0001
2FI	25.63	8	3.20	28.25	< 0.0001
Quadratic	0.91	5	0.18	1.61	0.2115
Cubic	0.096	1	0.096	0.85	0.3698
Pure Error	1.93	17	0.11	-	-

The lack of fit tests (Table 5.33) compared residual error with pure error from replicated design points. The suggested model was the quadratic model. The Prob > F had suggested that the quadratic model had an insignificant lack of fit which was desirable.

Table 5.34 Anova of particle size distribution for experimentation 3

Source	Sum of Squares	df	Mean Square	F Value	p-value Prob > F	Significance
Model	153.15	9	17.02	131.81	< 0.0001	Significant
A-Classifier speed	116.73	1	116.76	904.21	< 0.0001	Significant
B-Grinding gas pressure	10.38	1	10.38	80.40	< 0.0001	Significant
C-AFG weight	0.75	1	0.75	5.82	0.0246	-
AB	0.47	1	0.47	3.64	0.0694	-
AC	0.051	1	0.051	0.39	0.5379	-
BC	0.044	1	0.044	0.34	0.5635	-
A^2	23.47	1	23.47	181.79	< 0.0001	Significant
B^2	1.50	1	1.50	11.63	0.0025	-
C^2	0.0030	1	0.0030	0.24	0.6318	-
Residual	2.84	22	0.13	-	-	-
Lack of Fit	0.91	5	0.18	1.61	0.2115	Not Significant
Pure Error	1.93	17	0.11	-	-	-
Cor Total	155.99	31	-	-	-	-

The model F-value of 131.81in (Table 5.34) implied that the model was significant. The above table indicated that the classifier speed and grinding gas pressure had a major impact on particle size distribution. The lack of fit value of 1.61 indicated that the lack of fit was not significant.

Table 5.35 Model applicability and precision for psd design matrix 3

Std. Dev.	0.36	R-Squared	0.9818
Mean	8.21	Adj R-Squared	0.9743
C.V. %	4.38	Pred R-Squared	0.9571
PRESS	7.53	Adeq Precision	35.151

The predicted R-squared and the adjusted R-squared in (Table 5.35) were in agreement with each other. The adequate precision value of 35.151 indicated an adequate signal.

The final equation generated in terms of actual factors was:

$$PSD = (+385.66646) + (-0.076832 \times CS) + (-55.57563 \times GP) + (+0.41243 \times AFG) + (-2.425E^{-03} \times CS \times GP) + (-7.95E^{-05} \times CS \times AFG) + (+0.11920 \times GP \times AFG) + (+8.23745E^{-06} \times CS^2) + (+5.35275 \times GP^2) + (-7.59951E^{-03} \times AFG^2)$$

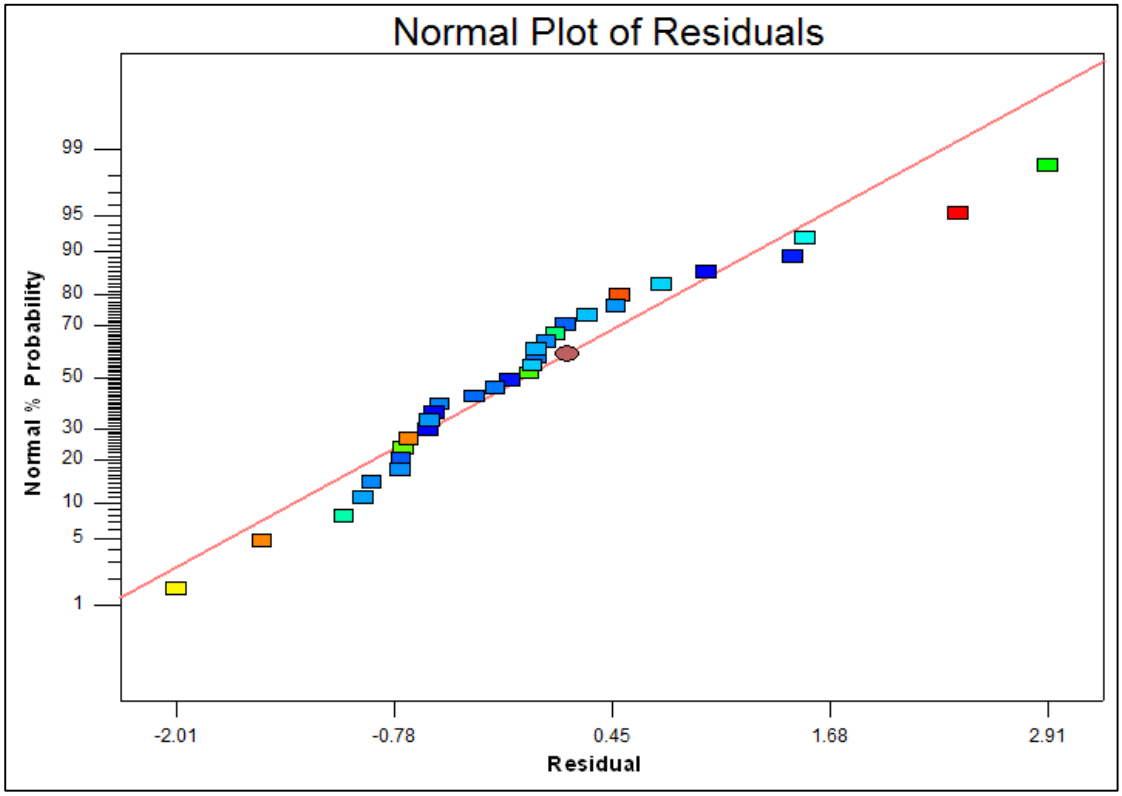

Figure 5.27: Normal plot vs. residual for psd.

The data points in (Figure 5.27) were distributed across the linear target line.

5.5.2 Response Variable Milling Time

Milling time analysis did not require a transform as the ratio between the minimum and maximum response value was 2.94.

Table 5.36 Model summary statistics for milling time

Std. Source	Adjusted Dev.	R-Squared	Adjusted R-Squared	Predicted R-Squared	PRESS
Linear	0.47	0.7540	0.7276	0.6643	8.61
2FI	0.47	0.7884	0.7376	0.4678	13.65
Quadratic	0.16	0.9777	0.9686	0.9443	1.43
Cubic	0.16	0.9816	0.9683	- 0.1126	28.53

The model summary (Table 5.36) indicated that the cubic model was aliased. The model suggested was the quadratic model as this had a maximum predicted R-squared and adjusted R-squared value.

Table 5.37 Lack of fit tests for milling time

Sum of Source	Mean Squares	F (df)	p-value Square	Value	Prob > F
Linear	5.96	11	0.54	26.60	< 0.0001
2FI	5.08	8	0.64	31.16	< 0.0001
Quadratic	0.23	5	0.045	2.22	0.1002
Cubic	0.13	1	0.13	6.20	0.0235
Pure Error	0.35	17	0.020	-	-

The lack of fit tests (Table 5.37) compared residual error with pure error from replicated design points. A significant lack of fit was represented by a low Prob > F value. The quadratic model was highlighted again as the suggested model and had shown an in-significant lack of fit.

Table 5.38 Anova of milling time for experimentation 3

Source	Sum of Squares	df	Mean Square	F Value	p-value Prob > F	Significance
Model	25.07	9	2.79	107.09	< 0.0001	Significant
A-Classifier speed	13.99	1	13.99	537.63	< 0.0001	Significant
B-Grinding gas pressure	5.32	1	5.32	204.40	< 0.0001	Significant
C-AFG weight	0.032	1	0.032	1.23	0.2788	-
AB	0.87	1	0.87	33.49	< 0.0001	Significant
AC	0.00045	1	0.00045	0.017	0.8966	-
BC	0.011	1	0.011	0.43	0.5176	-
A^2	4.81	1	4.81	184.88	< 0.0001	Significant
B^2	0.30	1	0.30	11.63	0.0025	-
C^2	0.13	1	0.13	4.84	0.0386	-
Residual	0.57	22	0.026	-	-	-
Lack of Fit	0.23	5	0.045	2.22	0.1002	Not Significant
Pure Error	0.35	17	0.020	-	-	-
Cor Total	25.65	31	-	-	-	-

The model F-value of 107.09 in (Table 5.38) implied that the model was significant. The above table indicated that the classifier speed and grinding gas pressure had a major impact on milling time. The lack of fit value of 2.22 indicated that the lack of fit was not significant.

Table 5.39 Model applicability and precision for milling time design matrix 3

Std. Dev.	0.16	R-Squared	0.9777
Mean	2.63	Adj R-Squared	0.9686
C.V. %	6.13	Pred R-Squared	0.9443
PRESS	1.43	Adeq Precision	34.742

The predicted R-squared and the adjusted R-squared in (Table 5.39) were in agreement with each other. The adequate precision value of 34.742 indicated an adequate signal.

The final equation generated in terms of actual factors was:

$$MillingTime = (+141.04193) + (-0.017753 \times CS) + (-16.84404 \times GP) + (-1.74578 \times AFG) + (-3.3E^{-03} \times CS \times GP) + (+7.5E^{-06} \times CS \times AFG) + (+0.06 \times GP \times AFG) + (+3.72919E^{-06} \times CS^{2}) + (+2.39421 \times GP^{2}) + (+0.015451 \times AFG^{2})$$

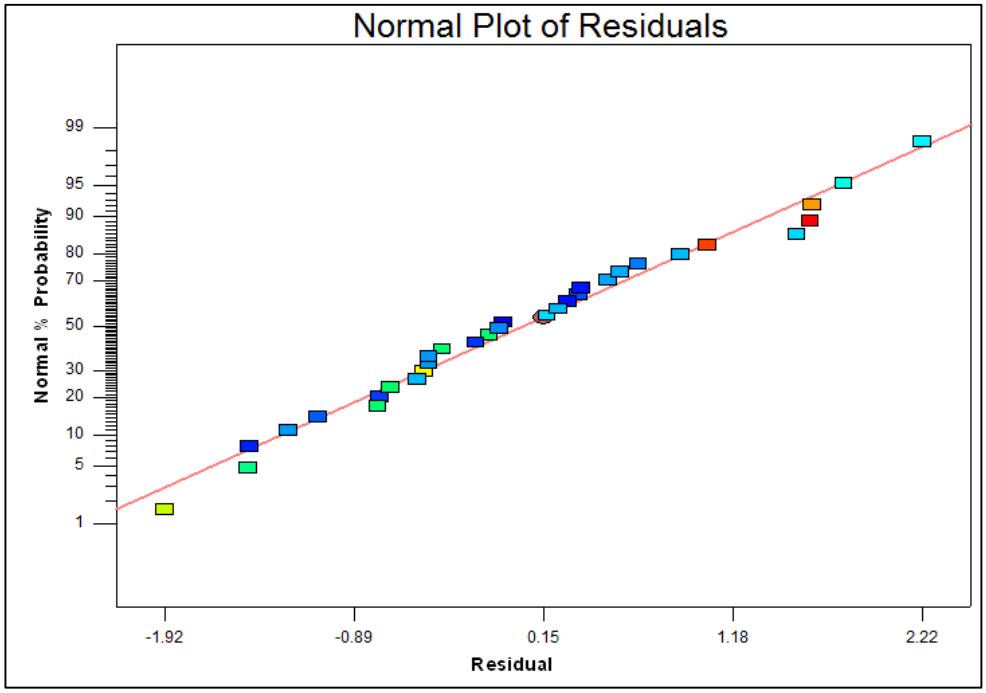

Figure 5.28 Normal plot vs. residual for milling time.

The data points in (Figure 5.28) were distributed much more evenly across the linear target line.

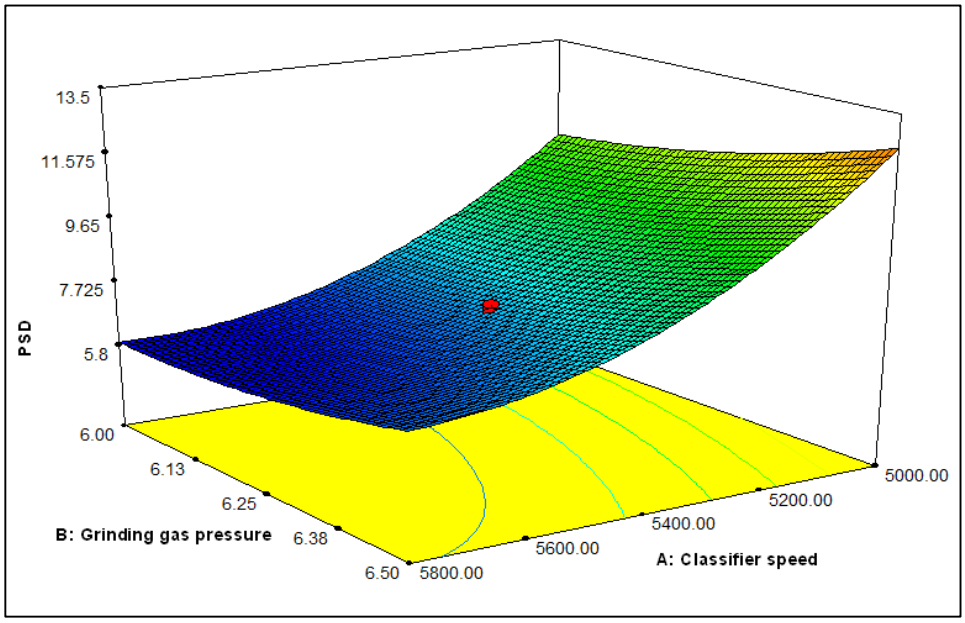

Figure 5.29: 3D surface model for psd vs. grinding gas pressure and classifier speed interaction.

Low grinding gas pressure and high classifier speed (Figure 5.29) resulted in lower particle size distribution.

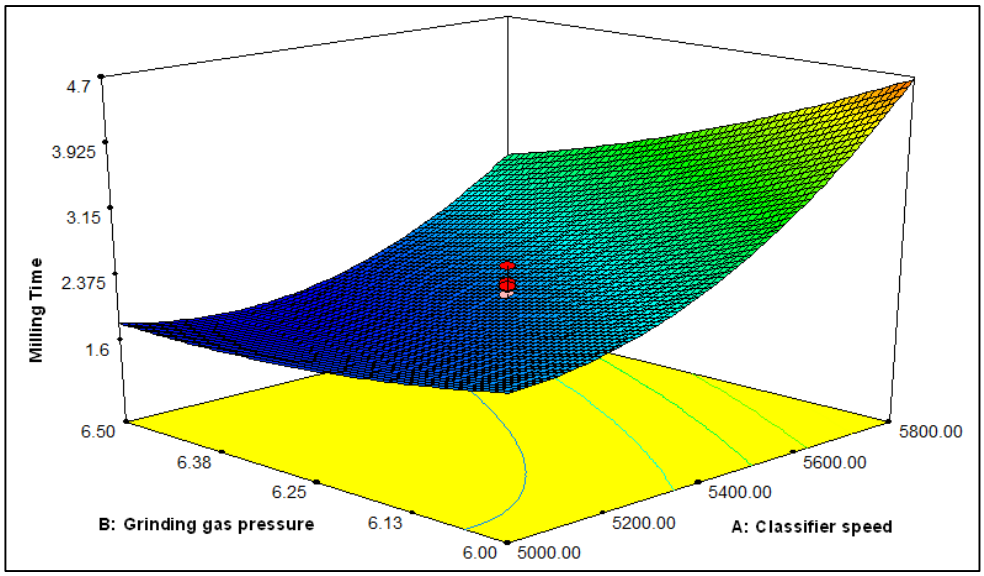

Figure 5.30: 3D surface model for milling time vs. grinding gas pressure and classifier speed interaction.

Low grinding gas pressure and low classifier speeds (Figure 5.30) resulted in longer milling time.

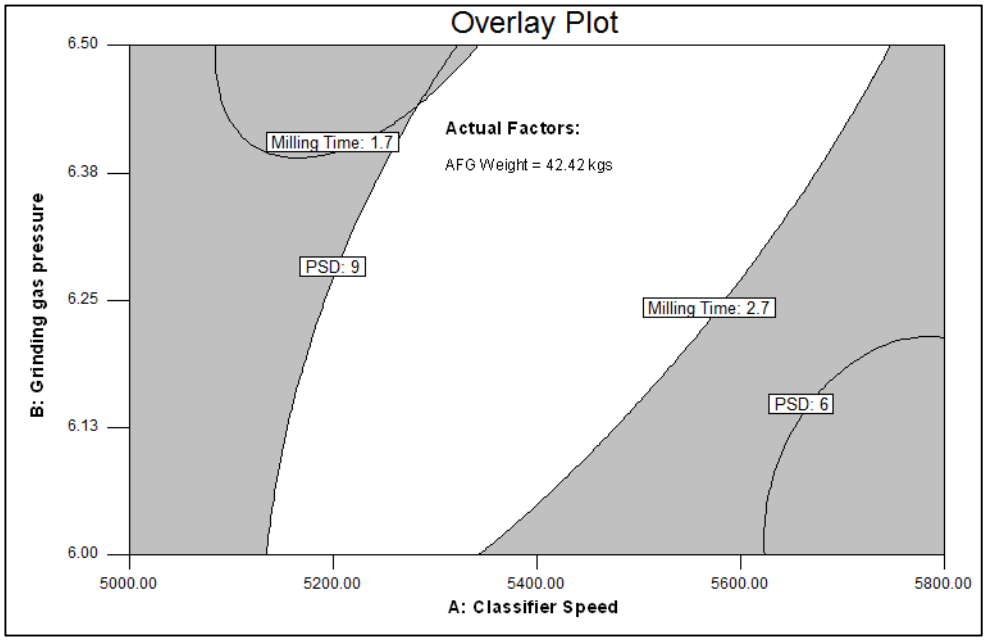

Figure 5.31 Overlay Plot highlighted in white indicating the area of the optimum results

Figure 5.31was an overlay plot which highlighted the area which both the response values are at its optimum. The area highlighted in white was at constant AFG weight. This area encompasses varying combinations of both classifier speed and grinding gas pressure in which the responses are within optimal range. This optimal range was at particle size distribution d_{90} (6.0 - 9.0 µm) and milling time (1.7- 2.7 hrs).

5.5.3 Trends observed for Jet mill Experimentation 3 (PSD and Milling time)

The last experimental design for the jet mill experiment consisted of 32 runs which included 6 center points and 3 axial points. Some of the runs in experiment 3 yielded powder with a particle size distribution d_{90} > 12 µm and milling time greater than 3 hours. The trend observed was that classifier speed had the single largest effect on particle size distribution and grinding gas pressure had the single largest effect on milling time. However a combination of all 3 operating variables changed the effects of the factors on the response variables positively and negatively. Having the axial point in the experimentation helped identify the significance of the AFG weight. A lower AFG weight reduced particle size distribution in combination with a high classifier speed. In experimentation 3 the AFG weight was maintained within a tight range as extreme fluctuations yielded inconsistent results. The suggested models for both milling time and particle size distribution were a quadratic model. Optimum particle size distribution and milling time were achieved at the following operating ranges (5400 - 5500 rpm) classifier speed, (6.25 - 6.0 bar) grinding gas pressure and (39 - 46 kgs) AFG weight.

5.6 Discussion of Furnace and Jet mill Experimentation

Sub-micron cobalt powder that was produced during the experimentation resulted in the powder reaching a particle size range of 0.70 - 0.80 µm, oxygen range of 0.40 - 0.65% and particle size distribution range d_{90} of 6.50 µm - 8.5 µm. Altogether there was 140 experimental runs that were conducted between the furnace and jet mill experimentation. Initially designs of experiments were used to screen important factors and their respective operating range to attain the desired response variables ranges. Response surface methods assisted in determining the optimal range for the operating factors.

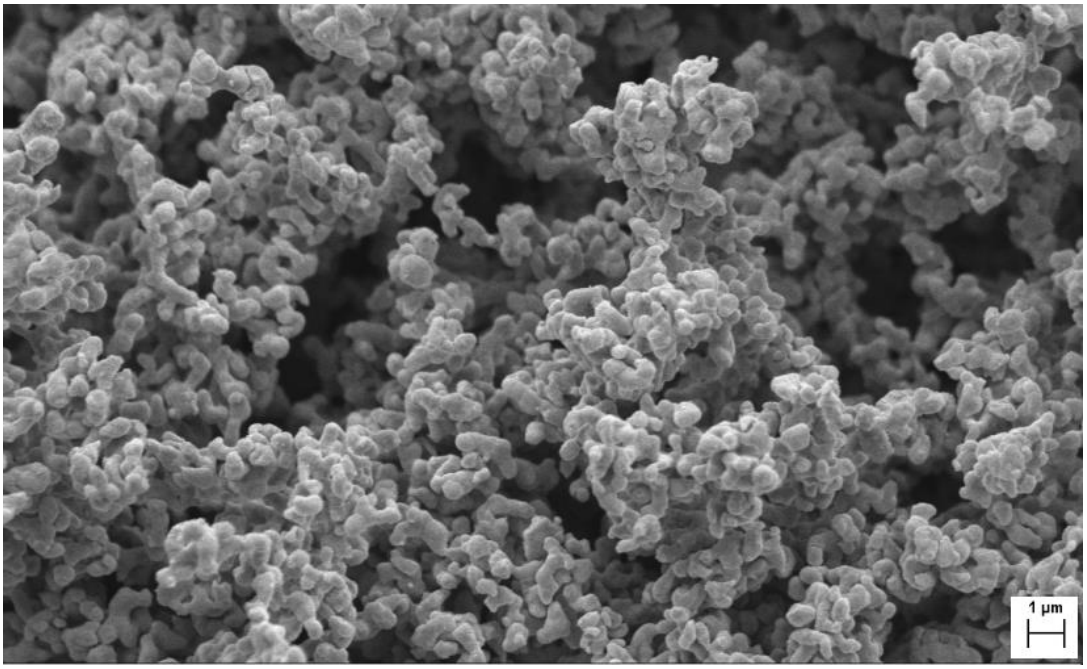

Figure 5.32: SEM of the sub-micron cobalt powder produced from the furnace (Moodlier., 2012a)

The SEM (Figure 5.32) is the scanning electron microscope image of the sub-micron cobalt powder produced from the furnace. It essentially looked at the powder under magnification to assess the structural morphology of the powder produced. The SEM confirmed that the sub-micron cobalt powder was less than 1 µm. There was uniformity in the individual particles in the sub-micron cobalt powder.

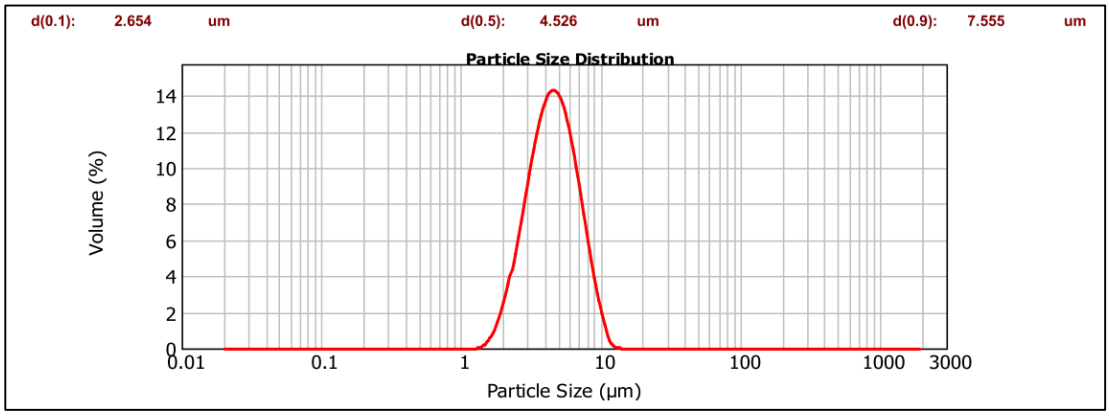

Figure 5.33: Particle size distribution from the jet mill experimentation (Moodlier., 2012b)

The particle size distribution in (Figure 5.33) was within desirable specification. The powder was homogenous and well de-agglomerated. The sub-micron cobalt powder produced in the above research had been used in industry. The application of the sub-micron cobalt powder had been in the hard metals and diamond tool industry. A comparison was conducted by customers using the sub-micron cobalt powder produced utilizing the above operational parameters and the sub-micron cobalt powder produced from the competitors. Factors such as compacity and hardness were tested in the diamond tool industry (Figure 5.34) and (Figure 5.35).

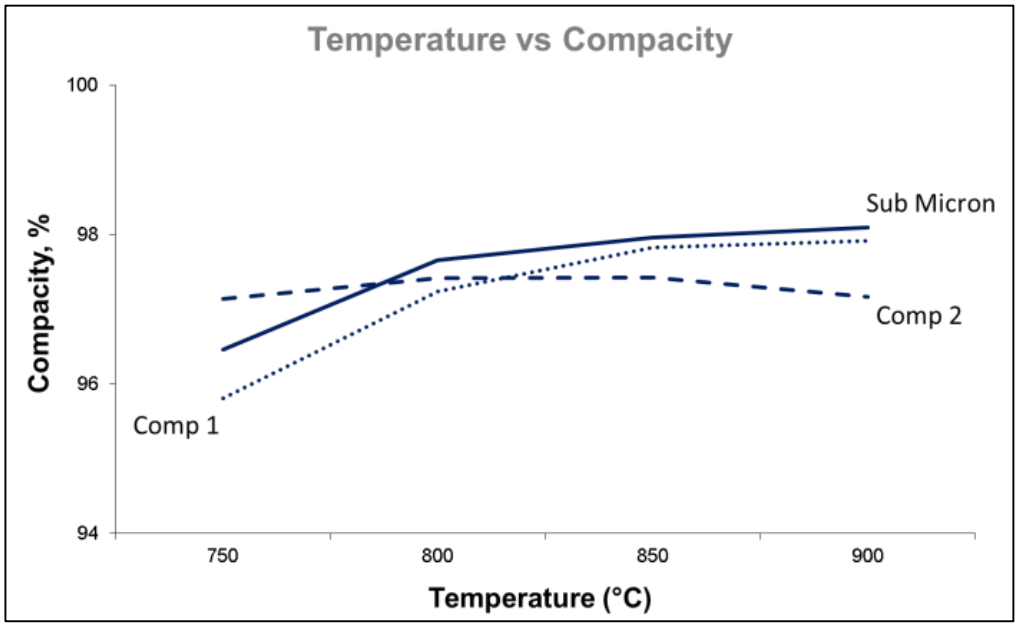

Figure 5.34: Compacity of this sub-micron cobalt powder in comparison to conventional powders (Moodlier., 2013a)

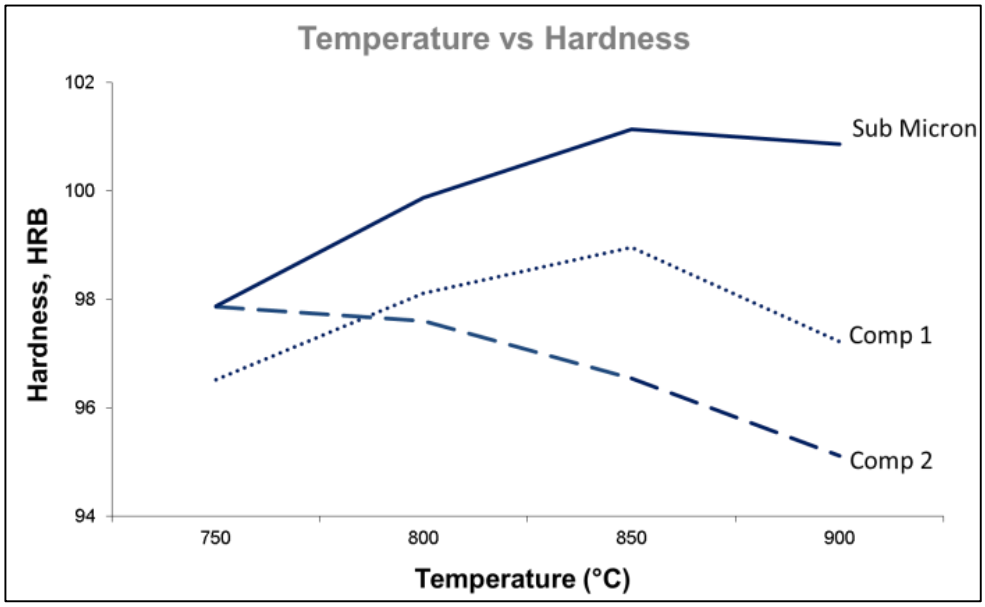

Figure 5.35: Hardness of this sub-micron cobalt powder in comparison to conventional powders (Moodlier., 2013b)

In the hard metal industry the sub-micron cobalt powder was used in the tungsten carbide application. It proved to be successful when bonded with tungsten carbide. (Figure 5.36) highlights the uniform distribution of the sub-micron cobalt powder with tungsten carbide.

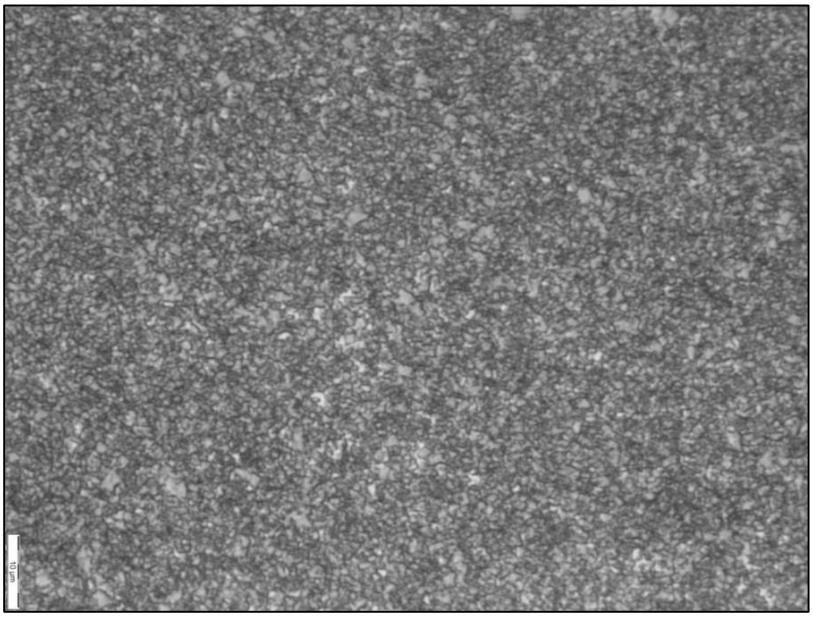

Figure 5.36: Microstructure achieved with this sub-micron cobalt powder (Moodlier., 2013c)

CHAPTER 6

CONCLUSIONS AND RECOMMENDATIONS

6.1 Conclusions

A production rate of 2.3 tons/day was achieved for sub-micron cobalt powder production. This was a record production rate in the cobalt industry as most commercial processes produce a maximum of 1.6 tons/day (De Schepper, 2006). The product quality had also been accepted in industry in terms of particle size, oxygen content and particle size distribution. Due to this research, production at the Shu Powders Africa facility had increased by 15 % due to new sales. Furthermore sub-micron cobalt powder was sold at a premium, hence making it very profitable to produce.

6.2 Recommendations

The recommendations arising from this study were to modify the use of carbon dioxide in the process in terms of where it entered the furnace. A few studies in the laboratory at Shu Powders Africa have shown that oxygen content in the sub-micron cobalt powder could be reduced by allowing the carbon dioxide gas to passivate the powder at temperatures of 40°C in the furnace cooling section. Temperature probes have been installed in the furnace cooling section where currently carbon dioxide gas enters the furnace. Temperature readings have highlighted that temperatures are below 30°C when carbon dioxide enters the furnace hence the impact of passivation is not fully utilized. This means that the hydrogen gas flow rate and temperatures of the furnace could potentially be lowered. The reasons for this are, currently high volume of hydrogen gas and temperature of furnace are being used to attain the required sub-micron cobalt powder specification. High volumes of hydrogen gas flow rate aid in the reduction of the raw material and subsequent reduction of oxygen in the sub-micron cobalt powder. Hydrogen gas is produced from anhydrous ammonia which is expensive. Hence reduction in the volume of hydrogen gas will reduce the operational costs. Lower temperatures would result in lower energy requirement in the process which in turn would reduce energy costs. More work should be conducted to achieve these findings.

On the jet mill experimentation a change in size of the nozzles in the grinding bin should be investigated as this could potentially assist in reducing the milling time which means higher throughput from the jet mill.

CHAPTER 7

REFERENCES

Anderson, M. J., and Whitcomb, P. J., 2005. *RSM Simplified: Optimizing processes using response surface methods for design of experiments*. New York: Productivity Press.

Anderson, M. J., and Whitcomb, P. J., 2007. *DOE Simplified: Practical tools for effective experimentation*. 2nd ed. New York: Productivity Incorporated.

Burrows, J. C., River C. Associates., 1971. *Cobalt: An industry analysis*. Vol. 1. New York: Heath Lexington Books.

Bhaskar, P., Verma, A., and Biday, A. C., 2012. Optimization of sintering parameters of sub-micron cobalt metal powder using the Taguchi method. *Journal of metallurgical engineering*, 1(1): (23-29).

Cobalt Development Institute (CDI), 2013. *Cobalt supply demand*. Fall: 1-10.

Chong, H. W., 2012. Low energy consumption industrial production of ultra-fine spherical cobalt powders. *Energy Conservation*, (pdf), Chapter 6, p. (149-163). Available: http://dx.doi.org/10.5772/52113. (2014-07-06).

Crundwell, F. K., Ramachandran, V., and Moats, M. S., 2011. *Extractive metallurgy of nickel, cobalt and platinum group metals*. Britain: Elsevier.

De Schepper. A., 2006. Cobalt production technologies in Industry. (Presentation). DES Consulting.

De Schepper, A., 2008. Production of cobalt carbonate. (Presentation). DES Consulting.

De Schepper, A., 2009. Cobalt in the diamond tool industry. (Presentation). DES Consulting.

De Schepper, A., 2007. Milling technologies. (Presentation). DES Consulting.

Erikkson. L., Johansson. E., Kettaneh-Wold. N., Wikstrom. C., Wold. S., 2008. *Design of experiments: Principles and applications*. 3rd Ed. MKS Umetrics AB.

Enghag. P., 2008. *Encyclopedia of the elements: Technical data, history, processing, and applications*. John Wiley & Sons.

Fisher sub-sieve sizer (online). 2012. Available: http://www.aimsizer.com/ (Accessed 13 April 2014).

Gurmen, S., Stopic, S., Friedrich, B., 2005. Recovery of sub-micron cobalt powder by acidic leaching of cemented carbide scrap. *Proceedings of EMC 2005*. (1-14).

Hannis, S., and Bide, T., 2009. British Geological Survey: Cobalt (Profile). United Kingdom.

Hareepersad. A, Musonge. P, Swalaha. F.M, Oehlers. M., 2013a. Single step high volume production of sub-micron cobalt powder. *18th Plansee Seminar International conference on Refractory metals and Hard metals*. 2013: 1003-1015.

Hareepersad. A., 2011. Furnace production. (Production record). Shu Powders Africa.

Hareepersad. A., 2012. Carbon dioxide capex file. (Presentation). Shu Powders Africa.

Hareepersad. A., 2014. Jet mill processing. (Production record). Shu Powders Africa.

Honhe, M., Mende, B., Eikemeyer, K., 2002. *Ultra-fine cobalt metal powder process for the production thereof and the use of the cobalt metal powder and of cobalt carbonate.* US Patent 6346137.

A guidebook to particle size analysis (online). 2012. Available: http://www.horiba.com/ (Accessed 13 April 2014).

Alpine fluidized bed opposed jet mill (online). 2010. Available: https://www.hosokawa-alpine.com/powder-particle-processing/machines/jet-mills/afg-fluidised-bed-opposed-jet-mill/ (Accessed 13 April 2014).

Montgomery, D. C., 2009. *Design and analysis of experiments*. 7th Ed. New York: Wiley & Sons.

Moodlier. D., 2011. Customer specifications. (Lab record). Shu Powders Africa.

Moodlier, D., 2010. Raw material specifications. (Lab Record). Shu Powders Africa.

Moodlier, D., 2012. Sem of raw material. (Lab Record). Shu Powders Africa.

Moodlier, D., 2013. Finished product analysis. (Lab Record). Shu Powders Africa.

Moodlier, D., 2014. Customer feedback records. (Lab Record). Shu Powders Africa.

Oehlers, M., Tybaert, C., and Peersman, J., 2000a, Comparison of different cobalt powders in cemented carbide grades. *Proceedings of the 2000 international conference on tungsten, hard metals and refractory alloys*. 25-27 September, (1-9).

Oehlert. G., 2000. *A first course in design and analysis of experiments: Response surface methods.* New York: W. H. Freeman.

Samsonov, G. V., 1968. *Handbook of the physicochemical properties of the elements: Cobalt*. Springer US.

Singh. G., 2012. Hydrogen reduction of heterogenite to make sub-micron cobalt metal powder for hard metal applications. *International journal of refractory metals and hard metals*. 35: 300-305.

Zhang, J., Chun, Y., Niao, J., Yang, W., Guan, F., 2000. Preparation of ultra-fine cobalt powder by chemical reduction in aqeuos solution. *Chinese Chemical Letters.* 12:555.

CHAPTER 8

APPENDIX A

8.1 Furnace Experimentation 2

8.1.1 Design of experiments 2 - Furnace

Design matrix 2 for the furnace experimentation is represented in this section. The design was based on a two level factorial design method. There was 6 center points selected for this design. Based on the response variables produced in design matrix 1, the selection of operational parameters was narrowed in order to optimize the experimental runs (Table 8.1).

Table 8.1 Furnace experimental parameters for design matrix 2

Factor	Range
Temperature	350 - 475 °C
Hydrogen Flow rate	150 - 200 Nm^3/h
Belt Speed	40 - 80 mm/min
Carbon Dioxide Flow rate	60 - 90 Nm^3/h

Design matrix two parameters were based on the responses variables generated for design matrix one. The first experimental run gave the feel for how the powder reacted with a variation of operational parameters. Hence major changes in the operational parameters in experimental run two were not made so as to ensure that the experimenter got to see the effect on the response variable by small changes made in operation.

Table 8.2 Analytical data of factors and response variables for furnace experimentation 2

STD	RUN	Factor 1 - A TEMP °C	Factor 2 - B H_2 Nm^3/h	Factor 3 - C CO_2 Nm^3/h	Factor 4 - D BS mm/min	Response 1 FSSS µm	Response 2 O_2 %
8	1[5]	475	200	80	60	1.3	0.18
15	2[5]	350	200	80	90	0.36	1.5
20	3[5]	412.5	175	60	75	0.65	1.1
16	4	475	200	80	90	0.99	0.48
12	5	475	200	40	90	0.98	0.54
9	6[5]	350	150	40	90	0.33	2.1
19	7[5]	412.5	175	60	75	0.63	1.06
4	8[5]	475	200	40	60	1.28	0.22
11	9[5]	350	200	40	90	0.37	1.62
21	10[5]	412.5	175	60	75	0.64	1.02
14	11	475	150	80	90	0.91	0.61
10	12	475	150	40	90	0.93	0.65
1	13[5]	350	150	40	60	0.45	1.39
7	14[5]	350	200	80	60	0.49	1.2
6	15[5]	475	150	80	60	1.3	0.26
5	16[5]	350	150	80	60	0.44	1.33
18	17[5]	412.5	175	60	75	0.67	1.08
13	18[5]	350	150	80	90	0.32	2
2	19[5]	475	150	40	60	1.32	0.31
3	20[5]	350	200	40	60	0.47	1.28
22	21[5]	412.5	175	60	75	0.61	1.08
17	22[5]	412.5	175	60	75	0.68	1.03

Experimental runs in 4, 5, 11 and 12 in (Table 8.2) produced powder that was getting closer to producing sub-micron cobalt powder.

[5] These runs consist of powder that is unreduced and highly oxidized to powder that is classified as normal cobalt powder.

8.1.2 Response Variable Fsss

The fsss analysis did not require a transform as the ratio between minimum and maximum response value was below 10. The effects of each factor on the response needed to be understood. The half normal plot or Pareto chart was used to graphically highlight the effects of the factors on the response variable.

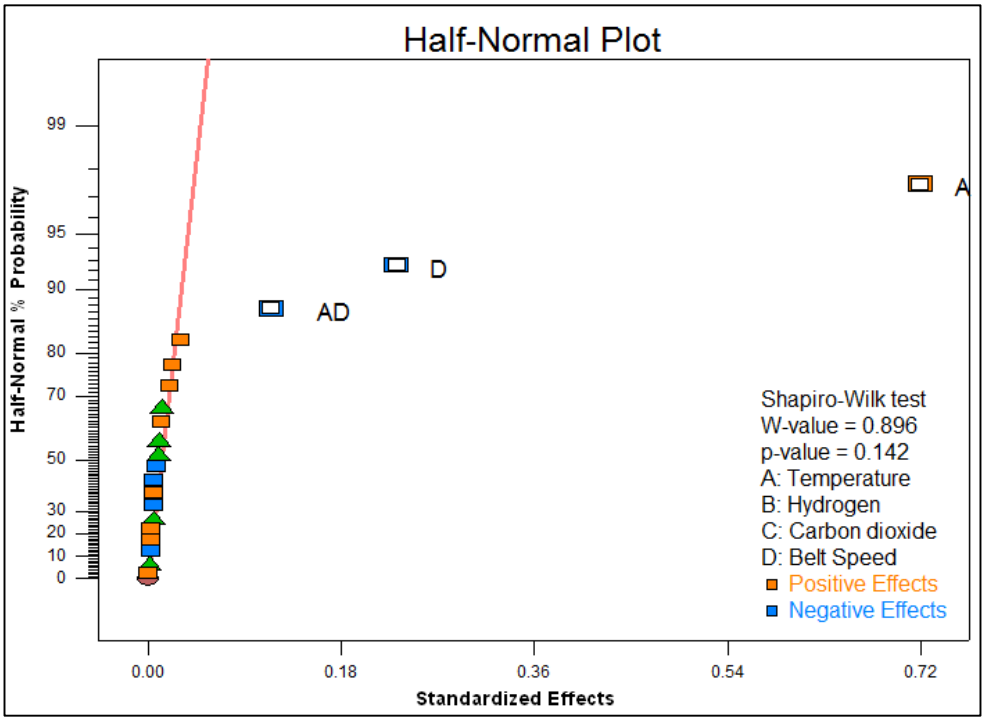

Figure 8.1 Half-normal probability for experimentation 2 for fsss (µm) selected effects.

Factor A (temperature), D (belt speed) and the two factor interaction AD (temperature × belt speed) are selected as main effects in (Figure 8.1). The *p*-value generated after the selection is 0.142.

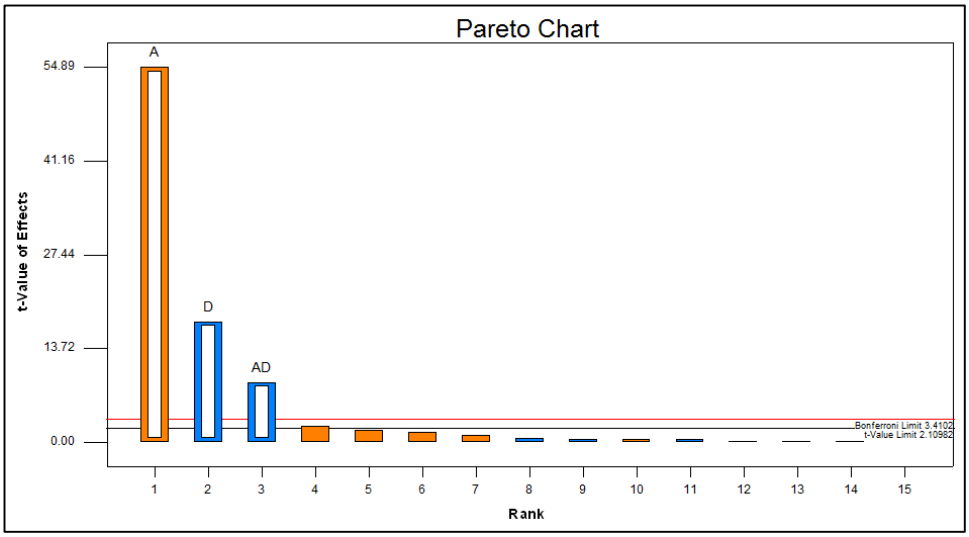

Figure 8.2 Pareto chart for experimentation 2 for fsss (µm) selected effects.

Figure 8.2 is the Pareto chart highlighting the magnitude of the effects in the experimentation. The above figure indicates that factor A (temperature) has a positive effect on particle size. Factor D (belt speed) and Factor AD (temperature and belt speed combined) have a negative effect on particle size.

Table 8.3 Anova of fsss for furnace experimentation 2

Source	Sum of Squares	df	Mean Square	F Value	p-value Prob > F	Significance
Model	2.36	3	0.79	1133.57	< 0.0001	Significant
A-Temperature	2.09	1	2.09	3012.43	< 0.0001	Significant
D-Belt Speed	0.22	1	0.22	311.95	< 0.0001	Significant
AD	0.053	1	0.053	76.32	< 0.0001	Significant
Curvature	0.061	1	0.061	88.15	< 0.0001	Significant
Residual	0.012	17	0.0006931	-	-	-
Lack of Fit	0.00845	12	0.0007042	1.06	0.5139	Not significant
Pure Error	0.003333	5	0.0006667	-	-	-
Cor Total	2.43	21	-	-	-	-

The model F value of 1133.57 in (Table 8.3) implied that the model was significant. There was only a 0.01% chance that a "Model F-value" this large could occur due to noise. When the values of Prob > F was less than 0.05 this indicated that the model terms are significant. The

curvature F value of 88.15 indicated that curvature was significant. The lack of fit F-value of 0.5139 implied that this value was not significant. There was a 51.39% chance that a lack of fit F-value this large could occur due to noise.

Table 8.4 Model applicability and precision for Fsss (µm)

Std. Dev.	0.026	R-Squared	0.9950
Mean	0.73	Adj R-Squared	0.9941
C.V. %	3.59	Pred R-Squared	0.9918
PRESS	0.020	Adeq Precision	76.087

The predicted r-squared of 0.9918 was in reasonable agreement with the adjusted r-squared of 0.9941 in (Table 8.4). Adequate precision measured the signal to noise ratio. A ratio greater than 4 was desirable. The ratio of 76.087 indicated an adequate signal.

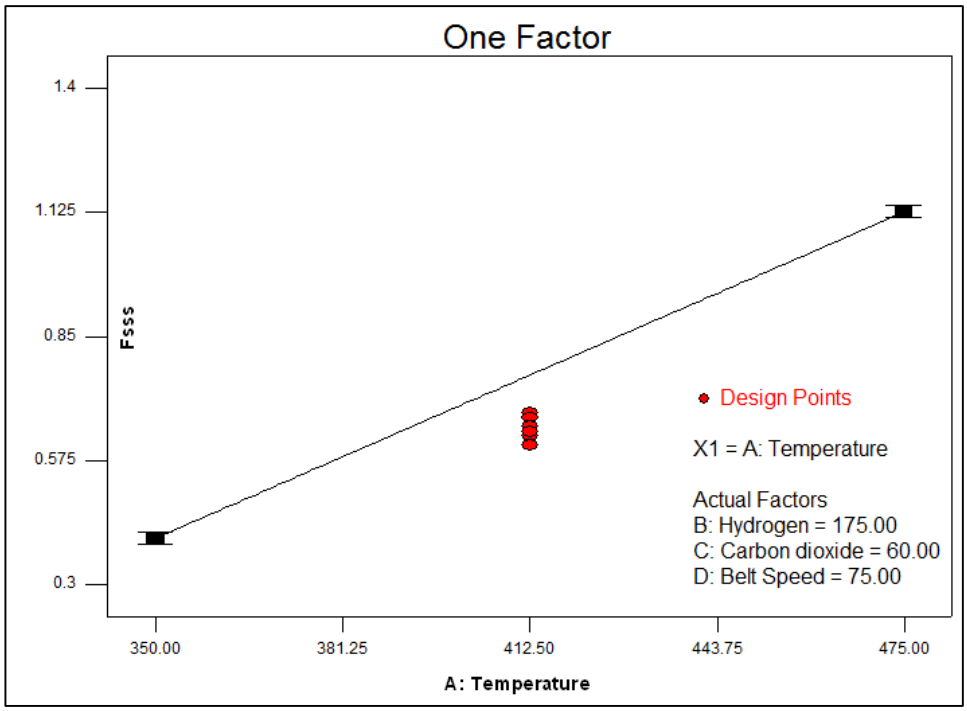

Figure 8.3 Model graph for the effects of temperature (°C) and fsss (µm).

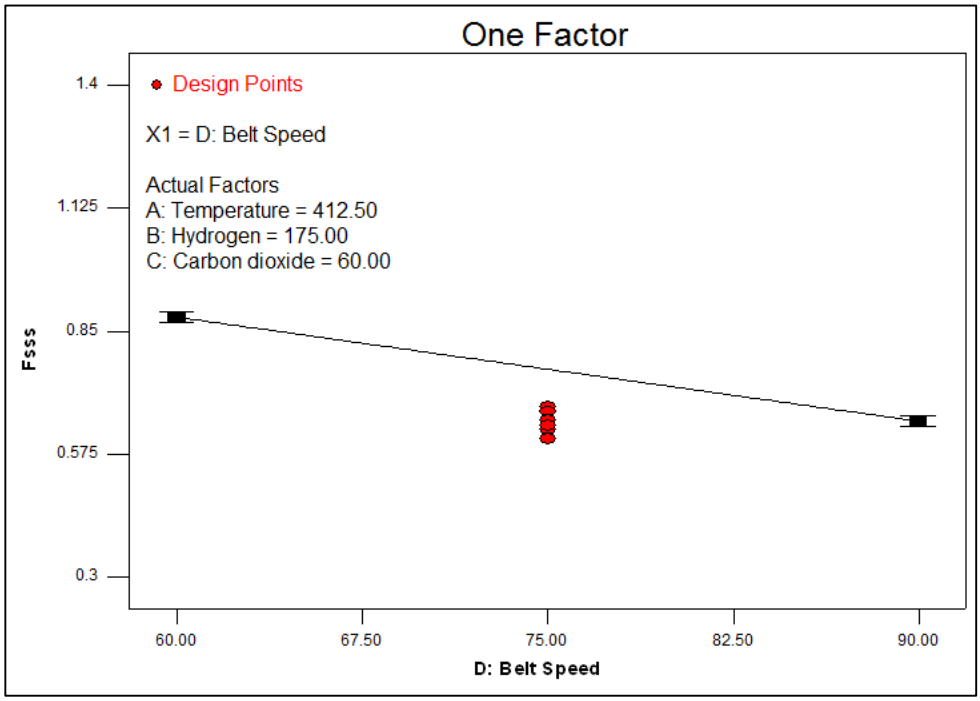

Figure 8.4 Model graph for the effects of belt speed (mm/min) and fsss (µm).

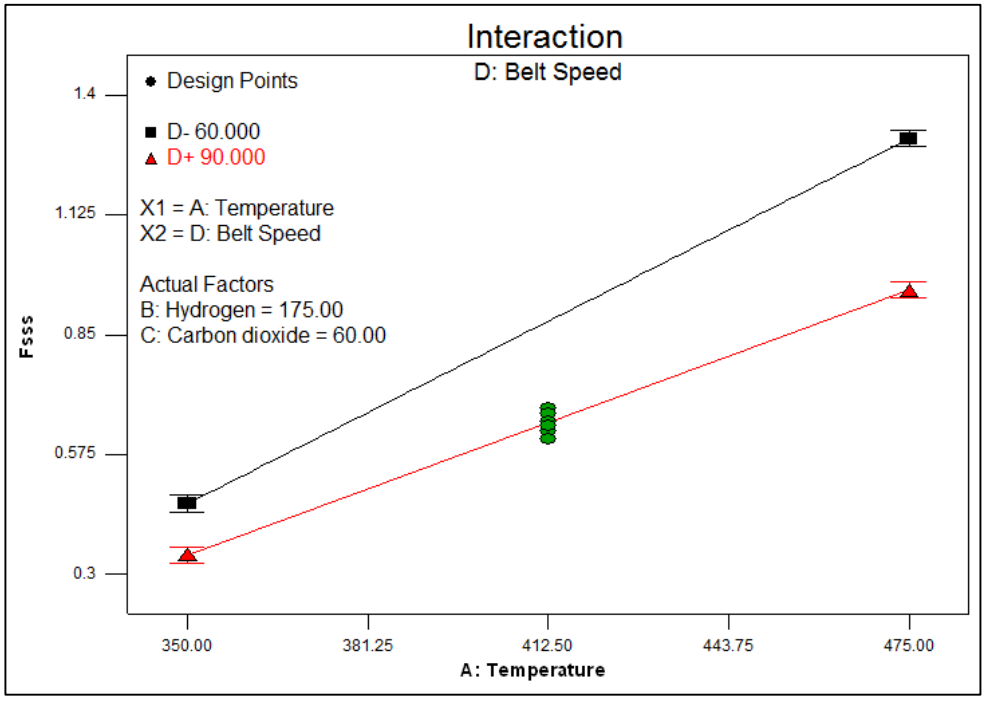

Figure 8.5 Model graph for the effects of temperature (°C) and belt speed (mm/min) on fsss (µm).

The interaction between fsss and temperature (Figure 8.3) highlighted that as temperature increased, fsss on the powder increased. The interaction between fsss and belt speed (Figure 8.4) highlighted that at higher belt speeds, the fsss decreased. The 2 factor interaction (Figure 8.5) of

belt speed and temperature on fsss illustrate that at some mid-point of temperature and belt speed a low fsss could be achieved.

8.1.3 Response Variable Oxygen

The oxygen analysis did require a transform as the ratio between minimum and maximum response value was greater than 10. The transform selected was a natural log.

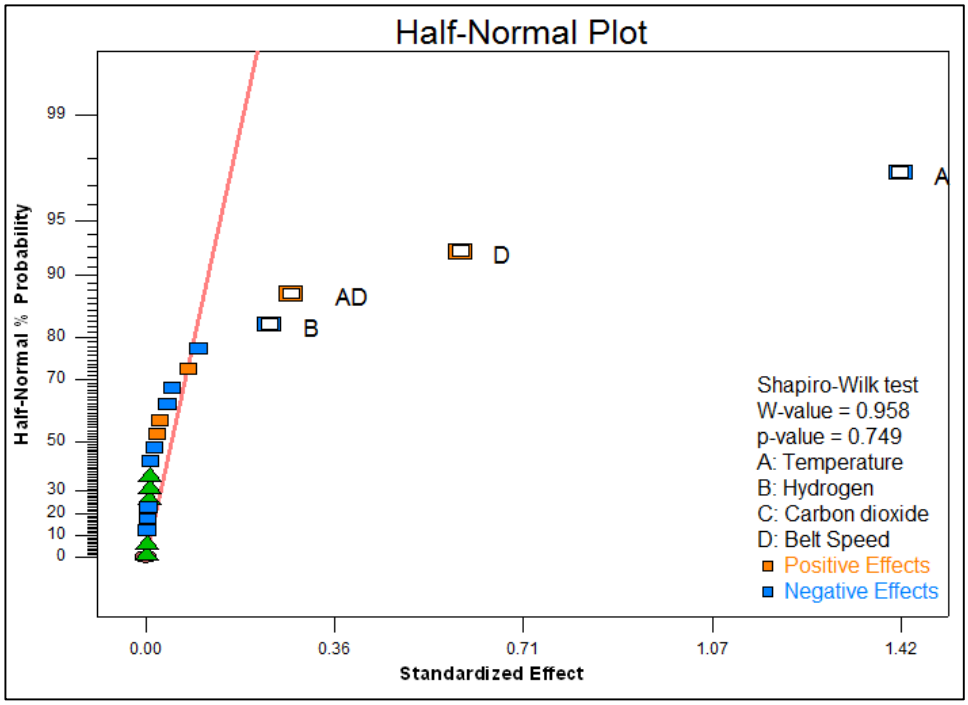

Figure 8.6 Half-normal probability for experimentation 2 for Oxygen (%) selected effects.

Factor A (temperature), factor D (belt speed), factor B (hydrogen flow rate) and the two factor interaction AD (temperature × belt speed) are selected as main effects in (Figure 8.6). The *p*-value generated after the selection is 0.749.

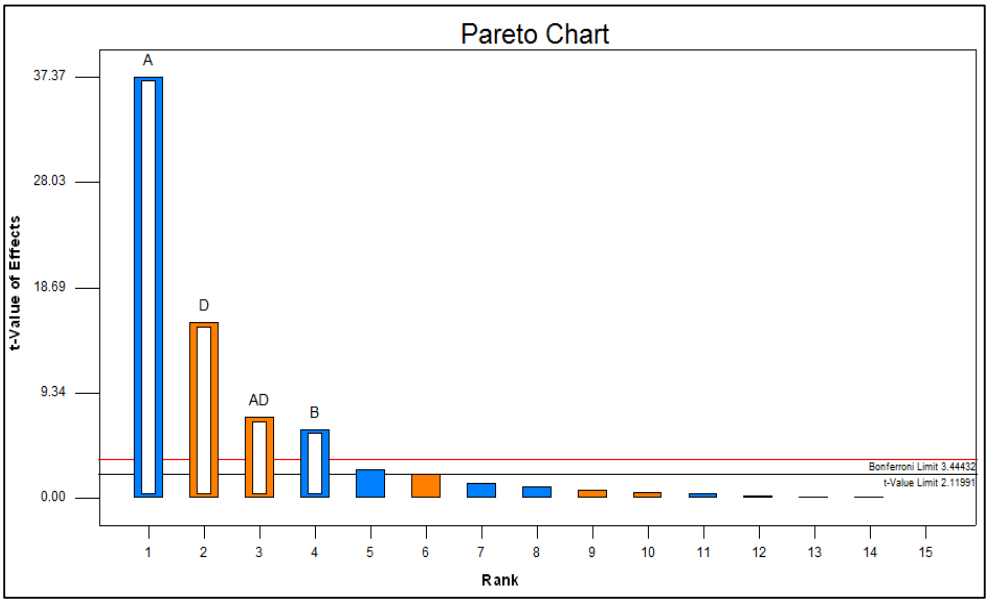

Figure 8.7 Pareto chart for experimentation 2 for Oxygen (%) selected effects.

Figure 8.7 indicated that factor A (temperature) and factor B (hydrogen flow rate) have a negative effect on oxygen content. Factor D (belt speed) and Factor AD (temperature and belt speed combined) have a positive effect on oxygen content.

Table 8.5 Anova of oxygen for furnace experimentation 2

Source	Sum of Squares	df	Mean Square	F Value	p-value Prob > F	Significance
Model	10.04	4	2.51	432.33	< 0.0001	Significant
A-Temperature	8.11	1	8.11	1396.84	< 0.0001	Significant
B-Hydrogen Flow	0.22	1	0.22	37.59	< 0.0001	Significant
D-Belt Speed	1.41	1	1.41	243.10	< 0.0001	Significant
AD	0.30	1	0.30	51.77	< 0.0001	Significant
Curvature	0.54	1	0.54	92.35	< 0.0001	Significant
Residual	0.093	16	0.005804	-	-	-
Lack of Fit	0.088	11	0.008045	9.21	0.0119	Significant
Pure Error	0.004366	5	0.0008732	-	-	-
Cor Total	10.67	21	-	-	-	-

The model F value of 432.33 in (Table 8.5) implied that the model was significant. There was only a 0.01% chance that a "Model F-value" this large could occur due to noise. When the values of Prob > F was less than 0.05 this indicated that the model terms are significant. The curvature F value of 92.35 indicated that curvature was significant. The lack of fit F-value of 0.0119 implied that the lack of fit was significant. This was not good.

Table 8.6 Model applicability and precision for oxygen (%)

Std. Dev.	0.076	R-Squared	0.9908
Mean	-0.20	Adj R-Squared	0.9885
C.V. %	39.99	Pred R-Squared	0.9819
PRESS	0.19	Adeq Precision	56.581

The predicted r-squared of 0.9819 was in reasonable agreement with the adjusted r-squared of 0.9885 in (Table 8.6). Adequate precision measured the signal to noise ratio. A ratio greater than 4 was desirable. The ratio of 56.581 indicated an adequate signal.

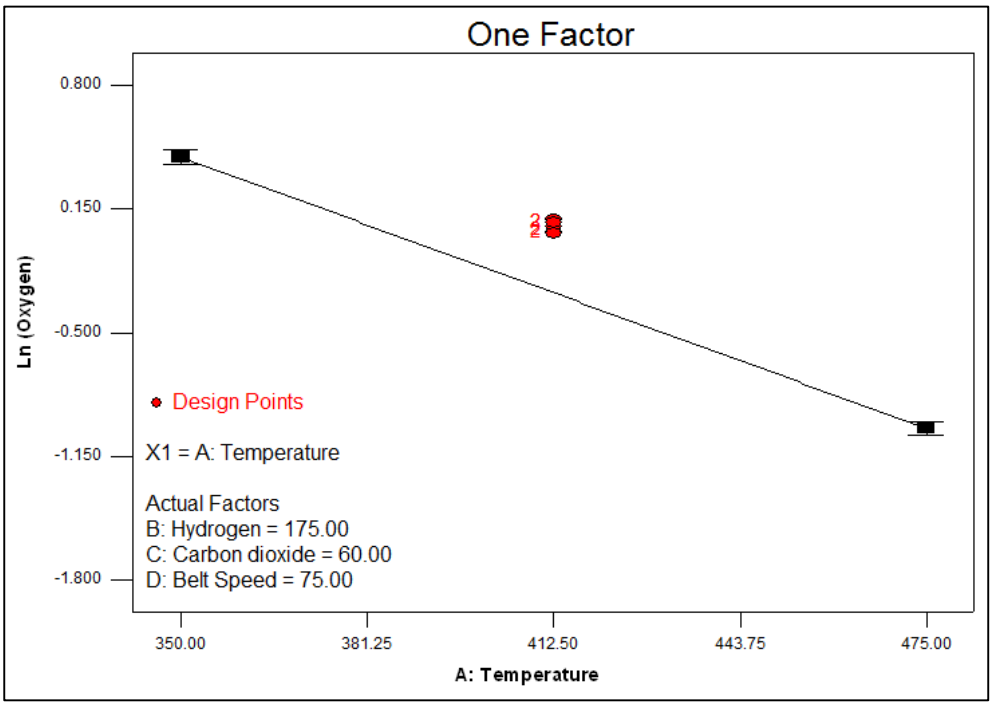

Figure 8.8 Model graph for the effects of temperature (°C) on oxygen (%).

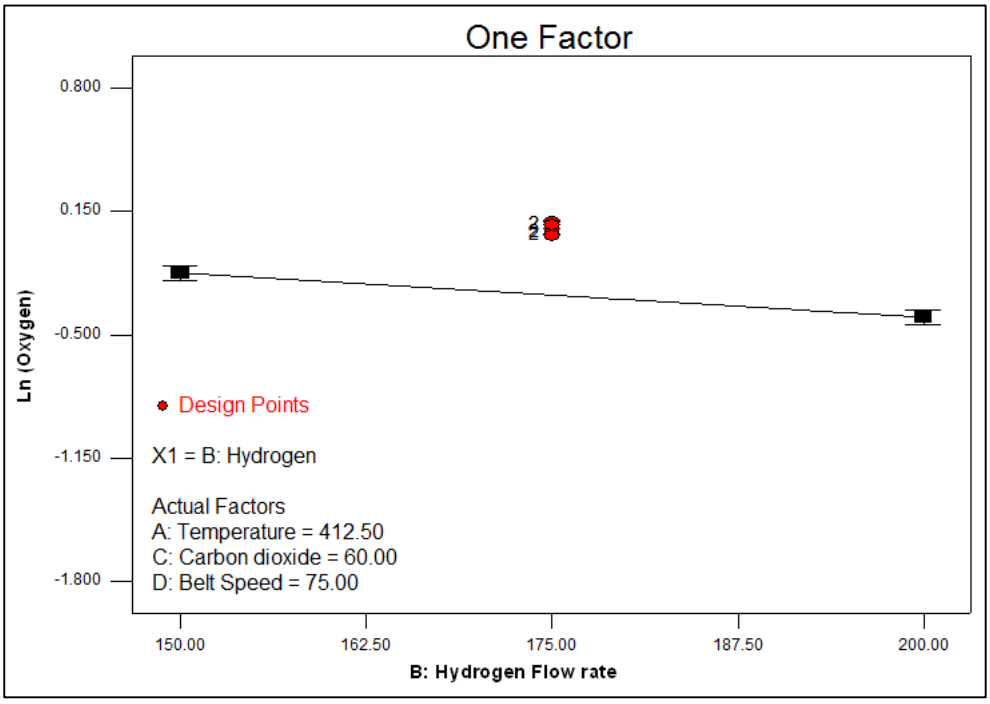

Figure 8.9 Model graph for the effects of hydrogen flow rate (Nm^3/h) on oxygen (%).

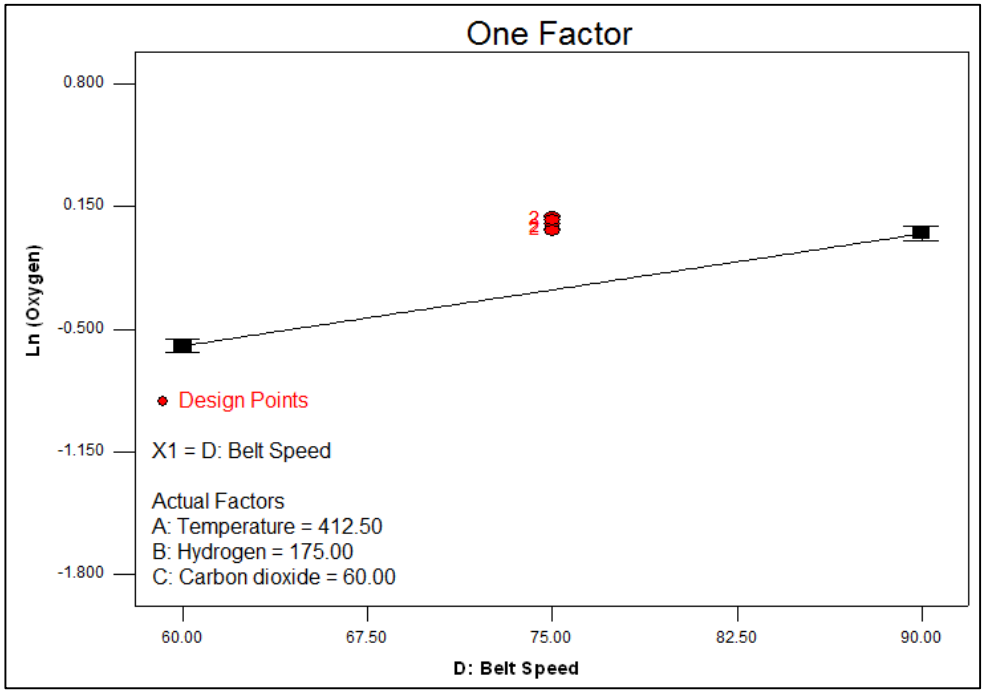

Figure 8.10 Model graph for the effects of belt speed (mm/min) on oxygen (%).

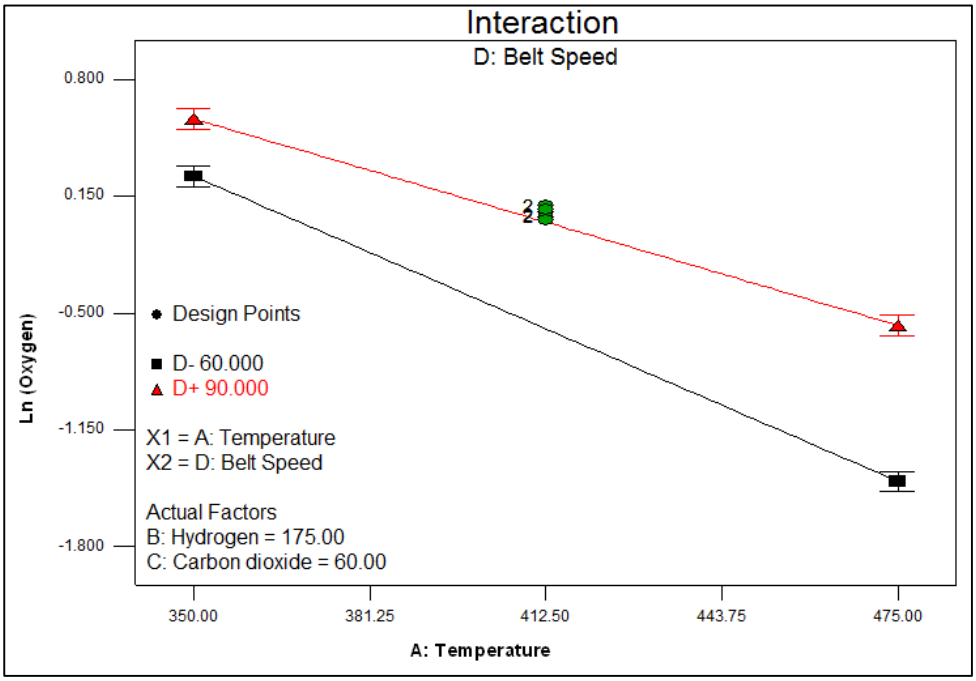

Figure 8.11 Model graph for the effects of temperature (°C) and belt speed (mm/min) on oxygen (%).

The interaction between oxygen and temperature (Figure 8.8) highlighted that as temperature increased, oxygen on the powder decreased. The interaction between hydrogen gas flow rate and oxygen (Figure 8.9) indicated that there was a minimal decrease in oxygen content at high hydrogen gas flow rates. The interaction between oxygen and belt speed (Figure 8.10) highlighted that at higher belt speeds, the oxygen content in the powder increased. The 2 factor interaction (Figure 8.11) of belt speed and temperature on oxygen illustrate that at some mid-point of temperature and belt speed, low oxygen content can be achieved.

8.1.4 Trends Observed for Furnace Experimentation 2 (Particle size and oxygen)

The second experimental design consisted of 22 runs. The trend observed for experimentation 2 in relation to the response variable particle size was that temperature, belt speed and the combination of temperature and belt speed had an impact on particle size (fsss). The second trend observed in relation to response variable oxygen was that temperature, hydrogen gas, belt speed and the combination of temperature and belt speed had an impact on oxygen content.

In design matrix 2 experimental runs 2, 3, 6, 7, 9, 10, 13, 14, 16, 17, 18, 20, 21 and 22 powder produced was highly oxidized and not decomposed properly. For runs 3, 6, 7, 9, 10, 13, 17, 20, 21 and 22 powder did combust as the flow rate of carbon dioxide was < = 60 Nm^3/h.

This experimental design concluded that at temperatures of 350°C, the precursor was not reduced properly and therefore the cobalt powder produced was in an unstable state in which it spontaneously combusted. Temperatures greater than and equal to 475°C yielded powder with a particle size greater than 1 micron however if the belt speed was greater resulting in a shorter residence time the particle size could be less than 1 micron. High volumes of hydrogen gas reduced oxygen content of the cobalt powder significantly even at high belt speeds and low temperatures. This experimentation also highlighted the importance of belt speed on both particle size and oxygen content. Hence for design matrix 3 higher belt speeds were selected.

8.2 Furnace experimentation 3

8.2.1 Response surface methodology for furnace experimentation 3

Design matrix 3 followed the design route response surface methodology using the central composite method. There was 1 axial and 1 factorial point selected for the design. The alpha value selected was at 1.71 which was an orthogonal quadratic alpha as it was least extreme as compared to the other alpha values. This set the cubical portion of the central composite design. Altogether there were 30 runs for experimentation 3 which consisted of 6 center points and 1 axial point for each factor. Table 8.7 represents the range in which the parameters were set.

Table 8.7 Furnace experimental parameters for design matrix 3

Factor	Range
Temperature	400 - 475 °C
Hydrogen Flow rate	150 - 250 Nm^3/h
Belt Speed	50 - 90 mm/min
Carbon Dioxide Flow rate	60 - 100 Nm^3/h

Table 8.8 The design range for experimentation 3

Factor	Units	-1 Level	+1 Level	(-) alpha	(+) alpha
Temperature	°C	400	475	362.5	512.5
Hydrogen gas	Nm^3/h	150	250	100	300
Carbon dioxide gas	Nm^3/h	50	90	30	110
Belt speed	mm/min	60	100	40	120

The design range was represented in (Table 8.8).

Table 8.9 Design summary for furnace experimentation 3

Factor	Name	Units	Type	Low Actual	High Actual	Low Coded	High Coded	Mean	Std. Dev.
A	Temperature	°C	Numeric	400	475	-1	1	437.5	33.541
B	Hydrogen gas	Nm^3/h	Numeric	150	250	-1	1	200	44.721
C	Carbon Dioxide gas	Nm^3/h	Numeric	50	90	-1	1	70	17.889
D	Belt speed	mm/min	Numeric	60	100	-1	1	80	17.889

The design summary for design matrix 3 was represented in (Table 8.9).

Table 8.10 Analytical data of factors and response variables for furnace experimentation 3

Std	Run	Factor 1 - A Temp (°C)	Factor 2 - B H_2 (Nm^3/h)	Factor 3 - C CO_2 (Nm^3/h)	Factor 4 - D BS (mm/min)	Response 1 Fsss (μm)	Response 2 Oxygen (%)
3	1[6]	400	250	50	60	0.70	0.97
29	2	437.5	200	70	80	0.80	0.85
15	3[6]	400	250	90	100	0.48	1.05
30	4	437.5	200	70	80	0.81	0.84
21	5	437.5	200	30	80	0.80	0.87
19	6[6]	437.5	100	70	80	0.8	1.1
10	7	475	150	50	100	0.87	0.88
2	8	475	150	50	60	1.22	0.32
8	9	475	250	90	60	1.2	0.18
14	10	475	150	90	100	0.86	0.85
5	11[6]	400	150	90	60	0.71	1.20
17	12[6]	362.5	200	70	80	0.38	1.5
23	13	437.5	200	70	40	1.1	0.40
13	14[6]	400	150	90	100	0.47	1.35
12	15	475	250	50	100	0.85	0.75
28	16	437.5	200	70	80	0.79	0.86
24	17	437.5	200	70	120	-	-
1	18[6]	400	150	50	60	0.69	1.25
18	19	512.5	200	70	80	1.45	0.22
6	20	475	150	90	60	1.21	0.28
4	21	475	250	50	60	1.22	0.2
7	22[6]	400	250	90	60	0.71	0.95
16	23	475	250	90	100	0.87	0.72
20	24	437.5	300	70	80	-	-
26	25	437.5	200	70	80	0.8	0.82
11	26[6]	400	250	50	100	0.48	1.09
22	27	437.5	200	110	80	0.8	0.79
27	28	437.5	200	70	80	0.81	0.85
9	29[6]	400	150	50	100	0.45	1.37
25	30	437.5	200	70	80	0.8	0.84

[6] These runs consist of powder that is unreduced and highly oxidized to powder that is classified as normal cobalt powder.

Experimental runs 17 and 24 in (Table 8.10) could not been conducted as the settings of the operational parameters exceeded the operational limit as per (Table 4.1). The response variables produced in experimentation 3, produced powder with sub-micron particle size however oxygen content was very high. The design trend between fsss and oxygen for experimentation 3 was represented in (Figure 8.12).

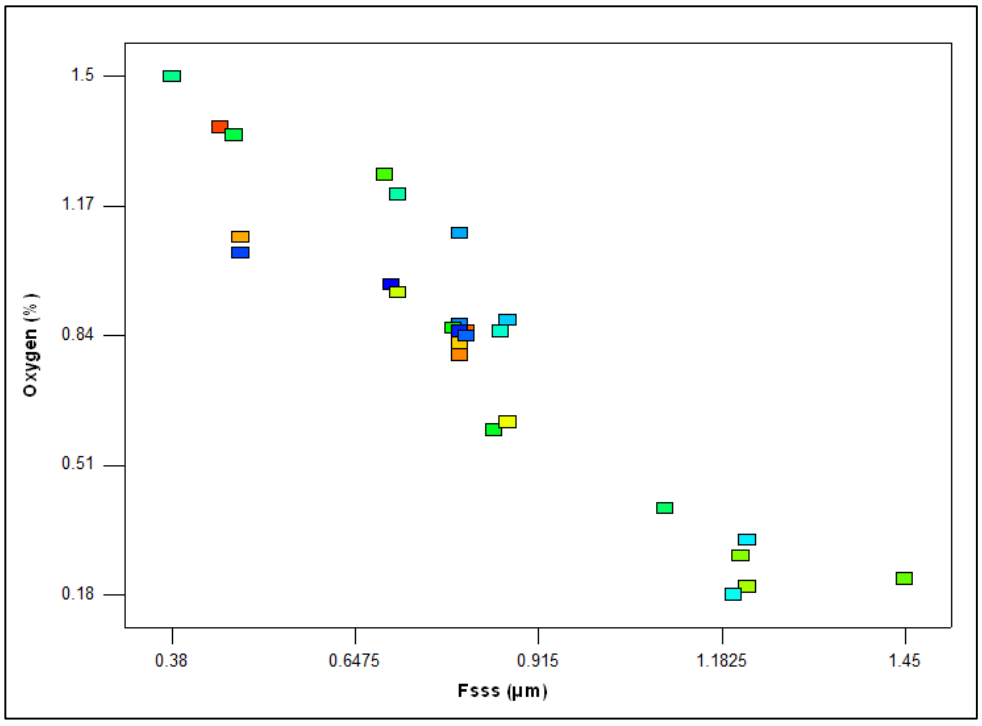

Figure 8.12 The design trend between fsss and oxygen for experimentation 3.

8.2.2 Response variable fsss

The fsss analysis did not require a transform as the ratio between the minimum and maximum response value was 3.81.

Table 8.11 Model summary statistics for fsss - experimentation 3

Std. Source	Adjusted Dev.	R-Squared	Adjusted R-Squared	Predicted R-Squared	PRESS
Linear	0.045	0.9747	0.9703	0.9596	0.074
2FI	0.043	0.9826	0.9724	0.9630	0.068
Quadratic	0.030	0.9937	0.9869	0.9531	0.086
Cubic	0.008559	0.9998	0.9989	-	+[5]

The model summary (Table 8.11) indicated that a cubic model was aliased. The model suggested was the quadratic model as this had a maximum predicted R-squared and adjusted R-squared value.

Table 8.12 Lack of fit tests for fsss - experimentation 3

Sum of Source	Mean Squares	F (df)	p-value Square	Value	Prob > F
Linear	0.046	18	0.002571	45.36	0.002
2FI	0.032	12	0.002644	46.67	0.0003
Quadratic	0.011	8	0.001422	25.09	0.0013
Cubic	0.000156	1	0.0001562	2.76	0.1577
Pure Error	0.000283	5	0.000056	-	+[7]

The lack of fit tests (Table 8.12) compared residual error with pure error from replicated design points. A significant lack of fit was represented by a low Prob > F value. The quadratic model was highlighted again as the suggested model as it did not show significant lack of fit.

[7] + Indicates that this is a case where the leverage is equal to 1, hence the press statistic could not be defined.

Table 8.13 Anova of fsss for furnace experimentation 3

Source	Sum of Squares	df	Mean Square	F Value	p-value Prob > F	Significance
Model	1.83	14	0.13	145.75	< 0.0001	Significant
A-temp	1.38	1	1.38	1536.23	< 0.0001	Significant
B-hydrogen gas	0.000002	1	0.000002	0.002278	0.9627	
C-carbon dioxide	0.000038	1	0.000037	0.042	0.8411	
D-belt speed	0.37	1	0.37	412.95	< 0.0001	Significant
AB	0.00031	1	0.00031	0.34	0.5690	
AC	0.00031	1	0.00031	0.34	0.5690	
AD	0.014	1	0.014	15.40	0.0017	Significant
BC	0.0000063	1	0.0000063	0.00697	0.9347	
BD	0.000056	1	0.000056	0.063	0.8062	
CD	0.000056	1	0.000056	0.063	0.8062	
A^2	0.018	1	0.018	19.91	0.0006	Significant
B^2	0.0003792	1	0.00038	0.42	0.5268	
C^2	0.0001823	1	0.0001823	0.20	0.6595	
D^2	0.0002143	1	0.0002143	0.24	0.6331	
Residual	0.012	13	0.0008967	-	-	
Lack of Fit	0.011	8	0.001422	25.09	0.0013	Significant
Pure Error	0.0002833	6	0.00005667	-	-	
Cor Total	1.84	27	-	-	-	

The model F-value of 145.75 in (Table 8.13) indicated that the model was significant. Model terms A, D, AD and A^2 are significant. Model terms A^2 and AD had a small effect on particle size in relation to model terms A and D. The lack of fit value of 0.0013 indicated that there was a significant lack of fit which was not good as we want the model to fit.

Table 8.14 Model applicability and precision for fsss (experimentation 3)

Std. Dev.	0.030	R-Squared	0.9937
Mean	0.83	Adj R-Squared	0.9869
C.V. %	3.63	Pred R-Squared	0.9531
PRESS	0.086	Adeq Precision	43.724

The predicted R-squared and the adjusted R-squared in (Table 8.14) were in agreement with each other. The adequate precision value of 43.724 indicated an adequate signal. The final equation generated in terms of actual factors was:

$$\begin{aligned} FSSS = {} & (+0.26936) + (-0.00585 \times T) + (+0.001713 \times H_2) + (+0.00328819 \times CO_2) + \\ & (+0.010554 \times BS) + (-2.33E^{-06} \times T \times H_2) + (-5.83E^{-06} \times T \times CO_2) + \\ & (-3.92E^{-05} \times T \times BS) + (-6.25^{-07} \times H_2 \times CO_2) + (+1.87E^{-06} \times H_2 \times BS) + \\ & (+4.69E^{-06} \times CO_2 \times BS) + (+1.86E^{-05} \times T^2) + (-2.01E^{-06} \times {H_2}^2) + \\ & (-6.598E^{-06} \times {CO_2}^2) + (-9.46E^{-06} \times BS^2) \end{aligned}$$

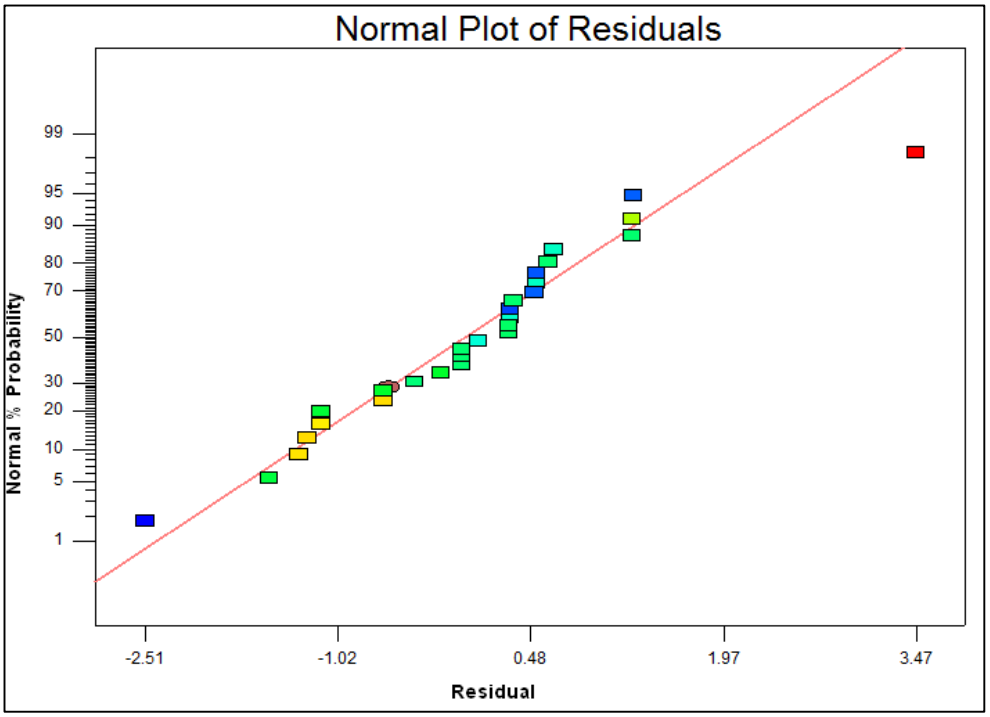

Figure 8.13 Normal plot vs. residual for fsss.

The data points in (Figure 8.13) represent a linear pattern which was desired as a non-linear pattern indicates non-normality in the error term.

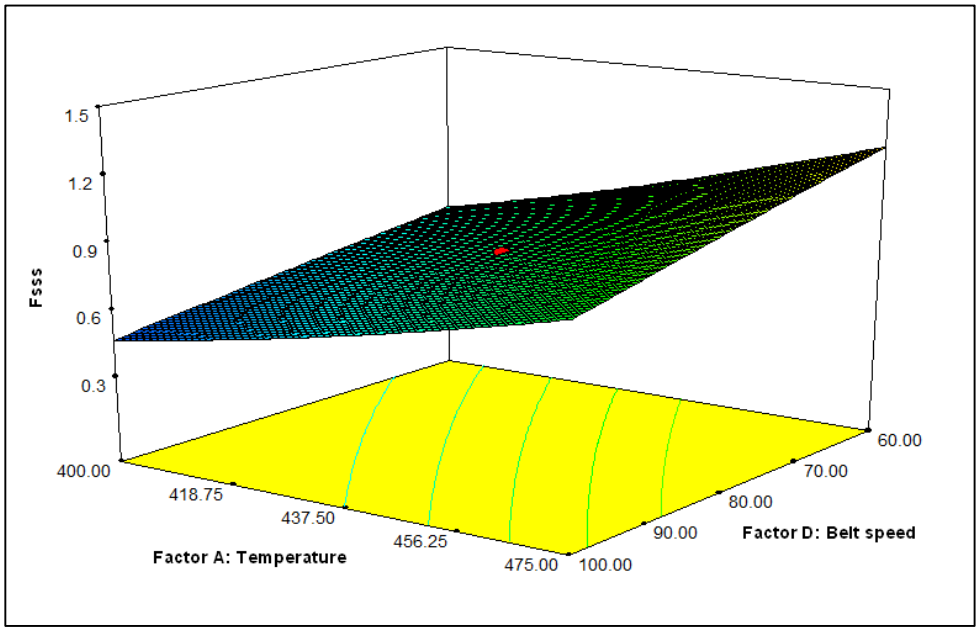

Figure 8.14 3D surface model for fsss vs. temperature and belt speed interaction.

Low temperatures and high belt speed (Figure 8.14) resulted in low particle size (fsss).

8.2.3 Response variable oxygen

The oxygen analysis did not require a transform as the ratio between the minimum and maximum response value was 8.31.

Table 8.15 Model summary statistics for oxygen - experimentation 3

Std. Source	Adjusted Dev.	R-Squared	Adjusted R-Squared	Predicted R-Squared	PRESS
Linear	0.088	0.9506	0.9421	0.9196	0.29
2FI	0.037	0.9935	0.9897	0.9798	0.072
Quadratic	0.022	0.9982	0.9963	0.9887	0.041
Cubic	0.015	0.9996	0.9983	-	+[8]

The model summary (Table 8.15) indicated that a cubic model was aliased. The model suggested was the quadratic model as this had a maximum predicted R-squared and adjusted R-squared value.

Table 8.16 Lack of fit tests for oxygen - experimentation 3

Sum of Source	Mean Squares	F (df)	p-value Square	Value	Prob > F
Linear	0.18	18	0.00979	52.47	0.0002
2FI	0.022	12	0.00186	9.96	0.0098
Quadratic	0.005438	8	0.00068	3.64	0.0854
Cubic	0.0004	1	0.0004	2.14	0.2031
Pure Error	0.00093	5	0.000187	-	+[6]

The lack of fit tests (Table 8.16) compared residual error with pure error from replicated design points. A significant lack of fit was represented by a low Prob > F value. The quadratic model was highlighted again as the suggested model as it did not show significant lack of fit.

[8] + Indicates that this is a case where the leverage is equal to 1, hence the press statistic could not be defined.

Table 8.17 Anova of oxygen for furnace experimentation 3

Source	Sum of Squares	df	Mean Square	F Value	p-value Prob > F	Significance
Model	3.58	14	0.26	522.40	< 0.0001	Significant
A-temp	2.57	1	2.57	5252.68	< 0.0001	Significant
B-hydrogen gas	0.22	1	0.22	452.22	< 0.0001	Significant
C-carbon dioxide	0.0054	1	0.0054	11.02	0.0055	
D-belt speed	0.40	1	0.4	823.84	< 0.0001	Significant
AB	0.009025	1	0.009025	18.42	0.0009	
AC	0.00023	1	0.000225	0.46	0.5099	
AD	0.14	1	0.14	279.35	< 0.0001	Significant
BC	0.0004	1	0.0004	0.82	0.3827	
BD	0.00723	1	0.007225	14.74	0.0020	
CD	0.00023	1	0.000225	0.46	0.5099	
A^2	0.000601	1	0.0006011	1.23	0.2881	
B^2	0.001013	1	0.001013	2.07	0.1741	
C^2	0.000192	1	0.000192	0.39	0.5421	
D^2	0.016	1	0.016	32.04	< 0.0001	Significant
Residual	0.00637	13	0.0004901	-	-	
Lack of Fit	0.005438	8	0.0006797	3.64	0.0854	Not Significant
Pure Error	0.00093	5	0.0001867	-	-	
Cor Total	3.59	27	-	-	-	

The model F-value of 522.40 in (Table 8.17) indicated that the model was significant. Model terms A, B, D, AD and D^2 are significant. Model terms D^2 and AD had a small effect on oxygen content in relation to model terms A, B and D. The lack of fit value of 0.0854 indicated that there was a non-significant lack of fit which was good as we wanted the model to fit.

Table 8.18 Model applicability and precision for oxygen (experimentation 3)

Std. Dev.	0.022	R-Squared	0.9982
Mean	0.83	Adj R-Squared	0.9963
C.V. %	2.68	Pred R-Squared	0.9887
PRESS	0.041	Adeq Precision	83.318

The predicted R-squared and the adjusted R-squared in (Table 8.18) were in agreement with each other. The adequate precision value of 83.318 indicated an adequate signal. The final equation generated in terms of actual factors was:

$$\begin{aligned} Oxygen = {} & (+10.15) + (-0.024465 \times T) + (-0.0078 \times H_2) + (-0.00374 \times CO_2) + \\ & (-0.029688 \times BS) + (+1.27E^{-05} \times T \times H_2) + (+5.0E^{-06} \times T \times CO_2) + \\ & (+1.23E^{-04} \times T \times BS) + (+5.0E^{-06} \times H_2 \times CO_2) + (-2.13E^{-05} \times H_2 \times BS) + \\ & (+9.38E^{-06} \times CO_2 \times BS) + (+3.41E^{-06} \times T^2) + (+3.29E^{-06} \times H_2^{\,2}) + \\ & (-6.77E^{-06} \times CO_2^{\,2}) + (-8.099E^{-05} \times BS^2) \end{aligned}$$

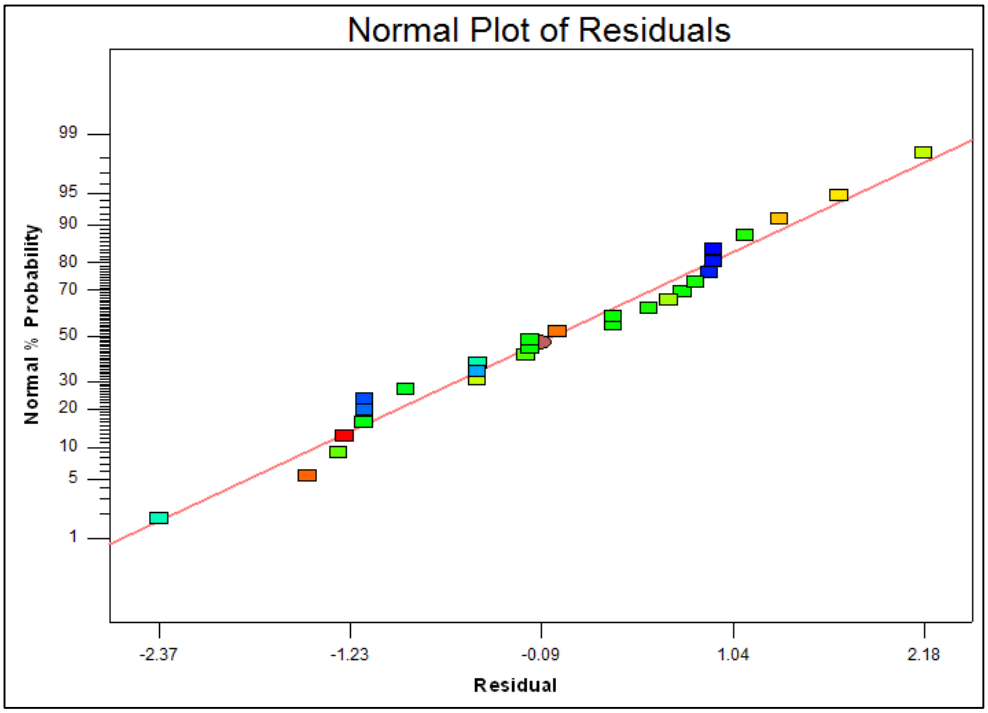

Figure 8.15 Normal Plot vs. Residual for oxygen.

The data points in (Figure 8.15) represented a linear pattern.

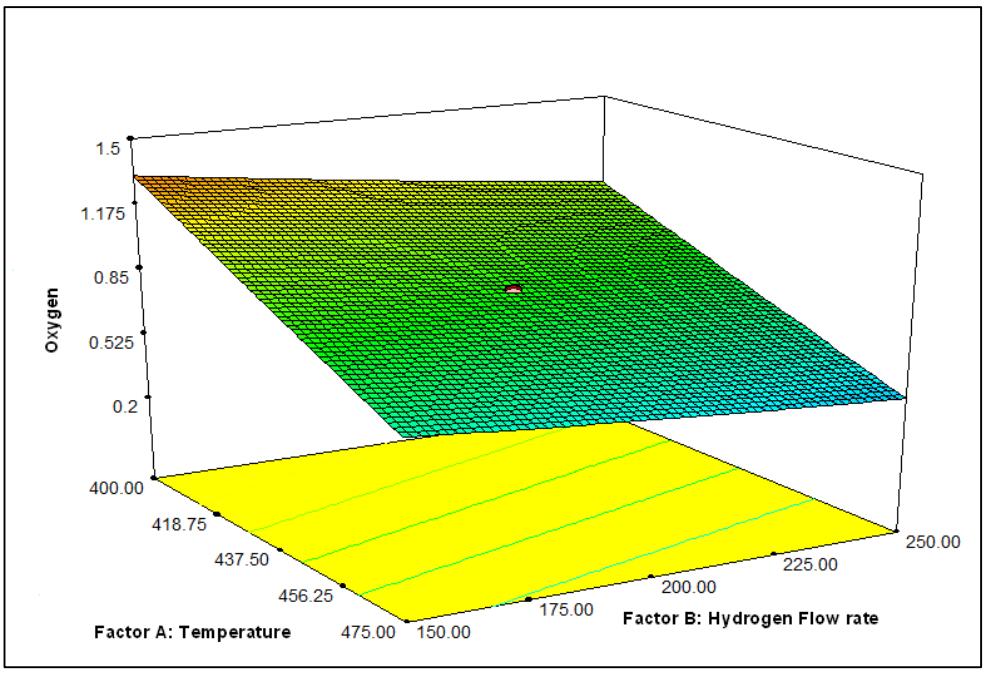

Figure 8.16 3D surface model for oxygen vs. temperature and hydrogen flow rate interaction.

High temperatures and high hydrogen gas flow in (Figure 8.16) resulted in low oxygen content.

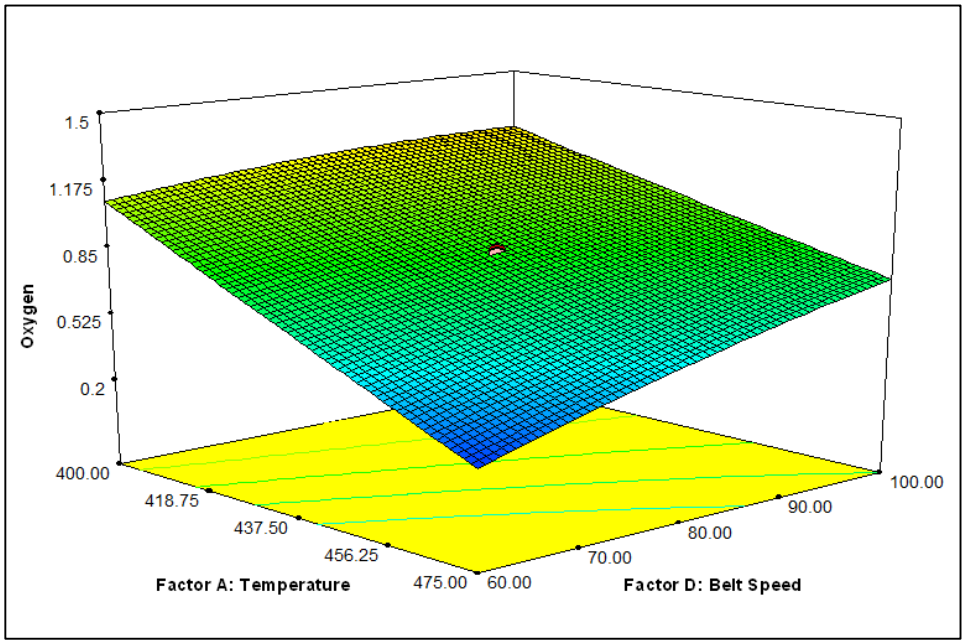

Figure 8.17 3D surface model for oxygen vs. temperature and belt speed interaction.

High temperatures and low belt speeds (Figure 8.17) resulted in low oxygen content.

8.2.4 Trends observed in furnace experiment 3 (Particle size and oxygen)

The third experimental design consisted of 30 runs. The trend observed for experimentation 3 in relation to the response variable particle size was that temperature, belt speed, and the combination of temperature and belt speed had an impact on particle size (fsss). The second trend observed in relation to response variable oxygen was that temperature, hydrogen gas, belt speed and the combination of temperature and belt speed had an impact on oxygen content.

In experiment 3 the following runs 1, 3, 6, 11, 12, 14, 18, 22, 26 and 29 produced powder that was highly oxidized and not decomposed properly. For runs 3, 11, 14 and 22 powder did not combust as the flow rate of carbon dioxide was > = 80 Nm^3/h. Experiment 3 concluded that at temperatures of < = 400°C, the precursor was not reduced properly and therefore the cobalt powder produced was in an unstable state in which it spontaneously combusted. This occurred even at high hydrogen gas flow rates and low belt speeds.

High hydrogen gas flow rates yielded low oxygen content powder. Belt speed in the right combination of operational parameters yielded particle size within sub-micron range.

The center point runs maintained a constant mid-point temperature whilst varying other operational parameters which helped give a clear indication of what the optimal range for all other parameters should be at. Operational parameters were further fine-tuned for experiment 4 on the furnace.

8.3 Jet mill Experimentation 2

8.3.1 Response surface methodology for jet mill experiment 2

For jet mill experiment two there were 1 axial point selected for the design. The alpha value selected was at 1.52 which was an orthogonal quadratic alpha as it was least extreme as compared to the other alpha values. This set the cubical portion of the central composite design. The ranges for the experimental parameters are represented in (Table 8.19).

Table 8.19 Jet mill operational parameters for experiment 2

Factor	Range
Classifier speed	3500 - 5500 rpm
Grinding gas pressure	4.80 - 6.80 bar
AFG weight	30 - 50 kgs

Table 8.20 The design range for jet mill experiment 2

Factor	Units	-1 Level	+1 Level	(-) alpha	(+) alpha
Classifier speed	rpm	3500	5500	2975	6025
Grinding gas pressure	bar	4.80	6.80	4.30	7.32
AFG weight	kg	30	50	25	55

Table 8.20 highlighted the design range for jet mill experiment 2.

Table 8.21 Design summary for jet mill experimentation 2

Factor	Name	Units	Type	Low Actual	High Actual	Low Coded	High Coded	Mean	Std. Dev.
A	Classifier speed	rpm	Numeric	3500	5500	-1	1	4500	795.2
B	Grinding gas pressure	bar	Numeric	4.80	6.80	-1	1	5.80	0.795
D	AFG weight	kg	Numeric	30	50	-1	1	40	7.95

The mean and standard deviation for experimentation 2 was represented in (Table 8.21).

The design matrix was generated which determined how each run would be conducted.

Table 8.22 Analytical data of factors and response variables for jet mill experimentation 2

Std	Run	Factor A	Factor B	Factor C	Response 1	Response 2
		Classifier Speed (rpm)	Grinding Gas pressure (bar)	AFG Weight (kg)	PSD - d90 (µm)	Milling Time (hrs)
20	1	4500	5.8	40	11.654	2.8
10	2	6025	5.8	40	-	-
2	3[9]	5500	4.8	30	11.311	5.29
11	4[9]	4500	4.3	40	13.259	6.15
7	5[9]	3500	6.8	50	14.325	1.32
15	6	4500	5.8	40	11.981	2.77
12	7	4500	7.3	40	-	-
3	8[9]	3500	6.8	30	14.010	1.55
14	9[9]	4500	5.8	55	14.258	2.52
1	10[9]	3500	4.8	30	16.345	4.98
13	11[9]	4500	5.8	25	11.265	3.2
9	12[9]	2975	5.8	40	16.981	2.0
19	13	4500	5.8	40	11.100	2.90
17	14	4500	5.8	40	11.281	2.85
18	15	4500	5.8	40	11.398	2.65
4	16	5500	6.8	30	11.421	2.1
6	17[9]	5500	4.8	50	11.852	6.01
16	18[9]	4500	5.8	40	13.568	2.5
5	19[9]	3500	4.8	50	16.241	4.68
8	20[9]	5500	6.8	50	12.954	1.82

Altogether there were 20 runs for experiment 2 which consisted of 6 center points and 1 axial point for each factor. No experimental run in (Table 8.23) produced powder with a particle size distribution d_{90} < 10 µm. Runs 2 and 7 could not be conducted as operational ranges were out of limit.

[9] These runs produced powder with a d_{90} value greater than 12 µm and powder that was milled longer than 3 hours.

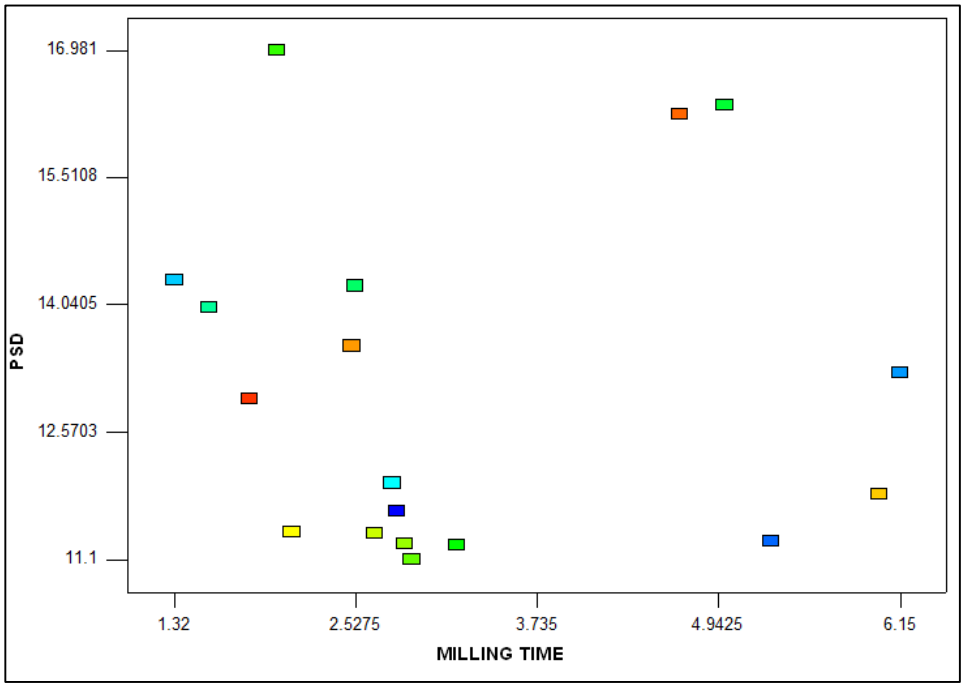

Figure 8.18 The design trend between PSD and Milling time for experimentation 2.

The design trend for particle size distribution (PSD) and milling are represented in (Figure 8.18).

8.3.2 Response variable particle size distribution

The particle size distribution analysis did not require a transform as the ratio between the minimum and maximum response value was 1.53.

Table 8.23 Model summary statistics for particle size distribution

Std. Source	Adjusted Dev.	R-Squared	Adjusted R-Squared	Predicted R-Squared	PRESS
Linear	1.26	0.6528	0.5784	0.4149	37.37
2FI	1.27	0.7219	0.5702	-0.1785	75.27
Quadratic	0.84	0.9124	0.8138	0.5754	27.12
Cubic	0.91	0.9359	0.7820	-	+

The model summary (Table 8.23) indicated that the cubic model was aliased. The model suggested was the quadratic model as this had a maximum predicted R-squared and adjusted R-squared value.

Table 8.24 Lack of fit tests for particle size distribution

Sum of Source	Mean Squares	F (df)	p-value Square	Value	Prob > F
Linear	18.08	9	2.01	2.45	0.1679
2FI	13.67	6	2.28	2.78	0.1407
Quadratic	1.50	3	0.50	0.61	0.6368
Cubic	0.00	0	-	-	-
Pure Error	4.10	5	0.82	-	-

The lack of fit tests (Table 8.24) compared residual error with pure error from replicated design points. The suggested model was the quadratic model. The Prob > F had suggested that the quadratic model had a significant lack of fit which was not desirable.

Table 8.25 Anova of particle size distribution for experimentation 2

Source	Sum of Squares	df	Mean Square	F Value	p-value Prob > F	Significance
Model	58.27	9	6.47	9.26	0.0023	Significant
A-Classifier speed	24.75	1	24.75	35.39	0.0003	Significant
B-Grinding gas pressure	1.37	1	1.37	1.93	0.1989	-
C-AFG weight	3.71	1	3.71	5.30	0.0503	-
AB	3.73	1	3.73	5.33	0.0497	Significant
AC	0.43	1	0.43	0.62	0.4536	-
BC	0.25	1	0.25	0.36	0.5673	-
A^2	6.45	1	6.45	9.22	0.0162	Significant
B^2	0.54	1	0.54	0.78	0.4042	-
C^2	1.34	1	1.34	1.91	0.2039	-
Residual	5.60	8	0.70	-	-	-
Lack of Fit	1.50	3	0.50	0.61	0.6368	Not Significant
Pure Error	4.10	5	0.82	-	-	-
Cor Total	63.87	17	-	-	-	-

The model F-value of 9.26 in (Table 8.25) implied that the model was significant. The above table indicated that the classifier speed and the combination of classifier speed and AFG weight had a major impact on particle size distribution. The lack of fit value of 0.61 indicated that the lack of fit was not significant.

Table 8.26 Model applicability and precision for psd design matrix 2

Std. Dev.	0.84	R-Squared	0.9124
Mean	13.07	Adj R-Squared	0.8138
C.V. %	6.40	Pred R-Squared	0.5754
PRESS	27.12	Adeq Precision	9.423

The predicted R-squared and the adjusted R-squared in (Table 8.27) were in agreement with each other. The adequate precision value of 9.423 indicated an adequate signal.

The final equation generated in terms of actual factors was:

$$PSD = (+83.54349) + (-0.016131 \times CS) + (-7.74667 \times GP) + (-0.45327 \times AFG) + (+6.828E^{-04} \times CS \times GP) + (+2.3287E^{-05} \times CS \times AFG) + (+0.017638 \times GP \times AFG) + (+1.06087E^{-06} \times CS^2) + (+0.3077 \times GP^2) + (+3.75401E^{-03} \times AFG^2)$$

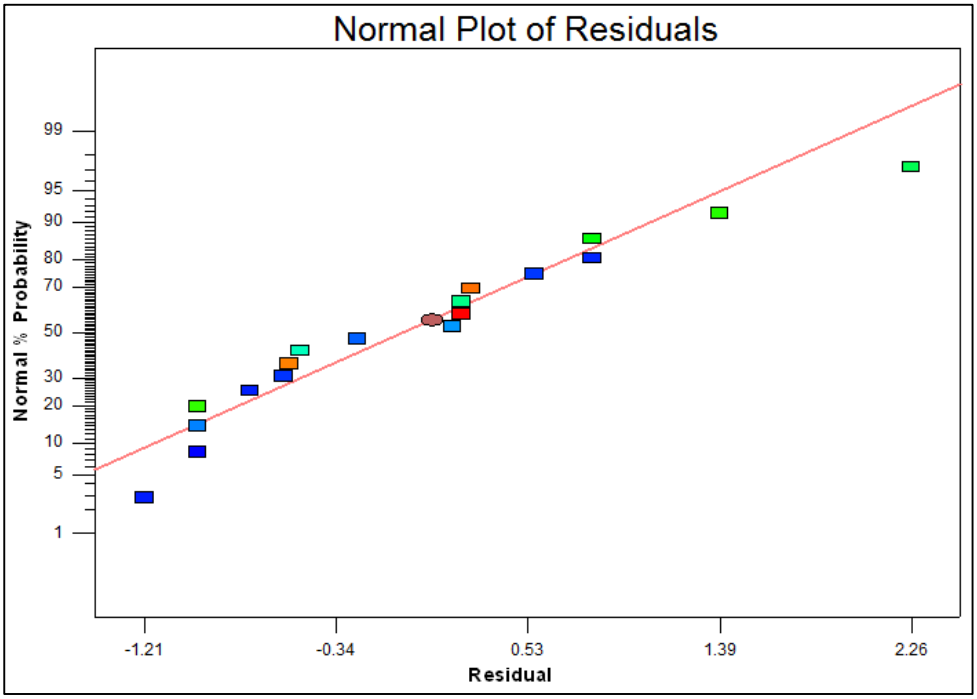

Figure 8.19 Normal plot vs. residual for psd.

The data points in (Figure 8.19) were distributed across the linear target line.

8.3.3 Response variable milling time

Milling time analysis did not require a transform as the ratio between the minimum and maximum response value was 4.66.

Table 8.27 Model summary statistics for milling time

Std. Source	Adjusted Dev.	R-Squared	Adjusted R-Squared	Predicted R-Squared	PRESS
Linear	0.46	0.9237	0.9073	0.8612	5.40
2FI	0.50	0.9306	0.8927	0.5612	17.08
Quadratic	0.29	0.9821	0.9620	0.7386	10.18
Cubic	0.15	0.9972	0.9906	-	-

The model summary (Table 8.27) indicated that the cubic model was aliased. The model suggested was the quadratic model as this has a maximum predicted R-squared and adjusted R-squared value.

Table 8.28 Lack of fit tests for milling time

Sum of Source	Mean Squares	F (df)	p-value Square	Value	Prob > F
Linear	2.86	9	0.32	14.77	0.0043
2FI	2.59	6	0.43	20.07	0.0024
Quadratic	0.59	3	0.20	9.09	0.0181
Cubic	0.00	0	-	-	-
Pure Error	0.11	5	0.022	-	-

The lack of fit tests (Table 8.28) compared residual error with pure error from replicated design points. A significant lack of fit was represented by a low Prob > F value. The quadratic model was highlighted again as the suggested model and had shown a significant lack of fit.

Table 8.29 Anova of milling time for experimentation 2

Source	Sum of Squares	df	Mean Square	F Value	p-value Prob > F	Significance
Model	38.24	9	4.25	48.86	< 0.0001	Significant
A-Classifier speed	1.32	1	1.32	15.20	0.0046	Significant
B-Grinding gas pressure	25.51	1	25.51	293.38	< 0.0001	Significant
C-AFG weight	0.10	1	0.10	1.15	0.3140	-
AB	0.044	1	0.044	0.50	0.4994	-
AC	0.12	1	0.12	1.35	0.2784	-
BC	0.11	1	0.11	1.24	0.2972	-
A^2	0.030	1	0.030	0.35	0.5723	-
B^2	1.30	1	1.30	14.89	0.0048	Significant
C^2	0.15	1	0.15	1.70	0.2284	-
Residual	0.70	8	0.087	-	-	-
Lack of Fit	0.59	3	0.20	9.09	0.0181	Significant
Pure Error	0.11	5	0.022	-		-
Cor Total	38.94	17	-	-		-

The model F-value of 48.86 in (Table 8.29) implied that the model was significant. The above table indicated that the classifier speed, grinding gas pressure and grinding gas pressure squared had a major impact on milling time. The lack of fit value of 9.09 indicated that the lack of fit was significant which was not desirable as we wanted the model to fit.

Table 8.30 Model applicability and precision for milling time design matrix 2

Std. Dev.	0.29	R-Squared	0.9821
Mean	3.23	Adj R-Squared	0.9620
C.V. %	9.14	Pred R-Squared	0.7386
PRESS	10.18	Adeq Precision	24.615

The predicted R-squared and the adjusted R-squared in (Table 8.30) were in agreement with each other. The adequate precision value of 24.615 indicated an adequate signal.

The final equation generated in terms of actual factors was:

$$\begin{aligned} MillingTime = {} & (+28.29214) + (-3.1949E^{-04} \times CS) + (-6.43632 \times GP) + \\ & (-0.095870 \times AFG) + (-7.375E^{-05} \times CS \times GP) + (+1.2125E^{-05} \times CS \times AFG) + \\ & (-0.011625 \times GP \times AFG) + (+7.25503E^{-08} \times CS^2) + (+0.47555 \times GP^2) + \\ & (+1.2478E^{03} \times AFG^2) \end{aligned}$$

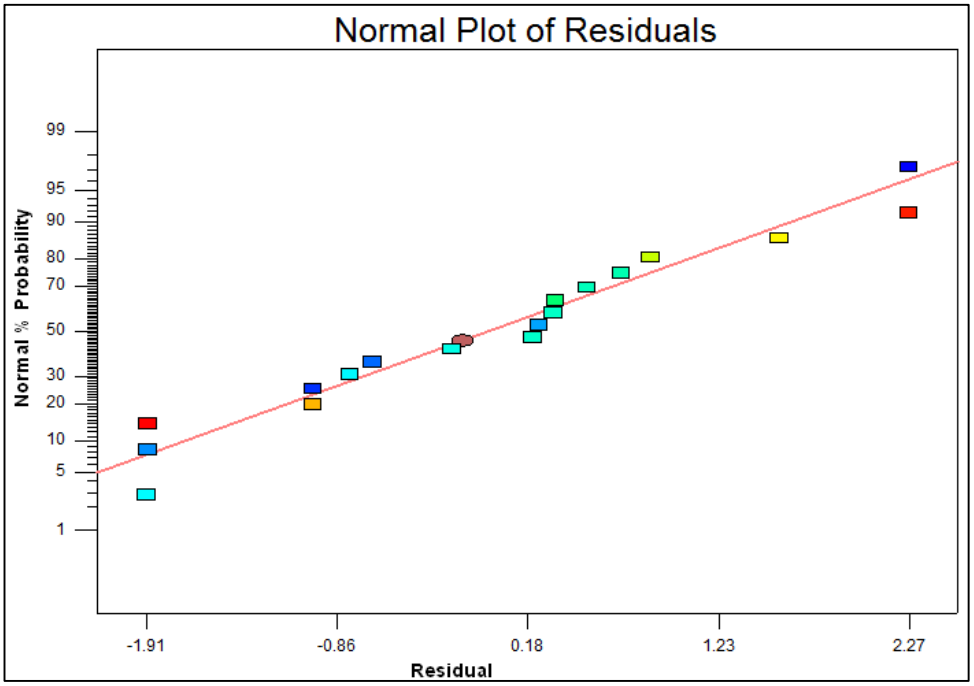

Figure 8.20 Normal plot vs. residual for milling time.

The data points in (Figure 8.20) were distributed much more evenly across the linear target line.

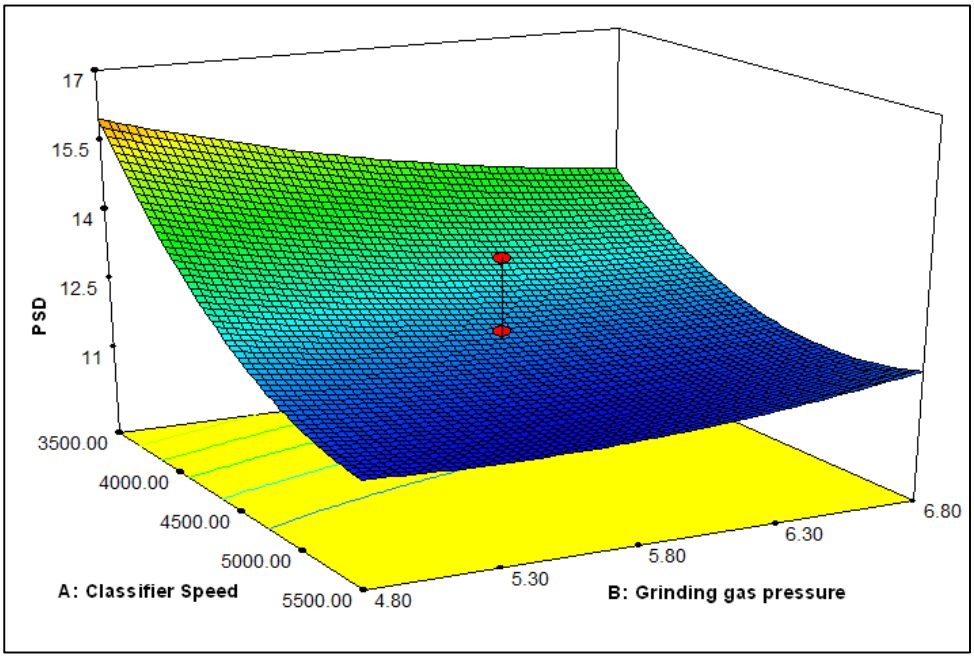

Figure 8.21 3D surface model for psd vs. classifier speed and grinding gas pressure interaction.

High grinding pressures and high classifier speeds in (Figure 8.21) resulted in lower psd.

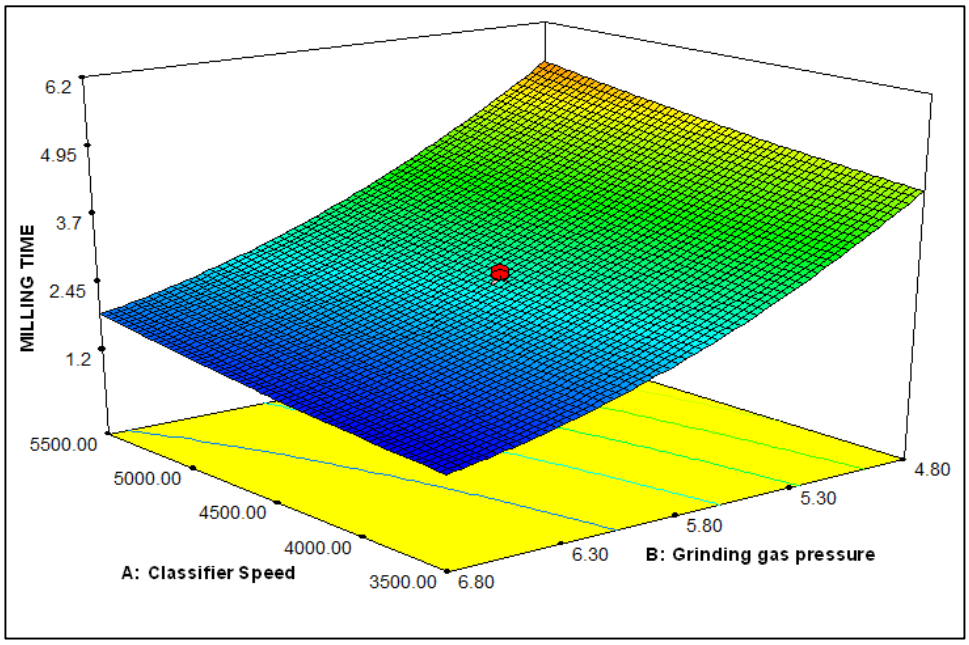

Figure 8.22 3D surface model for milling time vs. classifier speed and grinding gas pressure interaction.

Low classifier speeds and high grinding pressures in (Figure 8.22) resulted in lower milling time.

8.3.4 Trends observed for jet mill experiment 2 (Particle size distribution and milling time)

The design for the jet mill experimentation 2 consisted of 20 runs which included 6 center points and 1 axial point. None of the runs produced powder with a d_{90} < than 10 µm. The trend observed was that the optimal AFG weight laid approximately around 40 kgs in terms of being at the correct height above the nozzles in the jet mill. From the experimental runs it showed an AFG weight greater than 50 kgs increased the particle size distribution. Lower grinding gas pressure lowered particle size distribution but increased milling time exponentially. Higher classifier speeds usually produced lower d_{90} in combination with a change in AFG weight and grinding gas pressure, hence it demonstrated being very dependent. However AFG weight could not be treated as an independent variable due to the jet mill constraints, whereby the optimal weight of powder must be loaded which is slightly above the nozzles hence huge variation does not make sense. The suggested models for both response variables were a quadratic model.

The guidelines for experimentation 3 are applying a grinding gas pressure > 5.8 bar and < 6.8 bar. The AFG weight should be approximately within the range of 40 kgs. The classifier speed should be > 4500 rpm.

8.4 Design Expert Software

The approach used on design expert when running the experimentation for the furnace is detailed below.

1. Start design expert software.
2. Initially select the factorial design.
3. As there were two levels for each factor, a 2^4 factor design matrix was selected.
4. As the guideline, center points are important to be added.
5. Usually more than 4 center points are required to be added in order to get an adequate test for curvature. Note that the average response value from the actual center points is compared to the estimated center point. The estimated center point is the average of all factorial points.
6. There is a function whereby the design can be replicated or the number of blocking of factor runs can be added.
7. Blocking is conducted to restrict the randomization of a factor that is not being studied. In the above experiment conducted, no blocking, or replicating of runs were selected.
8. Once the design matrix is selected, factors have to be named, unit inserted and the range of each factor listed.
9. The software prompts the user to indicate the number of response variables that are present in the experimentation.
10. The response variable is essentially the variable that is measured during the experimentation. The response variable is usually numeric. What is important to take note of is the minimum change that must be detected to determine if it is statistically significantly. This is referred to as a signal. The standard deviation of each response variable needs to be understood. This can be determined by historic data, scientific knowledge, or a pilot study. The standard deviation is usually referred to as the noise.
11. The signal to noise ratio is the probability of detecting an effect if it truly exists.
12. A ratio of 80% and greater is recommended.

13. The next slide indicates the calculated power value to each response variable. The calculated power of a design is the ability of the design to detect which specific terms are statistically significant.
14. The next stage generates an experimental design matrix. The generated design matrix indicates how each factor should be set in every experimental run.
15. The experimental run is conducted on a plant scale and response values are generated.
16. These response values must be inserted into the design expert spreadsheet.
17. The next tab is called the design summary which gives a brief summary of the experimentation such as number of center points, minimum and maximum values for the factors and response variables. It also determines if there are any aliased effects which are due to a lack of design points.
18. The next tab is called the graphs columns which allows the user to look at the trends that is shared between the factors and the response variables.
19. Select the evaluation tab. This option allows the user to select the model that will evaluate the results. The model selected was a factorial model. The next tab under the evaluation section is called the results tab. The results tab indicates the degrees of freedom for evaluation. It looks at the VIF and leverage values. A good design will provide for 3 lack of fit degree of freedoms and 4 pure error degrees of freedom.
20. The next tab on the evaluation tab is called graphs. The software generates an FDS graph. This will assist the user to determine if the design space has useful information.
21. Select the analysis tab for the response variable. This tab assesses the response variables which were specified at the beginning.
22. The assessment looks at the transform function of the response. The ratio of the minimum and maximum response variable is calculated and if the ratio is less than 10, a transformation of the equation is not required. If the ratio is greater than 10, a transformation is required.
23. The type of transformation required will be dependent on the data and what the research aims to determine.
24. Once the transform is selected if required, select the effects tab.
25. The effects tab generates a half normal plot chart. At this stage, significant terms must be selected. Select effects that are larger than others.

26. Select the Pareto chart option. This enables the user to understand the terms that are significant by taking into consideration the Bonferroni and T-value limit.
27. Once these terms are selected, the next tab analysis of variance must be selected.
28. The software gives the user a warning if there are terms that are omitted which are significant and will prompt the user to select terms again.
29. The analysis of variance generates a summary of the design. It evaluates the operating factors in relation to the response variable. It will indicate if the model selected is significant. It also highlights which operating factor has the most effect on the respective response variable. ANOVA also generates an equation for the respective data.
30. It must be noted that the analysis of variance is generated separately for each response variable.
31. The next tab can be selected which is known as the diagnostics tab. The Box Cox plot can be selected in this diagnostics tab. The box cox usually indicates the recommended transform and it will also indicate if a transform is required or not. This is as a double check on the transform that was selected in point 23.
32. The next tab is called the model graphs. This generates a graph for each factor in relation to the response variable.
33. This stage of the design is crucial as it graphically allows the user to evaluate the relationship between factors and a response variable. It also guides the user to fine tune the process parameters for the next trial.
34. Depending on the number of response variables steps 21 will be repeated for the next response variable.
35. As new process parameter ranges are selected and the design is fine-tuned the data is inserted in the software once again however at this stage, response surface methodology design method will be applied.
36. Select the new design. This will allow the user to select the response surface method. At this stage select the central composite design route.
37. Insert the response data into the spreadsheet.
38. Go to the file tab and select new design.
39. It will give the user an option to keep existing data, select ok.
40. Select response surface method.
41. At this stage select central composite design.
42. Note the number of center points selected as per the initial design matrix will be maintained.

43. Go to options, on the central composite design sheet.
44. There is an option to increase the number of replicates that each factorial run is conducted. One is the default.
45. The second option is to increase the number of replicates for each axial point. As discussed, axial points are factors of the experimentation that are set to the mid-point of the operating range.
46. In the choice of the alpha, as per section 8.1 central composite design, the alpha choices can be made based on the experiment by looking at the number of factors and the value of the alpha generated by the software.
47. The number of response variables are selected and defined.
48. An experimental design matrix is generated which determines how each experimental run should be carried out.
49. The experimental run is conducted on a plant scale and response values are generated.
50. These response values must be inserted into the design expert spreadsheet.
51. The next tab is called the design summary which gives a brief summary of the experimentation such as number of center points, minimum and maximum values for the factors and response variables. It also determines if there are any aliased effects which are due to a lack of design points.
52. The next tab is called the graphs columns which allows the user to look at the trends that is shared between the factors and the response variables.
53. Select the evaluation tab. This option allows the user to select the model that will evaluate the results. The model selected was a factorial model. The next tab under the evaluation section is called the results tab. The results tab indicates the degrees of freedom for evaluation. It looks at the VIF and leverage values. A good design will provide for 3 lack of fit degree of freedoms and 4 pure error degrees of freedom.
54. The next tab on the evaluation tab is called graphs. The software generates an FDS graph. This will assist the user to determine if the design space has useful information.
55. Select the analysis tab for the response variable. This tab assesses the response variables which were specified at the beginning.

56. The assessment looks at the transform function of the response. The ratio of the minimum and maximum response variable is calculated and if the ratio is less than 10, a transformation of the equation is not required. If the ratio is greater than 10, a transformation is required.
57. The type of transformation required will be dependent on the data and what the research aims to determine.
58. Once the transform is selected if required, select the fit summary tab.
59. The fit summary tab highlights the recommended model for the experiment. It also highlights the lack of fit tests and design summary.
60. The next tab to be selected is the model option. In this tab, the process order should be selected based on the previous model recommendation.
61. The next tab is called ANOVA, which confirms if the model is significant. It evaluates the operating factors in relation to the response variable. It will indicate if the model selected is significant. It also highlights which operating factor has the most effect on the respective response variable. It indicates whether the lack of fit is significant or not.
62. It must be noted that the analysis of variance is generated separately for each response variable.
63. The next tab can be selected which is known as the diagnostics tab. The Box Cox plot can be selected in this diagnostics tab. The box cox usually indicates the recommended transform and it will also indicate if a transform is required or not. This is as a double check on the transform that was selected in point 57.
64. The next tab is called the model graphs. This generates a graph for each factor in relation to the response variable.
65. This stage of the design is crucial as it graphically allows the user to evaluate the relationship between factors and a response variable. It also guides the user to fine tune the process parameters for the next trial if the target response variable ranges have not been achieved.

8.5 Understanding the Terms and Options in Design Expert

The terms used in the design expert software and their meanings:

1. **VIF**

Variance inflation factors measure the increase of variance of the model coefficient due to the lack of orthogonality in the design.

2. **Leverage**

Leverage is points in the design that can effluence the model fit. Usually values closer to 1 should be replicated.

3. **Transforms**

Square root	-	Used for count and frequency data
Natural log	-	Used for variance and growth data
Base 10 log	-	Used for variance and growth data
Inverse square root and Inverse Power	-	Used for rate and decay data
Logit	-	Used for bounded and yield data
Arcin square root	-	Used for probability and fraction defective

4. **FDS**

Fraction of design space is a line graph. The function of the graph is to show the relationship between the volume of the design space and the amount of predication error. This curve indicates the percentage of the design that has a given prediction error. Lower and flatter curves lead to higher fraction of design space which is ideal as more of the design has useful precision.

5. **Bonferroni Limit**

Effects above this limit are certainly significant.

6. **T-limit**

Effects above the t-limit are possibly significant and should be selected. Effects below this limit are not likely to be significant.

7. **ANOVA**

ANOVA stands for analysis of variance. There are terms that are used in ANOVA that highlight the analysis of the data. For better understanding these terms are defined below and represented in (Table 8.1).

8. **Model**

The model is terms estimating factor effects.

9. **Term**

Terms are listed in the model and individual statistics are calculated for each term.

10. **Curvature**

Curvature tests for non-linearity between the factorial points. It is achieved by comparing the average response of the factorial points to the average response of the center points.

11. **Residual**

The residual factor consists of terms used to estimate experimental error.

12. **Lack of Fit**

Lack of fit is the variation of data around the model.

13. **Pure Error**

Pure error is the amount of variation in the response in the replicated design points.

Table 8.31 Meaning of terms in ANOVA

Conditions	Model	Term	Curvature	Residual	Lack of Fit	Pure Error
Sum of Squares (SS)	The square value of each term added up for the model.	The number of factorial experiments divided by 4×squared factor effect	The weighted difference between the center and factorial point averages.	Sum of squares for all terms are not included in the model.	Is the residual SS after removing pure error SS.	Pure error SS from replicated points.
Degree of Freedom (DF)	No of model terms - 1 (including the intercept)	No of levels for the term - 1	The amount of info to determine curvature.	Corrected total DF - Model DF	The amount of info available after accounting for blocking, model terms, curvature & pure error.	Amount of info available from replicated points.
Mean Square (MS)	Model (SS ÷ DF)	Term (SS ÷ DF)	Curvature (SS ÷ DF)	Provides the estimate for the process standard deviation.	Estimate of lack of fit.	Estimate of pure error variance.
F value	Model MS - Residual MS	Term MS - Residual MS	Curvature MS - Residual MS	-	Compares LOF variance with pure error variance.	-
Prob > F Proportion of the area under the curve F-distribution that lies beyond the observed F value.	Prob > F (less than 0.05) then the terms of model have a significant effect on the response.	Prob > F (less than 0.05) then the individual terms of model have a significant effect on the response.	Prob > F (less than 0.05) will result in the curvature being significant. Ideal value >0.10.	-	Prob > F (less than 0.05) will result in the lack of fit being significant.	-

CHAPTER 9

APPENDIX B

9.1 Sequence furnace start-up

There was a sequential start-up for the furnace during experimentation. Raw material with a particle size range of 0.40 - 0.50 µm was issued to production. The following steps were taken:

1. The furnace was heated up incrementally over three days to set point temperature.
2. The set point temperature was based on the temperature set out by the experimentation.
3. The furnace was purged with nitrogen gas at 100 Nm^3/h. This was done for a day.
4. The belt speed was set to a speed set-out by the experimentation.
5. The level system was set at 25 mm.
6. The purging of nitrogen was stopped prior to the commencement of feeding of the furnace.
7. Nitrogen gas to the cooling section was opened and set to 25 Nm^3/h. There are four ports on the cooling section through which the nitrogen entered.
8. Raw material was loaded into the feed tank of the furnace.
9. The furnace feeding system was initiated which allowed powder to fall onto belt of the furnace.
10. All plant personnel were made aware of the start-up of hydrogen gas.
11. Hydrogen gas was initiated and was fed through the furnace incrementally.
12. The stack flame was ignited to burn off excess hydrogen gas.
13. In the beginning of the start-up the flame leaving the stack was bright orange.
14. As powder filled the furnace, the flame turned to a blue colour. The blue colour was an indication that raw material which had been loaded onto the furnace was in the heating section and the hydrogen gas was reacting with the raw material.
15. Hydrogen gas was incrementally added to set point flow rate.
16. The flame on the stack stabilized after 30 minutes.
17. Carbon dioxide gas was then fed at a set point flow rate at the end of the furnace.
18. All gas flow rates and temperatures were monitored every 30 minutes.
19. The settings as per the experimental run were carried out for 3 days.
20. On the third day, the furnace feeder was stopped for five hours which stopped the raw material from falling onto the belt.

21. Within the five hours, changes to the process parameters were carried out.
22. After five hours, the furnace feeder was initiated and the process commenced.
23. Note after every experimental run steps 19 to 22 would have to be followed.

When process parameters are changed, there was delay time of 2-3 hours before the temperature of the furnace stabilized; hence there was a five hour delay in total before the startup of the next experimental run.

9.2 Sequence jet mill start-up

1. Sub-micron cobalt powder from the furnace was transferred to the jet mill.
2. The batches of powder from the furnace to be used in the jet mill were documented.
3. The settings of the jet mill were set before mill process is initiated.
4. The settings are made as per the experimental matrix generated for the jet mill.
5. The program is then started.
6. Nitrogen gas supply was initiated when the program started.
7. The next step in the program initiated the classifier wheel. The speed had to be manually selected by the operator. Once the speed was set, the classifier wheel started to spin at the set point speed.
8. The filter and discharge control valves thereafter automatically started up.
9. Grinding gas valve opened automatically. This was determined by the grinding gas pressure which was manually selected by the operator.
10. Feed flap valves and sensors initiated.
11. The jet mill process began.
12. Note that the experimentation was carried out over a three day period.
13. The settings of the jet mill were changed after the three day period.

Note after each experimental run, the jet mill was cleaned up, to remove any process material. Process parameters were set as per the experimental runs. It was important to carry out the experimentation after every three days to ensure that there was sufficient data that could be analyzed.

9.3 The fsss analysis procedure

1. Switch on the FSSS equipment.
2. The equipment was run for 20 minutes which allowed the system to stabilize.
3. Calibration was checked for the machine
4. The calculator chart was positioned such that the pointer aligned with the value of 0.75 for porosity.
5. The standard pipe was placed in position K. This was the sample tube holder.
6. The water level was allowed to rise in the manometer.
7. The level of the meniscus had to be at the value 5.1µm on the chart.
8. If not, the water knob was adjusted. I.e. increase or decrease the level.
9. The above method was used to calibrate the Fsss machine.
10. The pressure standard tube was inserted in the base block assembly J.
11. The standard tube was compressed.
12. The force used was noted. This was indicated on the wheel of the rack control.
13. This force noted was the force used to compress all samples to be tested.
14. Sample preparation was conducted.
15. The sample tube was positioned vertically on a flat surface onto the supporting device.
16. The filter paper disk was placed in the center on the end of the tube.
17. The porous plug was positioned with the perforated end down.
18. This plug was positioned onto the center of the filter paper disk.
19. The sample to be tested was weighed. Refer to (Table 9.1) which indicates the mass of sample required for the type of powder to be analyzed.
20. The mass reflected the true density in grams/cm^3 of the material.
21. Sample mass was accurate within 0.01gram.
22. The sample tube was inverted so that the inserted porous plug was at the bottom.
23. The powder funnel was used to transfer the weighed sample into the sample tube.
24. The sides of the funnel and sample tube were tapped.
25. This was to ensure that the entire sample settled into the sample tube.
26. The filter paper was positioned on the center of the sample tube.
27. The porous plug above was inserted.
28. The sample was placed into the base block assembly J.
29. The sample was compressed using the force as noted in point 12.
30. The sample was compressed thrice.

31. On the third compression, the wheel was held in position.
32. The pointer was aligned onto the standard line.
33. The sample was removed from the block assembly.
34. The sample was placed in the tube holder K.
35. The meniscus started to rise.
36. The porosity value from the X-axis was recorded.
37. The FSSS value from the Y-axis was recorded.

Table 9.1 Reference mass required for particle size analysis

Sample	Grams to be analyzed
Cobalt Carbonate	4.13
Furnace	4.45
Jet mill	8.90

9.4 The particle size distribution analysis procedure

1. The de-ionised water unit that is connected to the Malvern master-sizer must be opened. Note it was imperative that de-ionised water was used, as any contaminates in the water would affect the particle size distribution result.
2. The Master-sizer 2000 program was opened and the configure option was selected.
3. The accessories option was thereafter selected.
4. The clean option was selected.
5. The machine underwent the clean process before the analysis was carried out.
6. The system operation program on the Master-sizer 2000 was opened.
7. The sample bag was shaken to ensure that the sample was homogenous.
8. A small amount of powder was placed on the watch glass.
9. The syringe containing water or isopropyl alcohol was used to wet the powder.
10. Only one drop at a time was added.
11. This sample was mixed with a spatula until it reached a paste consistency.
12. A small amount of this sample was then added to the Hydro G dispersion unit.
13. Step 12 was conducted until the obscuration was in range (between 5 - 10%)
14. The sample was then analysed.
15. The particle size distributor provided three readings.
16. The average of the readings was taken as the final result.